INFORMATION TO USERS

This manuscript has been reproduced from the microfilm master. UMI films the text directly from the original or copy submitted. Thus, some thesis and dissertation copies are in typewriter face, while others may be from any type of computer printer.

The quality of this reproduction is dependent upon the quality of the copy submitted. Broken or indistinct print, colored or poor quality illustrations and photographs, print bleedthrough, substandard margins, and improper alignment can adversely affect reproduction.

In the unlikely event that the author did not send UMI a complete manuscript and there are missing pages, these will be noted. Also, if unauthorized copyright material had to be removed, a note will indicate the deletion.

Oversize materials (e.g., maps, drawings, charts) are reproduced by sectioning the original, beginning at the upper left-hand corner and continuing from left to right in equal sections with small overlaps.

Photographs included in the original manuscript have been reproduced xerographically in this copy. Higher quality 6" x 9" black and white photographic prints are available for any photographs or illustrations appearing in this copy for an additional charge. Contact UMI directly to order.

Bell & Howell Information and Learning
300 North Zeeb Road, Ann Arbor, MI 48106-1346 USA

UMI®
800-521-0600

The Role of North Atlantic Deep Water Formation in the Thermohaline Circulation

Paul Joseph Goodman

A dissertation submitted in partial fulfillment of the
requirements for the degree of

Doctor of Philosophy

University of Washington

2000

Program Authorized to Offer Degree: Atmospheric Sciences

UMI Number: 9964258

Bell & Howell Information and Learning Company
300 North Zeeb Road
P.O. Box 1346
Ann Arbor, MI 48106-1346

In presenting this dissertation in partial fulfillment of the requirements for the Doctoral degree at the University of Washington, I agree that the Library shall make its copies freely available for inspection. I further agree that extensive copying of the dissertation is allowable only for scholarly purposes, consistent with "fair use" as prescribed in the U. S. Copyright Law. Requests for copying or reproduction of this dissertation may be referred to Bell and Howell Information and Learning, 300 North Zeeb Road, Ann Arbor, MI 48106-1346, to whom the author had granted "the right to reproduce and sell (a) copies of the manuscript in microform and/or (b) printed copies of the manuscript made from microform."

Signature Paul Yoder

Date 15 MARCH 2000

University of Washington
Graduate School

This is to certify that I have examined this copy of a doctoral dissertation

Paul Joseph Goodman

and have found that it is complete and satisfactory in all respects,
and that any and all revisions required by the final
examining committee have been made.

Chair of Supervisory Committee:

Edward S. Sarachik

Reading Committee:

Edward S. Sarachik

David S. Battisti

Paul D. Quay

University of Washington

Abstract

The Role of North Atlantic Deep Water Formation in the Thermohaline Circulation

Paul Joseph Goodman

Chairperson of the Supervisory Committee:
Dr. Edward S. Sarachik
Atmospheric Sciences

An ocean general circulation model is used to explore the global ocean thermohaline circulation. North Atlantic Deep Water formation is an important component of this system and the role of this process in the ventilation, structure and variability of all the world ocean basins is studied. The production of deep water in the north Atlantic Ocean has profound effects on and around the Atlantic basin, and limited effects at certain locations downstream. A distinction is drawn between upwelling (the vertical motion of water parcels) and de-densification (the addition of buoyancy): upwelling in the model occurs primarily in the Southern Ocean and de-densification occurs mainly in the tropics between 30°S and 30°N.

There are two different time-scales associated with changes in the rate of NADW formation. The adjustment time scale is quite fast, on the order of 25 years, and this is the time scale on which the overturning and heat transport in the Atlantic respond to changes in the high-latitude surface forcing. Boundary layer waves connect all three northern ocean basins and all location begin to feel a change in the rate of NADW production within 25 years. The advective time scale is much slower, on the order of 300-1000 years. The Indian and Pacific Ocean are only slightly changed by the presence or absence of NADW production in the model.

Table of Contents

List Of Figures

List of Tables

Acknowledgements

I would like to gratefully thank and acknowledge my advisor, Dr. Edward Sarachik, for his considerable time, effort, guidance, and patience on my behalf. I would not have come nearly so far without his assistance. I would also like to thank the members of my committee, Dr. David Battisti, Dr. Paul Quay, and Dr. Ed Harrison, for their most helpful discussions, comments, and suggestions along the way. I want to thank all the wonderful people at JISAO, too numerous to name, especially the canine corps including Sophie, Sassy, and the late Margaret Black Lab. I need to give a special thanks to Dr. David McDermott who made my mistakes first and so could tell me where I went wrong.

My friends here in Seattle and elsewhere have given me strength and support through the many years of graduate school and all the late nights, working and otherwise. I want to thank and acknowlegde my parents for letting me begin life without student loans and for instilling my curiousity and love of learning. Last, but not least, I want to express my most sincere thanks and love to my wife Dr. Joellen Russell for her strength, support, mentoring, company and friendship. Without her, I was drifting; with her, I thrive.

Introduction

The density-driven overturning of the word ocean, the thermohaline circulation, is controlled by the inhomogeneous heating, cooling, evaporation, precipitation and runoff from the world's land masses. The global thermohaline circulation has been called a "Great Conveyor" [Broecker, 1991]. In the Atlantic basin, warm tropical water flows northward in the Gulf Stream and is evaporated and cooled until it reaches the vicinity of Greenland where it sinks to form the North Atlantic Deep Water (NADW) mass. This water mass then flows southward as a deep western boundary current along the coast of the Americas until it joins the Southern Ocean. This pattern of northward surface flow, sinking, and southward subsurface flow is reminiscent of a giant conveyor belt. The conveyor-like qualities of the other ocean basins, however, are more suspect: the formation of Antarctic Bottom Water is controlled by shelf processes [Carmack and Foster, 1977], the Southern Ocean and the Antarctic Circumpolar Current are dominated by the wind-driven upwelling, and there are no known sources of deep water production in either the Indian or Pacific basin.

This dissertation is an exploration of how the deep water production in the North Atlantic affects the global overturning with an ocean general circulation model (OGCM). I will focus on two main simulations, one with NADW production and the other without. The model forms a reasonable amount of NADW (16 Sv) when forced by restoring the surface properties (temperature and salinity) to the

current climatology as given in the Levitus Climatological Atlas (1994). In order to eliminate the production of NADW a negative salinity anomaly is imposed into the restoring boundary condition north of 40°N in the Atlantic This is the only change between the two simulations: all mixing parameters, time constants, and surface forcing (outside the North Atlantic) are identical.

In Chapter 1, the two different steady states are explored to examine the effects of North Atlantic Deep Water (NADW) formation on the thermohaline circulation (THC) and ventilation time-scales of the abyssal ocean. An idealized age tracer is included to gauge the ventilation in the model. The Atlantic branch of the THC is reversed and the ventilation of the deep Atlantic basin is severely reduced when NADW formation is prevented. The Southern Ocean forms bottom water in both experiments, but downwelling and upwelling in the Southern Ocean are both reduced when NADW is included due to increased stratification of the water column. The Indian and Pacific basins are upwelling regions in both experiments and upper-level upwelling is stronger there when NADW is included; this change leads to cooler temperatures and reduced ventilation of the upper ocean.

Chapter 1 notes that there is a need for the distinction to be drawn between upwelling, the vertical movement of water parcels, and positive buoyancy forcing, which converts denser water masses into lighter ones. A density-regime analysis reveals that most of the positive buoyancy forcing associated with the THC occurs equatorwards of 30° latitude in both hemispheres. The THC in the model ocean

seems more modular than the "conveyor-belt" metaphor implies; each high-latitude region functions quasi-independently, responding to its own heat and fresh water forcing. The newly ventilated sub-surface water masses formed in each region compete for space in the water column. The production of NADW increases the upper level stratification throughout the world ocean. The idealized age tracer reveals that the deep Pacific and Indian basins are primarily ventilated by southern bottom water and the inclusion of NADW causes only minor changes. The qualitative pattern of ventilation in the model is determined by the number and location of sub-surface water mass formation regions; the actual ages in the deep ocean are very sensitive to the vertical diffusion prescribed in the model.

In Chapter 2, the transient effects of the baroclinic adjustment due to deep water formation in the presence of a background circulation are studied. The advantage of using a GCM over the previous two-layer models is that the effects of higher-order modes are not arbitrarily eliminated. The initial condition for this study is the steady-state circulation in the OGCM with North Atlantic deep water (NADW) production artificially eliminated; the artifice is then removed and the development of the pressure and transport anomalies due to the initiation of NADW are followed. The incorporation of a passive water mass tracer into the model allows for a comparison between the baroclinic adjustment and the advection of the newly formed deep water. Chapter 2 describes how the time-scales and the spatial patterns of these two processes are distinctly different: adjustment fol-

lows the classical boundary layer path and the stratification at all locations north of the Antarctic Circumpolar Current begins to change within 20 years, advection follows the flow and the relevant time-scale for NADW in the North Pacific is about 1000 years. The majority of the passive tracer injected into the Atlantic north of 60°N, returns to the surface along the coast of Antarctica. Time-series of the transport anomalies at various locations are presented and the small differences in the baroclinic adjustment process due to the initiation and cessation of deep water production are discussed.

In Chapter 3, variability around the long-term mean is explored. This variability is imposed on the model as varying salinity anomalies are applied to the North Atlantic with a range of time-scales and amplitudes. The model responds at all locations with the same period as the imposed forcing. The amplitude of the response increases as the period increases and as the amplitude of the forcing increases. There is an adjustment time-scale of roughly 25 years in the Atlantic over which the overturning can respond to changes in the forcing. When the period of the forcing is less than 25 years, the overturning varies only weakly.

The amplitude of the response decreases as the distance from the North Atlantic increases. Changes in the overturning rate and Gulf Stream transport can be fairly large, but the response in the Indonesian Throughflow is a few percent at most. Changes in the stratification are largely confined to the North Atlantic except in the most extreme case studied; in this case, there were notable changes

in the Southern Ocean south of Australia and west of Chile, the sites of Sub-Antarctic Mode Water and Antarctic Intermediate Water formation, respectively. This interaction between the rate of NADW production and the stratification in the intermediate water formation regions is interesting and deserves further study.

Chapter 1

The Role of North Atlantic Deep Water Formation in an OGCM's Ventilation and Thermohaline Circulation

1.0 Introduction

The processes and time-scales associated with the ventilation of the deep and mid-depth ocean continue to be major unresolved questions in both oceanography and climatology. Much work has been done to date, both through observational analysis and computer modelling, but as yet no consistent, geographically-complete description exists. While it is known that new bottom and deep waters are created in the high-latitude Southern Ocean and North Atlantic as part of the global thermohaline circulation, the ventilation of the abyssal and mid-depth ocean away from these formation regions is still poorly understood. With the possible threat of global climate change due to anthropogenic factors, understanding of the ocean's potential to ameliorate or enhance these stresses is of critical concern.

The current description of the ocean's thermohaline circulation (THC), the so-called "global conveyor belt", as put forth by W. S. Broecker (1987, 1991, 1995), A. L. Gordon (1986, 1991) and others, suggests that it is driven primarily

by convection in the North Atlantic. North Atlantic Deep Water (NADW) advects a great quantity of salt into the Southern Ocean and the Antarctic Circumpolar Current (ACC). The salinity-enhanced Circumpolar Deep Water (CDW) briefly upwells, loses its heat to the atmosphere, and sinks to the bottom as Antarctic Bottom Water (AABW). Elsewhere, deep and bottom waters absorb heat diffusively, upwell gradually, and eventually return to the sinking regions.

A study by Schmitz (1995) [S95, hereafter] reviewed much of the observational evidence from a wide variety of sources and compiled a coherent summary of the global THC. This report concluded that NADW is first converted into CDW and it is this water mass which then fills the deep Indian and Pacific basins. It is notable in the S95 analysis that the only region in which upper water is converted into deep water is the North Atlantic and that all bottom water is converted from CDW. Contrary to S95, however, recent work by Broecker, et al, (1998) concluded that the only way to explain the phosphate star (PO_4^*) evidence [see Broecker, et al. (1991) for discussion] is if equal volumes of Antarctic surface water and North Atlantic surface water are converted into deep or bottom water. Observational studies [Carmack and Foster (1975), Foster and Carmack (1976), Foster (1995)] have located only about one third as much bottom water formation at various sites along the coast of Antarctica compared to the estimated rate of NADW formation, but large uncertainties due to the analysis technique, as well as potential spacial and temporal variability, still exist. S95 also concluded that all deep water

upwelling occurs in the Indian Ocean and the Southern Ocean, although he acknowledged that the vertical exchange processes in the Indian and Pacific Oceans are poorly established.

Sedimentary evidence ($\delta^{13}C$) indicates that NADW production was less plentiful, if not entirely eliminated [Boyle and Keigwin (1987)] during the last glacial period than at present, while AABW production (or rather, strong convection between the surface and deep water in the Southern Ocean) was comparable or more vigorous [Duplessy, et al. (1988)]. Modelling results consistently indicate that AABW production remains roughly constant whether or not NADW production is present [Fichefet, et al. (1994); Stocker, et al. (1992); England (1993); Cai and Greatbatch (1995)]. Radiocarbon evidence ($\Delta^{14}C$) also indicates that water in the deep, tropical Pacific was about 70 ± 105 years older relative to the surface during the last glacial period than at present [Broecker, et al. (1990), Duplessy, et al. (1992)].

This highlights an obvious question: if NADW production and export is the main process behind the ventilation of the abyssal ocean, then how could the deep Pacific Ocean experience such a small change in deep water ages at a time when NADW production was sharply curtailed? The obvious alternative is that the formation of recently ventilated AABW occurred independently of NADW production during the last glacial period, and the deep Pacific was ventilated by AABW.

The role of AABW in the global THC and ventilation of the deep ocean has been largely ignored or deemed secondary in importance to that of NADW.

The present study will examine this question in an OGCM simulation under two related, yet distinct, sets of boundary conditions: one which includes NADW production, and one in which this critical water mass is eliminated. The purpose of this study is twofold: to provide a thorough analysis of the model's circulation, in terms of mass transport and density regime conversion, and to distinguish between these two processes; and to present a coherent description of the model's THC in order to examine the role of NADW on the global overturning. It should be noted that water masses in OGCM's are generally not equivalent to the real-world water masses in terms of their temperature and salinity characteristics. The model water masses discussed in this paper are given the same names as their real counterparts, because they seem to function the same in the context of the model circulation.

An idealized passive age tracer is included to gauge the ventilation time-scales throughout the model ocean. The idealized age tracer used in these experiments is derived from that of Haidvogel and Bryan (1992) and was recently incorporated into an OGCM by England (1995); it gives an indication of the time elapsed since a fluid parcel was last at the surface. Since the 'atmosphere' plays no role in its final structure, the age profile derived from this idealized age tracer is

solely dependent on the model circulation. In this regard, it can serve as a benchmark on which to compare the oceanic portion of various modelling efforts.

Modelling studies of the ocean's general circulation provide a wealth of information not currently obtainable from the real ocean. Due to the lack of hard numbers needed to evaluate or contradict model performance, however, most researchers have concentrated on process studies or sensitivity studies, or have limited their analyses to those particular features where observational data have been recorded. Rigorous analyses of model results are useful in and of themselves, in that all relevant data is available; until we can understand model results more completely, we can not hope to describe fully the more complex, real-world ocean. The intercomparison of different models, model configurations and parameters, and boundary conditions provides essential information about the models, and may be the only way to increase our confidence in the simulations they provide. They also can guide observational studies to opportune geographical locations for data collection. Accordingly, many of the physical features simulated by the model will be discussed quantitatively, despite the paucity of data regarding the deep ocean circulation.

Results indicate that the largest effects of NADW formation are found in the Atlantic, but there are distinct and important changes to the rest of the world ocean as well. Contrary to the standard picture of a single "global conveyor", the model ocean basins seem to function quasi-independently, with each northern

basin and the Southern Ocean responding to its own high-latitude heat and fresh water balance. Water of southern origin fills the deepest model levels regardless of the presence or absence of NADW. Most of the upwelling in the model occurs in the circumpolar region, but most of the positive buoyancy forcing occurs between 30°S and 30°N. Low-salinity southern subpolar intermediate water is much more prevalent throughout the world ocean when NADW is removed. NADW formation also affects the upper-level upwelling in the Indian and Pacific; intermediate waters there are both colder and less ventilated (older) when NADW production is included.

The structure of the paper is as follows: section 2 describes the model formulation; section 3 presents the global circulation for the Control Experiment; section 4 presents the global circulation in the model when NADW formation is artificially eliminated (referred to as the No-NADW Experiment); a cartoon depicting the model's THC is presented in section 5 which summarizes the results and offers some conclusions.

2.0 The Model

2.1 Geometry

The experiments are carried out on the GFDL Modular Ocean Model [Pacanowski, et al. (1991)] in an idealized topography. The geometry [Figure 1] consists of three basins to represent the Indian, Pacific and Atlantic Oceans, along

with a reentrant channel in the south that allows for the formation of an ACC. The total zonal extent of the model is 240°; the Indian and Atlantic basins span 60° of longitude, and the Pacific covers 120°. The southern extreme of the model is 72°S, and the northern extremes for the Indian, Pacific and Atlantic Oceans are 24°N, 60°N and 72°N, respectively. The grid spacing is coarse: 3.75° (zonal) by 4° (meridional). The geometry includes a representation of Australia and an Indonesian Passage. Both Australia and Antarctica are treated as true islands and the model calculates the barotropic transport about them.

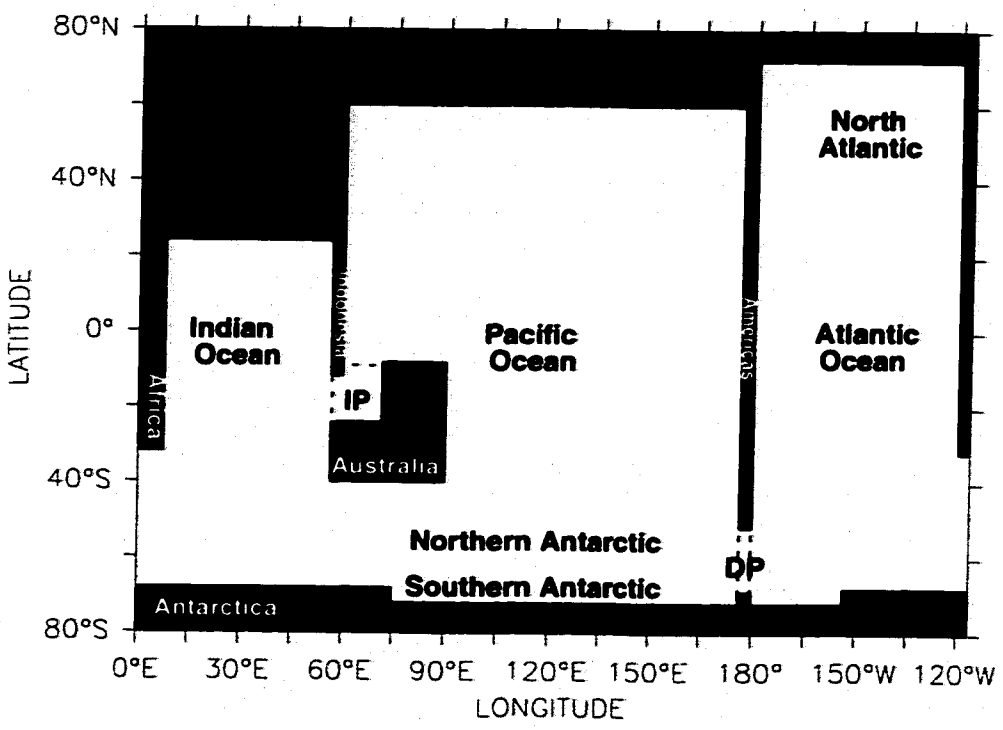

FIGURE 1 : The model domain. Names indicate regions referred to in this study and are adopted from Cox (1989). DP refers to the location of the Drake Passage; IP, the Indonesian Passage. Southern Ocean in the text refers to both the Northern and Southern Antarctic, while the "high-latitude" Southern Ocean refers to the Southern Antarctic only.

The bathymetry is divided into 20 levels of increasing thickness from 50 meters at the surface to 449 meters at the bottom comprising a total of 5000 meters everywhere. There is no bottom topography except in the Drake Passage where the sill depth is 2500 meters, and in the Indonesian Passage where there is a plateau at 1551 meters. This idealized geometry captures the basic elements necessary to differentiate among the distinct ocean basins and to simulate a global thermohaline circulation, within the constraints of the model resolution.

2.2 Surface Forcing

Restoring boundary conditions for both temperature and salinity are applied at the surface with a Haney-type restoring scheme [Haney (1971)] using a fixed restoring time-scale of 50 days. Zonally- and annually-averaged quantities from the 30-meter level of the Levitus (1982) climatological atlas are used, with some modifications. The global zonal average is applied south of 40°S; the Levitus data is fairly uniform along the latitude circles there. North of 40°S, each basin is forced with its own zonal average. North of 60°N in the Atlantic, the restoring salinity is calculated from the values east of Greenland only. Labrador Sea surface salinities are much lower and their inclusion in the basin average severely restricts the formation of northern deep water in the model. The other modification to the Levitus dataset is to smoothly increase the restoring salinity off the Antarctic coast from climatology at 60°S to 35‰ at 70°S, as was done by England (1993). Together, these changes create a reasonable balance between deep water production in

both hemispheres, and simulate the global salinity profile more accurately than the enhancement of either hemisphere alone or no enhancement at all. It must be noted that observational studies near Antarctica have indicated the importance of shelf processes in the formation of AABW [Foster (1995)]; these processes are not explicitly modeled in this or most other OGCM simulations.

Toggweiler and Samuels (1995) stated that the use of artificially high restoring salinities over the high-latitude Southern Ocean induces a surface freshwater flux which implies a rate of ice formation and export much higher than observed. They attribute the poor salinity structure in coarse-resolution models to a failure of the modeled NADW to transport enough salt into the ACC. Duffy and Caldeira (1997), however, report that the simulation of the global salinity profile is greatly enhanced, without affecting the diagnosed freshwater flux, when the salt rejected from Antarctic sea ice formation is incorporated into the top 160 meters of the water column, instead of the surface box alone. It is known that the Antarctic data in the Levitus dataset was collected in the austral summer and as a result, the upper-level salinities are excessively fresh compared to the deep water in this location [Levitus (1982)]. The restoring salinities used in this experiment are closer to the observed deep water characteristics, and since the focus of this paper is not on the diagnosed salinity flux, this modification is considered appropriate.

To test the sensitivity of the model to the enhanced salinities in both the North Atlantic (GIN seas salinity only) and the high-latitude Southern Ocean, various runs were conducted with either one enhancement or the other or neither. When neither hemisphere was enhanced, *i.e.* when using the actual Levitus data, the global circulation was similar to the one discussed in this paper, but the globally-averaged vertical salinity profile was exceedingly fresh. When the enhancement was applied to only the northern hemisphere, the southern hemisphere still produced deep water, but the global deep and bottom salinities were still too fresh (about 0.5‰ lower than observed), and the rate of NADW formation was much larger than observed (over 28 Sv). Increasing the Antarctic surface salinities, while including the Labrador Sea salinities in the North Atlantic restoring salinity value caused North Atlantic Deep Water production to cease. Further sensitivity studies focused on the bathymetry and boundary conditions, as well as the effect of sea ice in the Antarctic sector are needed.

The zonal component of the zonally- and annually-averaged wind stress from Hellerman and Rosenstein (1983) is applied uniformly at all longitudes. No meridional wind stress is applied anywhere. The model employs no-slip boundary conditions at the walls and there is no bottom friction. Viscous and diffusive mixing are prescribed in a Cartesian frame with constant coefficients, except for the vertical diffusivity, which varies from 0.3 cm^2s^{-1} at the surface to 1.1 cm^2s^{-1} at the bottom. It is parameterized by a depth-dependent function identical to that of

Robitaille and Weaver (1995), which is based on, but different from, the original formula presented in Bryan and Lewis (1979). All the parameters employed in these experiments are given in Table 1.

TABLE 1. Ocean Model Parameters

Parameter	Value
Horizontal Diffusivity	$1x10^7$ cm^2s^{-1}
Horizontal Viscosity	$6x10^9$ cm^2s^{-1}
Vertical Diffusivity	0.3 -1.1 cm^2s^{-1}
Vertical Viscosity	1.0 cm^2s^{-1}
Surface Relaxation Time (1/τ)	
Temperature & Salinity	50 days
Passive Age Tracer	0 days

2.3 Idealized Age Tracer

The idealized age tracer used in these experiments was suggested by Haidvogel and Bryan (1992). The surface age is set to zero everywhere at each time step, equivalent to a zero-day restoring time-scale. At each internal grid box, the age tracer act likes a running clock with time being added at each time step, according to the formula:

$$AGE\ (t + \Delta t) = AGE\ (t) + L(t) + \Delta t \qquad \text{(EQ 1)}$$

where t is time, Δt is the length of the model time step, and L represents all the advection and mixing from adjoining grid boxes. The idealized age tracer acts like a stopwatch which is reset at the surface and keeps track of the time after a parcel descends into the water column, rather than modelling a decaying quantity, such

as ^{14}C, which must be compared to a reference value to determine the elapsed time. By removing the need for an arbitrary reference, it is closer to a Lagrangian estimate of the average time elapsed since a parcel was at the surface and does provide an accurate indication of ventilation times in the model.

Sensitivity studies indicate that the qualitative pattern of ages is primarily a function of the surface forcing, *i.e.* the number and location of deep water sources. Away from the convecting regions, however, the modeled ages are highly sensitive to the parametrization of the vertical diffusion employed. It should be noted at this point that 'ventilation' is defined as the process of moving a parcel of water from the surface to a given subsurface location, and 'ventilation age' or 'age' as the time it takes to get to a given location from the surface. Ventilation can occur through convection, subduction, advection and diffusion.

2.4 Experiments

In the Control Experiment, NADW formation is observed when the model is forced at the surface with present day climatological values. In the No-NADW Experiment, NADW formation is halted by imposing a negative salinity anomaly on the North Atlantic north of 40°N, which nearly eliminates the convective activity in this region. The low salinity anomaly is imposed by reducing the previously mentioned restoring salinity values over this sector by 1‰ and letting the model achieve a new steady state. Many studies have explored the existence of multiple equilibria in OGCM's (e.g. Manabe and Stouffer (1988), Marotzke and Willebrand

(1991), Power and Kleeman (1993), Hughes and Weaver (1994), and others), but the present study does not fall into this category. Multiple equilibria, by definition, exist under identical forcing: the steady state equilibrium being determined solely by the initial conditions. As stated above, the purpose of this study is to compare and contrast the two *differently-forced* steady states, without delving into how the system gets from one equilibrium to the other. This transition will be the subject of future work.

3.0 Control Experiment (with NADW)

Under the control (*i.e.* present day) forcing, the model produces many of the features observed in today's ocean. Deep water is formed in both hemispheres [Figure 2a], driven by high-latitude convection [Figure 2b]. A strong ACC develops with a transport of 205 Sv (1 Sv = 10^6 m^3s^{-1}) through Drake Passage [Figure 2c]. This value is higher than the observed estimates of 125 Sv (± 15 Sv) [Whitworth, et al. (1982)], but is typical of OGCM results [Semtner and Chervin (1988), Hirst and Godfrey (1993), Cai and Greatbatch (1995)]. The flow through the Indonesian Passage from the Pacific into the Indian basin measures 22.2 Sv [Figure 2c], again higher than the observations (extrema in the throughflow were reported by Fieux, et al. (1996) as -2.6 Sv and 18.6 Sv westward flow, and Meyers, et al. (1996) determined that ENSO-induced variability was ± 5 Sv around a mean of 11 Sv), but in accord with other modelling results [Hirst and Godfrey (1993), England (1993), Cai and Greatbatch (1995)] given the idealized model topography. The

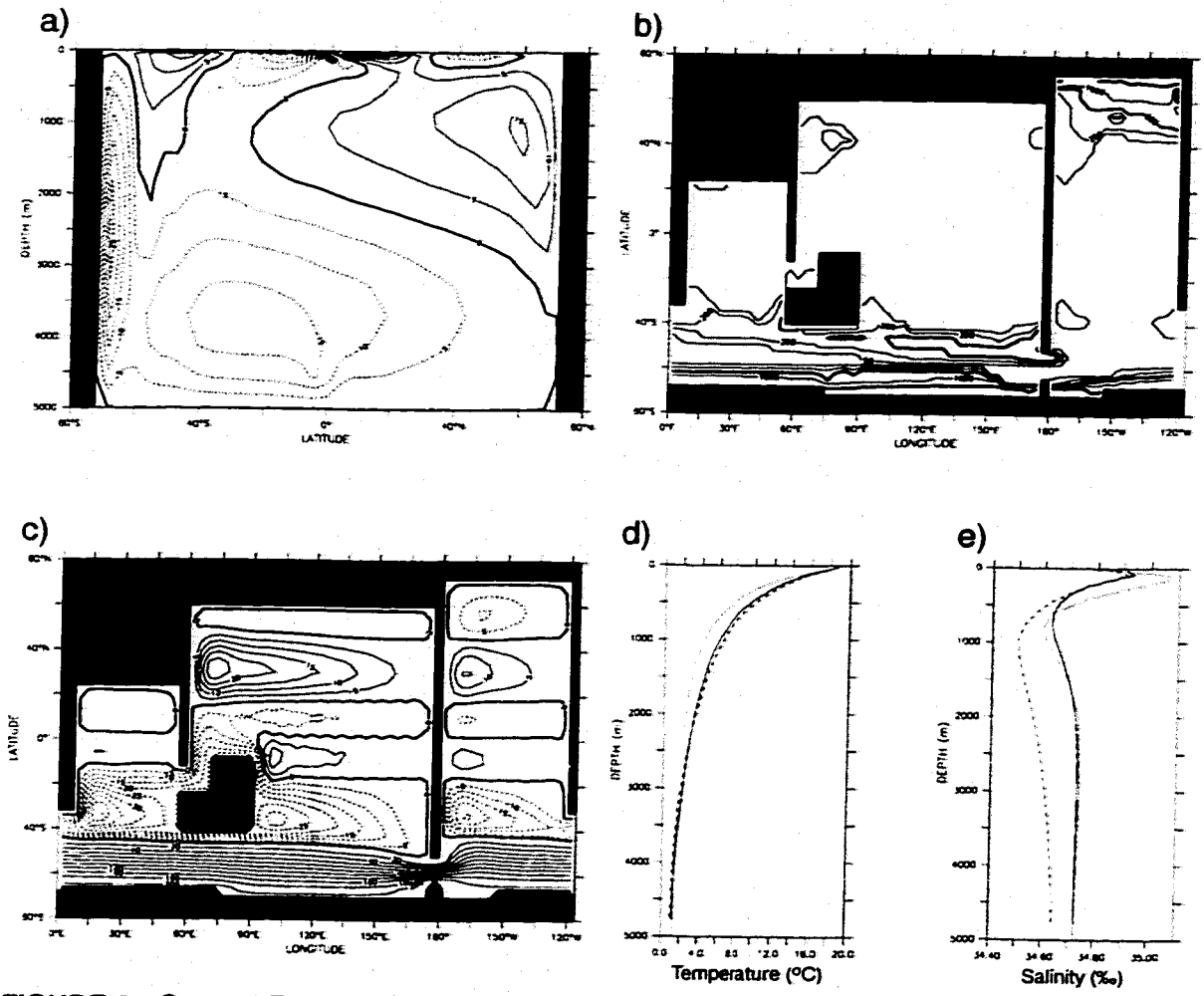

FIGURE 2 : Control Experiment: a) Meridional overturning streamfunction, contour interval is 5 Sv; b) Depth of convection from the surface, contours at 50, 250, 500, 1000, 2500, and 5000 meters, with the 500 and 2500 meter contours darkened; c) Barotropic streamfunction, contour interval is 5 Sv, except in the ACC where it is 20 Sv; d) Globally averaged temperature from the Control Experiment (solid), No-NADW Experiment (dashed), and Levitus (1982) (dotted); e) Globally averaged salinity from the Control Experiment (solid), No-NADW Experiment (dashed), and Levitus (1982) (dotted). Note that in a) and c) solid (dashed) contours denote clockwise (counter-clockwise) circulation.

westward portion of the flow south of Africa, known as the Agulhas Leakage, extends down to 1550 meters and measures 16.3 Sv with over 15 Sv of the transport in the upper kilometer. Although it is believed that the majority of the transport is in the form of baroclinic eddies which are not resolved by this model, Gordon, et

al. (1992) stated that there is still a large uncertainty in the Agulhas Leakage transport (3-20 Sv westward) which may be the result of a wide temporal variation in the flow itself and not an artifact of the observational method.

The globally averaged temperature and salinity profiles are plotted as a function of depth along with the Levitus (1982) profiles in Figure 2d and Figure 2e. As with most coarse resolution OGCM's, the thermocline is too diffuse compared to the observations; the maximum error is about 2°C too warm at 600 meters. The salinity profile is simulated well; the salinity minimum associated with Antarctic Intermediate Water (AAIW) is clear, although the upper level halocline is also a bit too diffuse. The model's globally averaged temperature and salinity are 4.1°C and 34.72‰, compared to the Levitus (1982) averages of 3.4°C and 34.73‰.

3.1 Antarctic Sector

As seen in Figure 2a, a net of 27 Sv sink below 2500 meters in the southernmost grid box, loosely corresponding to the Ross and Weddell Seas. This Antarctic overturning is slightly weaker than other modelling results (~34 Sv in Cai and Greatbatch (1995) and over 40 Sv in England (1993)) despite the enhanced restoring salinity. The sinking, south of 68°S, is divided into three regimes: the Weddell Sea in the Atlantic sector transports about 29 Sv downward; the southeastern Ross Sea between model longitudes 157°E and 180°E in the Pacific sector transports about 29 Sv downward; and the southwestern and central Ross Sea is an upwelling region that carries 31 Sv of deep and bottom water toward the sur-

face. A large percentage of the water downwelled west of the Antarctic Peninsula flows westward along the coast at the bottom and most of this upwells in the Indian and Pacific sectors of the high-latitude Southern Ocean. The meridional overturning [Figure 2a], south of 60°S, conceals stronger, zonal overturnings in both the Indo-Pacific sector and the Atlantic sector of 55 Sv and 27 Sv (measured at 2500 meters), respectively.

The vertical transport is upward nearly everywhere between 68°S and 60°S, except along the northwestern edge of the Antarctic Peninsula. As many authors have proposed, the largest part of the model ocean's upward vertical transport occurs in the Antarctic sector of the model, south of 60°S [Broecker (1991), Gordon (1991), Toggweiler and Samuels (1993), Shriver and Hurlburt (1997)]. Contrary to the standard description presented by these studies, however, this vertical motion is generally not associated with the conversion of denser water masses to lighter ones. This will be discussed further in section 3.4.

Despite these strong overturnings, a net of only 7.9 Sv actually flow northward across 60°S in the bottommost 1300 meters. The meridional flow across this section is divisible into the same three regimes as the vertical motion: 15.5 Sv move southward at 60°S in the Indian and western and central Pacific sectors to supply the upwelling; 9.8 Sv of newly downwelled water flow northward in the far-eastern Pacific, immediately west of the Drake Passage sill; and, 13.6 Sv flow northward across 60°S in the Atlantic. Nearly all of the bottom water formed in the

Atlantic sector flows northward below the ACC into the basin as a deep western boundary current [Figure 3], although a portion is entrained into the eastward flowing ACC.

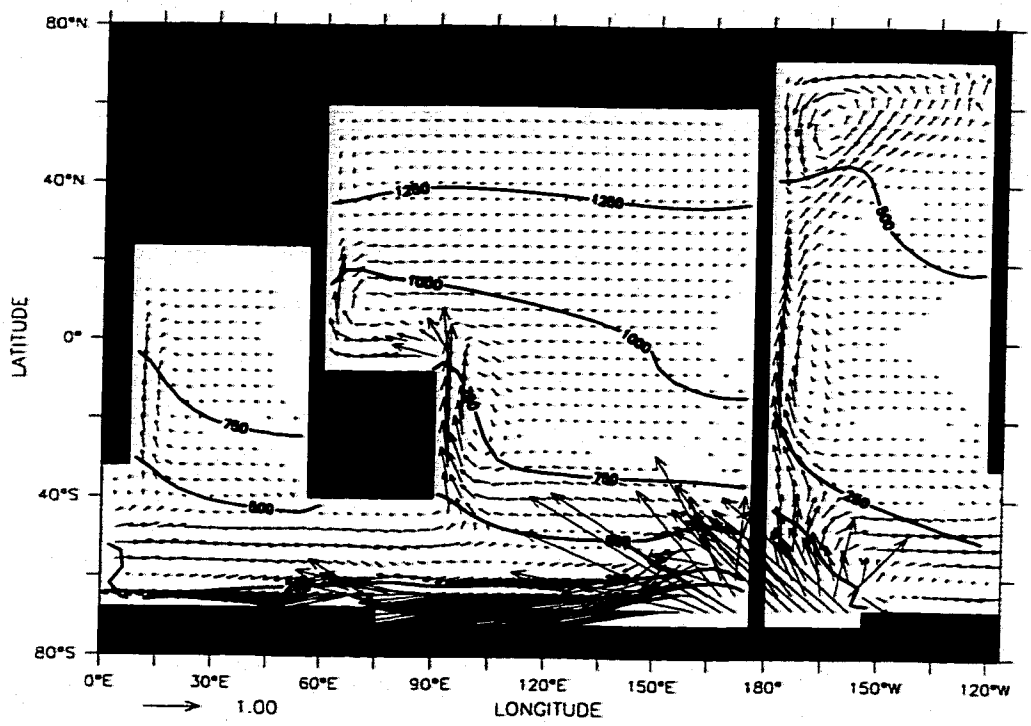

FIGURE 3 : Idealized ages and velocity vectors averaged over the bottom 1320 meters of the water column (levels 18 - 20); contours are 100, 250, 500, 750, 1000, and 1250 years. Note vector lengths, units are in cm/s.

The modeled ages and velocity vectors for the bottom 1320 meters of the ocean [Figure 3] show the paths by which bottom water travels northward into the individual basins. The youngest water is adjacent to Antarctica and is less than 100 years old. The outflow regions from the downwelling in the Weddell and Ross Seas are obvious. The dominant feature in each of the northern basins is a western boundary current, and the youngest water in each ocean is located near 30°S

along the western boundary. Bottom water in the Atlantic basin is younger than the other regions due to both the strong flow of newly formed AABW directly from the Weddell Sea and the "insulating effect" of young NADW directly above it in the water column. This is consistent with the results of Mantyla and Reid (1983) who found that 'true' AABW is only found in the Atlantic, whereas bottom water in the Indian and Pacific Oceans is actually the densest component of CDW, and therefore generally less recently ventilated.

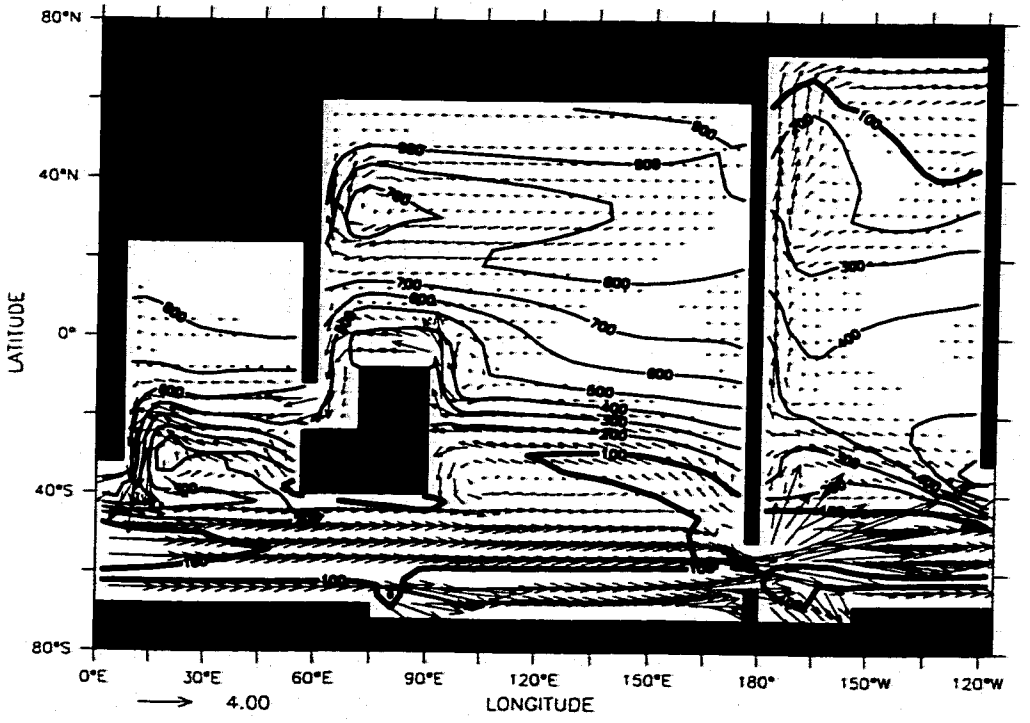

FIGURE 4 : Idealized ages and velocity vectors at 600 meters. The contour interval is 100 years with the 100 year contour darkened. Note vector lengths, units are cm/s.

Surface convection in the Southern Ocean [Figure 2b] occurs in two main regions: adjacent to the Antarctic coast, as discussed above; and in a swath extending from the southern tip of South America to the southern Australian coast

to the southern African coast. Convection in the sub-polar Southern Ocean has a maximum depth of 1000 meters at the South American coast, the main formation region for 'AAIW' in the model, and a lesser maximum at the southwest corner of Australia. Most of the area between 60°S and 50°S is stably stratified; the surface forcing can not overcome the wind-driven upwelling of upper CDW in this region. Figure 4 shows the ages and velocity vectors at 600 meters. The age minima in the vicinity of South America and Australia correspond to the maxima in convection. In the South Atlantic, wind-driven upwelling between 60°S and 40°S brings recently ventilated lower water to this level.

The age structures and flow patterns near South America and Australia are quite similar. These sites are in the path of the ACC where convergence along the coast leads to the downwelling of surface water into the water column. The age minima at the land masses spread toward the west-northwest, as does the outflow from the convecting regions. This figure is reminiscent of those presented in Hirst and Godfrey (1993, their figures 8b,9b and 10a); whenever the model ACC is influenced by a meridional wall, the flow develops a characteristic undercurrent structure (between 600 and 1000 meters in depth) which they liken to the observed Leeuwin Undercurrent (in the southeastern Indian Ocean).

3.2 Atlantic Sector

In the northeast Atlantic Ocean, 15.8 Sv are overturned down to 3000 meters, again driven by convection [Figure 2b], and 8.7 Sv of newly overturned

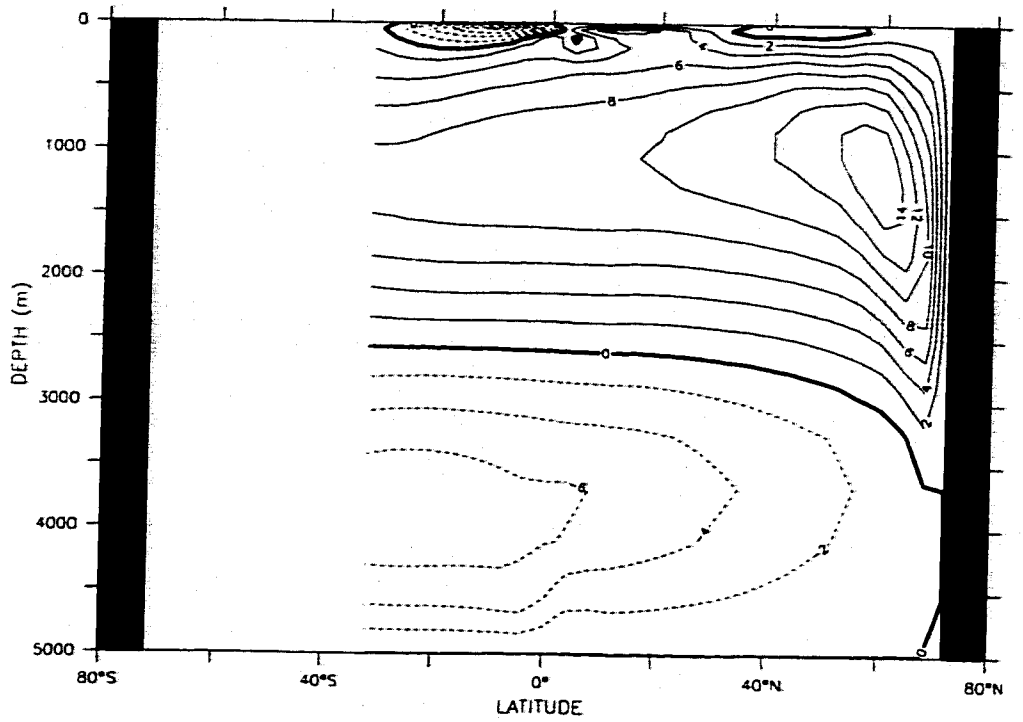

FIGURE 5 : Meridional overturning streamfunction for the Atlantic Ocean only, contour interval is 2 Sv. Solid (dashed) contours denote clockwise (counter-clockwise) circulation. (The streamfunction is undefined south of 32°S.)

water eventually cross 30°S, leaving the basin to join the ACC [Figure 5]. These values are similar to other modeling results [Manabe and Stouffer (1988), England (1993), Hirst and Godfrey (1993), Cai and Greatbatch (1995)]. More of the model's NADW upwells in the extratropical Atlantic than is reported in S95, his analysis indicates that all 14 Sv of the water downwelled in the North Atlantic flows southward out of the basin. This is a common shortcoming in OGCM experiments that employ Cartesian mixing: recent work by Böning, et al. (1995) and Weaver and Eby (1997) has shown that the artificial upwelling, due to the Veronis effect (anomalous upwelling on the coastal side of strong western boundary cur-

rents, Veronis (1975)), can be eliminated by the use of the Gent and McWilliams (1990) mixing parameterization. The effect of this parameterization on these results will be the subject of future work.

Below the North Atlantic cell, 7.2 Sv of southern bottom water (AABW) flow in across 30°S and 4.4 Sv eventually cross 30°N (see also Figure 3). The first value is consistent with the hydrographic analysis by Speer and Zenk (1993) who found a 6.7 Sv northward flow of bottom water at 30°S, and the second with the "best estimate" of the volume of bottom water converted into NADW, derived from water mass analyses, cited by Broecker (1991) and S95 as 4 Sv. The total outflow from the Atlantic at 30°S between 1300 and 3700 meters is 15.9 Sv (8.7 Sv in the upper cell and 7.2 Sv in the lower cell), but the deep western boundary current there measures 16.6 Sv. This value is close to the S95 estimate of 18 Sv of net deep water outflow across 30°S.

The idealized ages and velocity vectors at 2687 meters are shown in Figure 6. The water at the northern wall is under 100 years old and the strong western boundary current that carries newly formed NADW southward is apparent. Considering the idealized topography of the model, the age simulation in the Atlantic basin is quite good. The newly formed NADW matches the radiocarbon derived age (Δ°C) from GEOSECS [Stuiver and Ostlund (1980); Ostlund and Stuiver (1980); Stuiver and Ostlund (1983); a map of the radiocarbon ages at 3000 meters, compiled from the GEOSECS surveys, was presented in Andrée, et

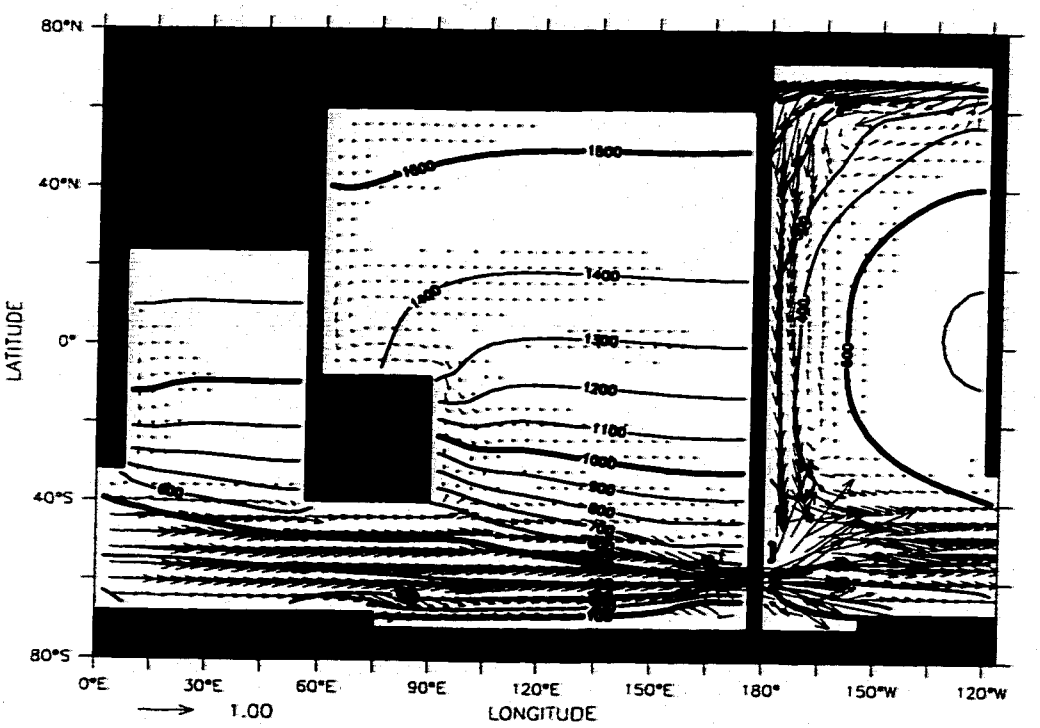

FIGURE 6 : Idealized ages and velocity vectors at 2687 meters. The contour interval is 100 years with the 100, 500, 1000, and 1500 year contours darkened. Note vector lengths, units are cm/s.

al. (1986)]. The water is about 400 years old as it enters the ACC, slightly younger than the calculated radiocarbon age (over 500 years), but similar to the average ages throughout the model's circumpolar region. The deep outflow from the Atlantic is replaced by an upper-level inflow from two different sources. The circulation vectors and ages in Figure 4 show both the inflow of older water from the Indian Ocean (the Agulhas Leakage) and the inflow of younger water from the northern edge of the ACC. There is also a moderately strong northward cross-equatorial flow at this level.

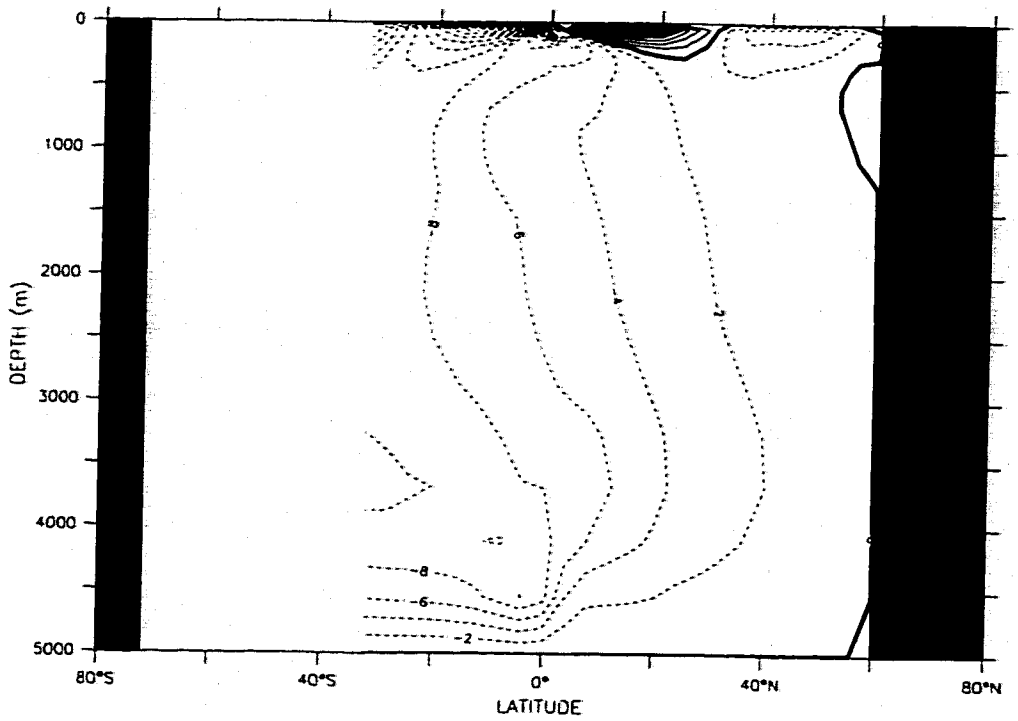

FIGURE 7 : Meridional overturning streamfunction for the Indian and Pacific Oceans combined, contour interval is 2 Sv. Solid (dashed) contours denote clockwise (counter-clockwise) circulation. (The streamfunction is undefined south of 32°S.)

3.3 Indo-Pacific Sector

The Pacific and Indian basins are primarily upwelling regions [Figure 7]. There is a moderate inflow of about 10 Sv along the bottom at 30°S [see also Figure 3] and a weak net outflow at 3000 meters with a total southward transport of less than one Sv, occurring mostly in the Indian basin [Figure 6]. The net effect of the Indian and Pacific basins north of 30°S is to convert 10 Sv of bottom water into 10 Sv of upper water. About half of the upwelling occurs north of the equator and generally the Pacific converts twice as much as the Indian basin. The model's Indo-Pacific circulation seems to be at odds with several observational studies

which conclude that there are roughly 20±5 Sv of lower water converted to upper water in the Indian Ocean and very little in the Pacific Ocean [Warren (1994), S95, Macdonald and Wunsch (1996)]. Warren (1994) proposed that the differences in meridional overturning between the Indian and Pacific Oceans were due to a larger local heat flux over the Indian Ocean surface. This mechanism is consistent with these model results; the average heat flux at the surface in the tropical Indian is only about half that of the Pacific, despite the warmer temperatures to which the Indian surface is restored.

Several authors have also reported that the bottom water inflow into the Pacific Ocean flows out again at mid-depth without contacting the surface [Toggweiler and Samuels (1993), S95]. Toggweiler and Samuels (1993) concluded that the magnitude of the mid-depth outflow was directly related to the strength of the bottom water inflow, although their series of experiments did not include an Indonesian throughflow. This discrepancy probably results from the lack of intermediate water production in the North Pacific; the presence of a locally formed water mass of increased density will increase the local stratification and will prevent the upwelling from below. This effect will be discussed further in section 4.2.

The pattern of ventilation revealed in the age profiles [Figures 3, 4, and 6] are consistent with the observations and the model circulation. The oldest water in the model ocean is found along the northern Pacific boundary. The idealized ages are over 1500 years between 1680 and 2760 meters with a maximum of 1535

years in the northwestern corner at 2330 meters. Ages in the Indian Ocean are younger, but the maximum is still along the northern boundary (1149 years at 1998 meters in the northeastern corner). Comparing Figure 3 with Figure 6 shows that the ages are older at 2687 meters than below at all locations in the Indian and Pacific basins, a clear sign of bottom water upwelling. Note the bowl shaped feature in the North Pacific at 600 meters [Figure 4], where downwelling in the subtropical gyre allows lower age surface water to diffuse down to this level. Also worth noting is the link exhibited by the circulation vectors connecting the downwelling near the southern tip of South America to the Agulhas Leakage, via the Indonesian throughflow [Figure 4], providing a possible pathway for the return of water into the Atlantic need to balance the deep water export.

3.4 Thermohaline Composite for the Control Experiment

In order to examine further the model's THC and to locate those regions where water mass transformations are occurring, the movement of water in different density regimes was analyzed. The four regimes are as follows: surface water, with potential density (σ_0) less than 26.5 kg-m°; intermediate water, with σ_0 between 26.5 and 27.5; deep water, with σ_0 between 27.5 and 27.8; and bottom water, with σ_0 greater than 27.8. This analysis is similar to that performed by Rintoul (1991) and Cai and Greatbatch (1995), although those studies defined deep and bottom waters solely according to model depth. The defining isopycnals for

this study were chosen to delineate the model's water masses and in that regard, this study is closer to the observational analysis of S95.

Properly speaking, this is not truly an analysis of water mass conversions, but rather a geographical census of density regimes in order to determine those locations where changes are occurring. Volume transports in the layers at various locations are given in Table 2 (similar to Table 1 in S95) and a 4 diagram schematic of the volume flux for each water type in the latitude bands 80°S-30°S, 30°S-0°, 0°-30°N, and 30°N-80°N over each of the three ocean sectors is presented in Figure 8.

TABLE 2. Key Sectional Thermohaline Component Transports for the Control Expt. (Positive transport denotes eastward or northward flow. All transports in Sv.)

Location	Surface	Intermediate	Deep	Bottom
Drake Passage (E,W)	---	108.2	92.2	5.1
Atlantic Basin at 30°S (N,S)	2.9	5.0	-14.4	6.5
Atlantic Basin at 0° (N,S)	4.0	5.5	-15.7	6.2
Atlantic Basin at 30°N (N,S)	5.5	5.3	-15.2	4.4
South of Africa (model 0°E) (E,W)	-0.9	97.5	100.6	8.3
Agulhas Leakage, N of 42°S (E,W)	-8.5	-7.8	2.6	-0.4
Indian Basin at 30°S (N,S)	-17.2	-7.2	-0.9	3.1
South of Australia (model 60°E) (E,W)	11.1	113.3	102.6	0.7
Pacific Basin at 30°S (N,S)	8.5	6.4	0.6	6.7
Indonesian Throughflow (E,W)	-14.6	-7.6	---	---
Pacific Basin at 0° (N,S)	-4.1	-0.4	0.0	4.5
Globally-Averaged Temperature (°C)	14.1	6.6	2.4	0.7
Globally-Averaged Salinity (‰)	34.72	34.65	34.70	34.75
Percent of Total Ocean Volume	7.4%	20.8%	55.1%	16.7%

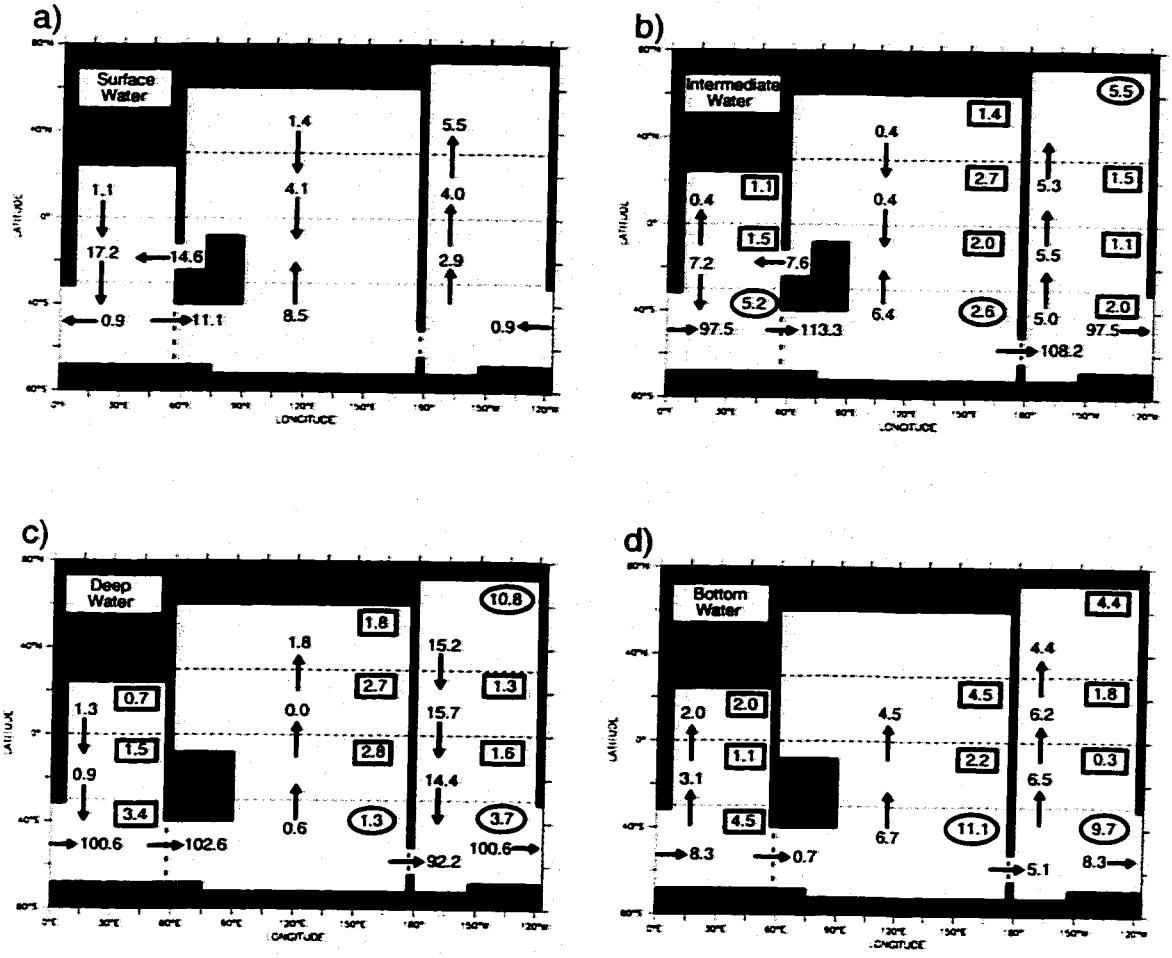

FIGURE 8 : This figure shows the balance for each water mass type in the Control Experiment for each of the three oceans, for the latitude bands 80°-30°S, 30°S-0°, 0°-30°N, and 30°-80°N. Arrows indicate direction of net flow and the net volume fluxes in Sv are noted. The figures outlined in circles (rectangles) indicate downwelling (upwelling) through the top of each box, *i.e.* exchange with the above water mass. The four figures show: a) Surface Water; b) Intermediate Water; c) Deep Water; and d) Bottom Water. (Note: The sill depth in the Drake Passage is 2500 meters; d) indicates that 5.1 Sv of bottom water flow through the Passage above this depth.)

The overall circulation in the Atlantic sector is remarkably similar to S95. Surface and intermediate water are converted into deep water in the North Atlantic where 10.8 Sv of newly downwelled water join 4.4 Sv of upwelled bottom water to form the core of the NADW mass [Figure 8c,d]. The model's upper circulation

(defined as surface and intermediate water together) is about 3-4 Sv weaker than observed, which leads to the deficit between the observed 18 Sv outflow of NADW across 30°S in S95 and the model's 14.4 Sv. This is less than the mass transport of 15.9 Sv cited in Section 3.2 because the least dense component of the southward deep western boundary current has a σ_0 less than 27.5 kg-m^o and is classified as intermediate water. The ~7 Sv flow of bottom water into the South Atlantic noted in section 3.2 is also found in the density regime analysis.

There is a large spread in the temperatures and salinities of water in the deep water regime. The average temperature and salinity for deep water in the Atlantic basin (north of 30°S) below 1000 meters are 3.3°C and 34.80‰, respectively, whereas deep water in the Southern Ocean (south of 40°S) has values of 2.2°C and 34.71‰. These differences agree with the observations that NADW is warmer and saltier, while the CDW shows more influence from the colder and fresher AABW. This analysis method can not distinguish between different source regions, so it is not possible to determine the relative fraction of NADW and CDW moving across a given section. It does seem that these two water masses are somewhat separable in the South Atlantic and virtually uniform in the South Pacific, agreeing with the observation by Broecker (1991) who noted that NADW loses its unique character after only half a circuit around the Antarctic continent.

It is important to note that the only two regions in which bottom water is formed are the Atlantic and Pacific sectors of the Southern Ocean, the regions

containing the two Antarctic Seas [Figure 8d]. The model continually forms 20.8 Sv of bottom water (σ_0 greater than 27.8), which upwells everywhere else as it absorbs heat diffusively from above and mixes with the overlying water masses. S95 (his Plate 9) indicates that 9 Sv of deep water are converted into bottom water in the Weddell Sea, similar to the 9.7 Sv converted in the model. Bottom water formation in the Pacific sector of the Southern Ocean is much weaker in the model with only 11.1 Sv of net deep water conversion, whereas the S95 analysis implies a net conversion of at least 30 Sv. The zonally integrated flow across 60°S in the lowest 1300 meters is 7.9 Sv as indicated in Section 3.1 and all of this flow is tagged as bottom water. There is, however, southward flow of bottom water higher in the column so that the net flow of bottom water across 60°S is only 5.8 Sv. The total bottom water transport at thais latitude can be decomposed into the three geographical regimes previously discussed as follows: 15.0 Sv moving northward in the Atlantic sector; 13.3 Sv moving northward in the far-eastern Pacific; and, 22.5 Sv flowing southward in the Indian and west and central Pacific.

There has been much debate about the return route of upper waters needed to compensate for the deep water export from the Atlantic basin. The controversy rests on whether the return flow is primarily Indian Ocean water which has travelled westward around Africa through the Agulhas Leakage, known as the warm-water route, or whether the return flow is mostly Antarctic Intermediate Water from the Drake Passage, known as the cold-water route. Gordon, et al. (1992), in an

observational study, concluded that the return flow is primarily composed of AAIW, but a significant portion (50-65%) was modified during a transit through the southern Indian Ocean before returning to the South Atlantic via the Agulhas Leakage in the form of baroclinic eddies, which as stated before, are not resolved by this model. The modelling study of Cai and Greatbatch (1995) [CG95, hereafter] also indicated the importance of AAIW but determined that at most 35% of the compensating return flow of upper water had travelled through the Agulhas Leakage. The model in CG95 was also unable to resolve the small-scale eddies and relied on the integrated flow in various density classes.

This model is compatible with the results of both Gordon, et al. (1992) and CG95, with some minor discrepancies. In this study, the upper-level northward flow into the Atlantic, needed to compensate for the deep water export, is 63% intermediate water, somewhat higher than CG95 (54%) and much higher than S95 (29%); these differences result from the choice of the defining isopycnal surface which separates surface from intermediate water. Figure 15 shows that approximately 50% of the upper return flow travelled through the Agulhas Leakage; this will be discussed further in Section 4.4.

A significant difference between the model and the observational analysis is the generally weak flow of bottom waters into the Pacific basin, and the subsequent lack of deep water outflow, as discussed previously. Figure 8c indicates a net flux of 0.6 Sv of deep water moving northward across 30°S; this conceals a

recirculation of approximately 6 Sv, but is not at all similar to the 20 Sv of deep water outflow reported in S95. No water with σ_0 greater than 27.8 kg-m$^\circ$ crosses 10°N in the model Pacific, consistent with the Levitus climatology [Levitus (1982)] which also shows no water greater than this density in the bottom 1000 meters of the central or northern Pacific. Wijffels, et al. (1996) reported that 8 Sv of lower CDW with a potential temperature below 1.2°C crosses 10°N from the south, but no water in the model's deep Pacific is this cold. It should also be noted that the Pacific and Indian basins north of 30°S, as well as the tropical Atlantic (between 30°S and 30°N), are entirely upwelling regions.

Veronis (1975) showed that coarse resolution OGCM's suffer from anomalous upwelling on the coastal side of western boundary currents. As Böning, et al. (1995) point out, this anomalous upwelling is largely responsible for the deficit in both deep water outflow and northward heat transport. This model does indeed exhibit a weak Veronis effect, but its existence does not greatly affect the results presented in this section. Except in the North Atlantic, the surface western boundary currents in the wind-driven gyres are confined to the upper 1000 meters of the water column and so are contained entirely within the intermediate and surface water regimes above the 27.5 kg-m$^\circ$ isopycnal surface.The Veronis effect may alter the balance between intermediate water and surface water, but this distinction is not crucial to the results presented here. In the Atlantic basin, the northward flowing Gulf Stream does extend below this isopycnal, but the upwelling

across it, south of 30°N, is less than 0.8 Sv. North of 30°N, the Veronis effect reduces the net creation of deep water; at 60°N, 14.7 Sv of intermediate water flow northward and 16.4 Sv of deep water flow southward, implying a loss of 1.2 Sv of deep water due to this effect between 60°N and 30°N.

Drijfhout, et al. (1996) employed a particle tracking method to determine where water downwelled in the North Atlantic was last below 1500 meters. Their results indicate that 27% of the water had upwelled in the Atlantic Ocean, 14% in the Indian Ocean, 43% in the Pacific Ocean and 16% in the Southern Ocean. Their model circulation, however, did not include an Agulhas Leakage, and their Indonesian Throughflow was only about 2 Sv, which will effect the results of the back-calculated particle trajectories. Although it is not possible to differentiate between NADW and CDW in this experiment, the net gain of 15.8 Sv of deep water (conversion from the intermediate regime) in the model is balanced by a positive buoyancy forcing induced loss of 18% in the Atlantic, 14% in the Indian, 46% in the Pacific, and 22% in the Southern Ocean [Figure 8c].

Unlike the analysis of the overturning circulations alone, the density regime analysis reveals that most of the positive buoyancy forced water mass conversion (from denser to lighter, typically equated with upwelling) occurs in the equatorial band between 30°S and 30°N. This region accounts for over 57% of the upwelling of bottom water, 66% of the upwelling of deep water, and 74% of the upwelling of intermediate water. The strong vertical transports in the Antarctic sector are

mostly associated with recirculations and not water mass conversions. It is possible that the limited zonal extent of these simulations (240°) leads to an underestimation of the wind-driven upwelling of deep water in the ACC. Further studies are needed, but it seems likely that convection and the surface forcing in this region would keep the balance between intermediate and deep water roughly constant.

4.0 No-NADW Experiment

In order to evaluate the effects of NADW on the global ocean circulation, an experiment without this water mass was conducted and the results of the two experiments are compared. Sedimentary evidence from the last glacial period seems to indicate that NADW production was severely reduced, if not eliminated entirely, at the last glacial maximum [Boyle and Keigwin (1987)]. Several studies have described and compared global circulations both with and without NADW [Manabe and Stouffer (1988), Stocker, et al. (1992), Power and Kleeman (1993), CG95]. All employed global models but generally limited the scope of their analyses. This study's focus is on the global THC, but the changes reported in those previous works will be compared to this one.

Rather than try to duplicate the glacial ocean by forcing the model with the poorly known glacial climatology, this study limits its scope to studying the effects of reduced NADW formation. This is accomplished by imposing a negative 1‰ salinity anomaly into the restoring salinity values of the Control Experiment over

the Atlantic basin, north of 40°N. The salinity forcing outside of this region remains unchanged, as do temperature and wind stress values everywhere. The model is then run until a new steady state is reached (about 6000 years). It should be noted that the final state of the ocean in this No-NADW Experiment did not depend on the initial conditions; the anomalous salinity forcing was applied to both an isothermal ocean at rest and to the final steady state of the Control Experiment —the results were identical.

Some of the effects of NADW production on the global circulation are visible by comparing Figure 2 and Figure 9. The most obvious change is that there is no longer any deep water formation in the northern hemisphere [Figure 9a]. Apart from the surface Ekman cells, the overturning circulation north of the equator is much weaker than in the southern hemisphere. Figure 2d shows that the elimination of NADW causes the model's globally averaged temperature in the upper 2300 meters to warm, by over 0.5°C at 500 meters, while the bottom 2700 meters cool slightly (by 0.25°C at 3500 meters). The surface salinity anomaly north of 60°N in the North Atlantic severely reduces the average (maximum) convective depth there from 1400 (4100) meters to 400 (1100) meters [compare Figure 2b and Figure 9b]. There is also an increase in the convection in the Southern Ocean when NADW is eliminated; the 500 meter contour expands between 40°S and 60°S, and the 1000 meter contour shifts further away from the Antarctic coast. Figure 2e shows that the removal of NADW causes the global salinity to decrease

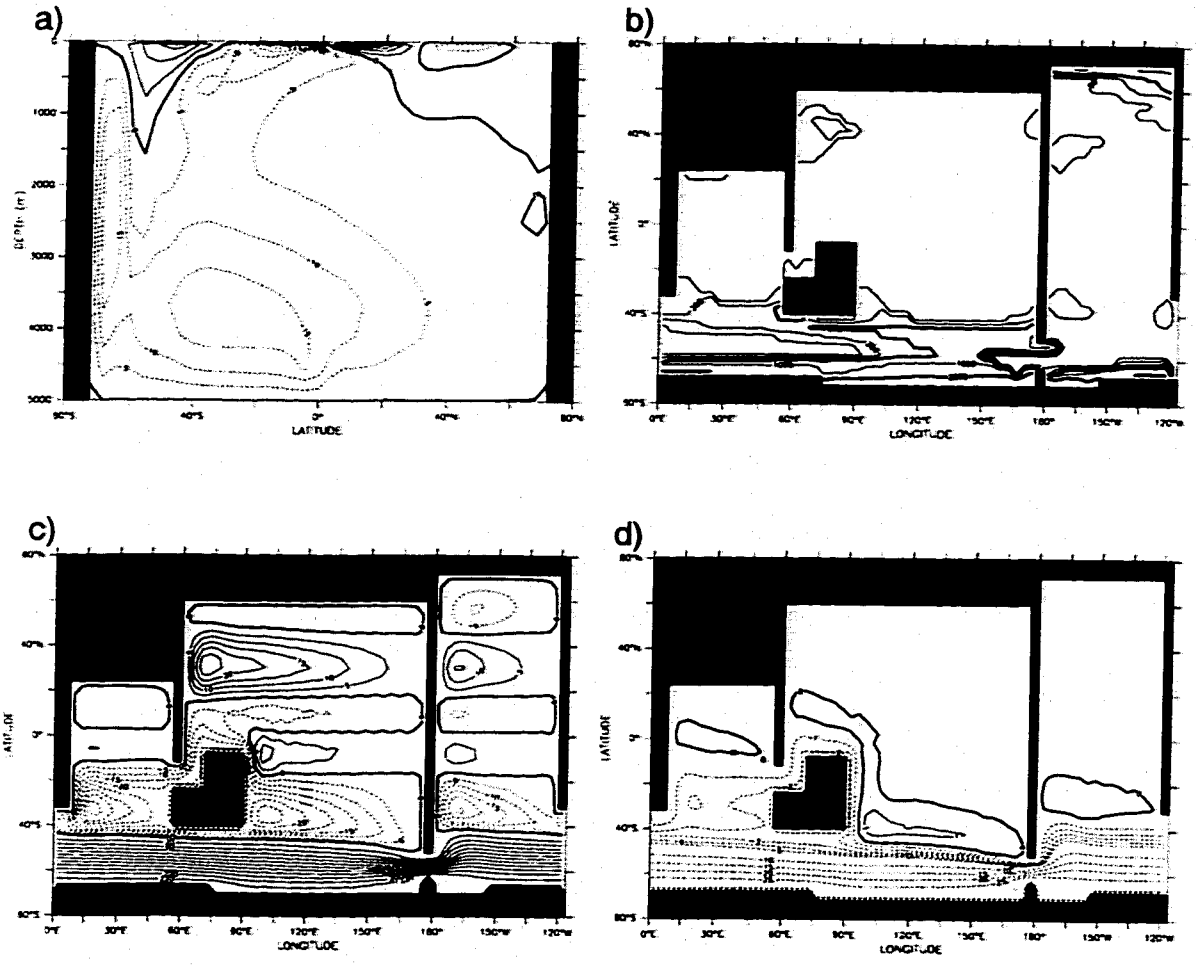

FIGURE 9 : No-NADW Experiment: a) Meridional overturning streamfunction, contour interval is 5 Sv; b) Depth of convection from the surface, contours at 50, 250, 500, 1000, 2500, and 5000 meters, with the 500 and 2500 meter contours darkened; c) Barotropic streamfunction, contour interval is 5 Sv, except in the ACC where it is 20 Sv; d) Change in the barotropic streamfunction due to the production of NADW (Control Experiment - No-NADW Experiment), contour interval is 5 Sv in the ACC and 1 Sv elsewhere. Note that in a), c) and d) solid (dashed) contours denote clockwise (counter-clockwise) circulation.

at all levels, including a change of over 0.1‰ between 700 and 3800 meters. The causes and effects of these changes will be discussed in the next section.

The ACC transport has increased from 205.5 to 235.1 Sv and the Indonesian Throughflow and the barotropic Agulhas Leakage are both about 2 Sv

weaker [Figure 9c,d]. The structure of the Agulhas Leakage is modified by the presence of NADW; without this water mass, the westward transport in the upper 1000 meters is reduced from 15.1 Sv to 9.0 Sv. The westward flow below this depth, however, increases from 1.2 Sv to 3.7 Sv and extends down to 3000 meters as opposed to the 1550 meter level when NADW production is active. The decrease in transport through the Indonesian Passage and the decreased upper level transport around the tip of Africa are both consistent with the 'warm-water route' of the conveyor-type circulation proposed by Broecker and Gordon. Figure 9d shows that the horizontal streamfunctions for both experiments are identical north of the equator. Since there is no bottom topography in the model's northern hemisphere, the JEBAR term is identically zero and the barotropic streamfunction (or more accurately, the vertically integrated vorticity equation) is solely a function of the wind forcing [Holland (1973), Mertz and Wright (1992)], which is the same in both model runs.

4.1 Antarctic Sector

The net Antarctic downwelling in the southernmost grid box has been reduced by one third, from over 27 Sv [Figure 2a] to just over 18 Sv [Figure 9a]. Nearly all of this reduction in the net downwelling is actually due to an increased upwelling in the southwestern and central Ross Sea. The downwelling regions in the Weddell Sea and the southeastern Ross Sea are virtually unchanged. The change in the Antarctic overturning circulation is due to a complex series of inter-

actions involving the ACC. The absence of the comparatively saline NADW outflow reduces the salinity below 1000 meters at the northern edge of the ACC throughout the southern subpolar ocean. Reduced salinity lowers the density of the water at and above the depth of the Drake Passage sill on the northern edge, while the density at the southern edge of the ACC is closely bound to the surface restoring profile and has not changed. These effects combine to increase the density gradient across the ACC, which increases the baroclinity of the flow, and acts through the JEBAR term in the vorticity equation [Mertz and Wright (1992)] to increase the strength of the barotropic transport through Drake Passage by 14% in the No-NADW Experiment. This change is similar to the one seen in CG95; their ACC increases from 202.9 Sv to 233.3 Sv when NADW formation is cut off.

Nearly all of the change in the Antarctic overturning seen by comparing Figure 2a and Figure 9a occurs in the Indo-Pacific sector. The enhanced ACC in the No-NADW Experiment leads to greater convergence at the northwestern tip of the Antarctic Peninsula. Increased horizontal convergence in a weakly stratified region leads to vertical motion in the model, which in this case is increased downwelling. As in the Control Experiment, most of the vertical motion between 68°S and 60°S in the No-NADW Experiment is still upward, but the sinking at the tip of the peninsula increases by over 8 Sv, while the rest of the region continues to upwell at the same rate in both experiments. Some of the increased downward flow feeds an increased export of AABW into the southeastern Pacific and the rest

of this extra downwelling eventually upwells in the southwestern Ross Sea. So despite the appearance of a weakened South Antarctic overturning in the No-NADW Experiment, the vertical transports, both upward and downward, are intensified. The net zonal overturnings south of 60°S in the No-NADW Experiment for the Indo-Pacific and Atlantic sectors, which are hidden by the zonal integral, are 66 Sv and 36 Sv (again, measured at 2500 meters), respectively, compared to 55 Sv and 27 Sv in the Control Experiment.

The average heat flux (out of the ocean) south of 60°S increases very slightly (~0.6 Wm°) when NADW is removed, but the equivalent salt flux (the net evaporation minus precipitation, which can be thought of as ice export) into the ocean increases substantially from 0.06 m-yr° to 0.32 m-yr°, to balance the lack of southward salt transport by NADW. These differences are also explained by the increase in convection in the No-NADW Experiment; the restoring boundary condition has to work harder when more deep is 'exposed' to the surface.

Despite the reduction in the net downwelling at the southern wall in the absence of NADW production, the increase in total downwelling leads to an increase in the northward flow across 60°S in the bottom 1300 meters from 7.9 Sv in the Control Experiment to 10.4 Sv in the No-NADW Experiment. Comparing the three regimes discussed in section 3.1, the increased outflow across 60°S is confined to the region between 165°E and the American continent. The northward meridional flow at the bottom in the Atlantic sector decreases by a small amount

(~ 0.8 Sv), and the southward meridional flow into the southwestern and central Ross Sea increases slightly.

Circumpolar Deep Water is the end product of strong mixing in the ACC. In the Control Experiment, it is composed of the three main subsurface water masses, AABW, NADW and AAIW. When NADW is missing, the new CDW is generally much fresher and a bit colder; this causes a decrease in its density at all levels and reduces the stratification in the ACC above 1500 meters. The increased convection along with the increased convergence at the northern edge of the ACC, causes the production (and volume) of AAIW to increase substantially. This inverse correlation between the production of AAIW and NADW seems consistent with the study of Michel, et al. (1995), although their main conclusion, that Subantarctic convection formed the global deep water mass during the glacial period, is not seen in the model.

In summary, NADW production has four main effects on the Antarctic region: 1) the ACC transport is weaker when NADW is present; 2) the downwelling and upwelling in the high-latitude Southern Ocean are both decreased in magnitude when NADW is present; 3) the net outflow of bottom water across 60°S is weakened when NADW is present, although the outflow in the Atlantic sector increases slightly; and 4) the formation of AAIW is also reduced when NADW is present.

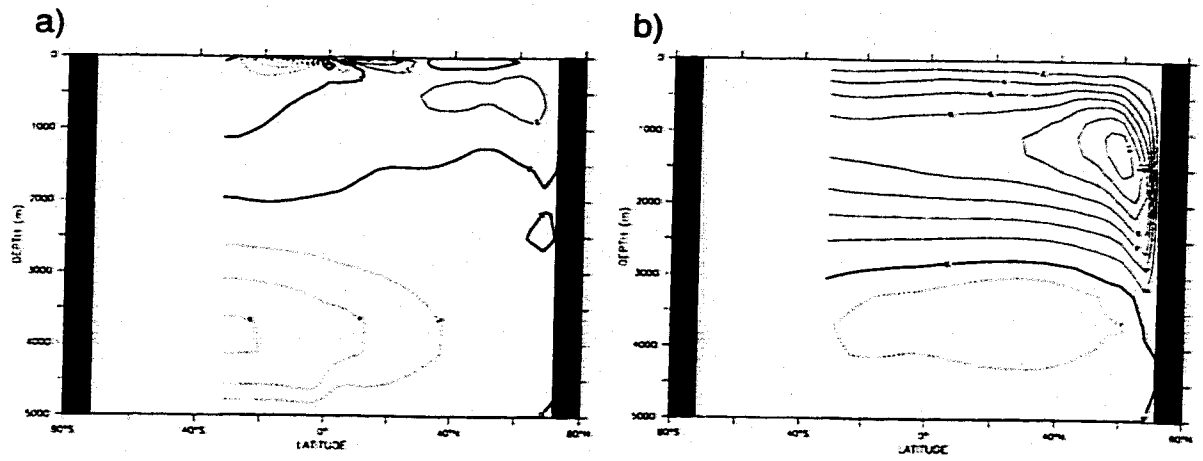

FIGURE 10 : a) No-NADW Experiment, meridional overturning streamfunction for the Atlantic Ocean only; b) Change in meridional overturning due to NADW production (Nominal Experiment - No-NADW Experiment). Contour interval in both figures is 2 Sv, with the -1 contour included in b). Solid (dashed) contours denote clockwise (counter-clockwise) circulation. (The streamfunction is undefined south of 32°S.)

4.2 Atlantic Sector

The changes to the Atlantic overturning are obvious and fairly easy to explain [compare Figure 5 and Figure 10a]. The northern overturning is restricted to the upper 1500 meters and is reduced from 15.8 Sv to just over 3 Sv. In the No-NADW Experiment, less than 1 Sv of surface water from the North Atlantic flows southward across 30°S between 1500 and 2000 meters. The bottom cell transport is reduced by 1 Sv, but bottom water now upwells to 2000 meters before exiting the basin to the south. The dense NADW mass, owing primarily to its salt content, suppresses the upwelling of bottom water by 1000 meters between the two model runs.

Figure 10b shows that an extra 8.6 Sv of water from south of 30°S are drawn into the basin, flow northward across the equator, and return southward at depth

after passing through the North Atlantic sinking region. This affects the stratification in the Atlantic basin, as expected. The influx of upper water needed to supply the downwelling in the north comes from the Southern Ocean as AAIW and Agulhas Leakage water. This water is generally colder than the tropical water present at upper levels in the No-NADW Experiment, leading to a cooling of upper ocean. At depth, NADW replaces AABW leaving the deep ocean warmer in the Control Experiment. These changes increase the stratification in the upper ocean, above 1500 meters, and weaken it below there. The northward heat transport in the Atlantic increases from 0.16 PW in the No-NADW Experiment to 0.52 PW in the Control Experiment. This increase of 0.36 PW in the heat transport is seen at all latitudes between 30°S and 40°N, implying that thermal energy from the Southern Ocean is released to the atmosphere over the North Atlantic, equivalent to an additional 26 Wm° of heating north of 40°N. Notice that NADW formation also causes an increase in the flow of bottom water through the basin, as was indicated in the previous section.

Figure 10a gives a clue as to why the model's Pacific Ocean does not produce a mid-depth outflow of bottom water as is seen in the observations. Even with the negative salinity anomaly imposed on the North Atlantic, the surface density is still large enough for the water to sink to intermediate depths whereas the model's Pacific surface water is too light. Yasuda (1997) concluded that North Pacific Intermediate Water (NPIW) is largely composed of cold, low-salinity water

from the Sea of Okhotsk mixed with some warmer, saltier water from the Western Subarctic Gyre. The lack of Okhotsk Sea Mode Water [Yasuda (1997)], and thus NPIW, in the model decreases the stratification in this region and allows bottom water to upwell without constraint to the surface, whereas even the artificial North Atlantic Intermediate Water in the No-NADW Experiment is enough to cap the upwelling of bottom water, thus causing it to flow southward out of the basin.

An interesting finding is that the salinity balance in the upper North Atlantic is between the northward advection of salt by the Gulf Stream and the convective mixing with deep water, consistent with the results of Manabe and Stouffer (1988). In both the Control and the No-NADW Experiments, the restoring boundary condition in the model removes salt from (rains on) the North Atlantic surface. In the No-NADW run, despite the reduced restoring salinity, the amount of salt removed is significantly less than in the Control run due to the large reduction in advective transport by the Gulf Stream. The model 'rains' more (equivalent to removing more salt) there when NADW is formed, implying that the high surface salinities in the model North Atlantic are due to the existence of the thermohaline overturning and not to the restoring salinity boundary condition. Manabe and Stouffer (1988) also determined that the difference between evaporation and the sum of precipitation and runoff was virtually identical in their coupled model, in both the NADW and No-NADW Experiments. It is notable, however, that their salinity flux adjustment, which removes the equivalent of 5 meters per year of surface water in the

North Atlantic near Iceland, is not enough to induce convection and deep water formation there, apparently due to the lack of poleward salinity advection in their Gulf Stream.

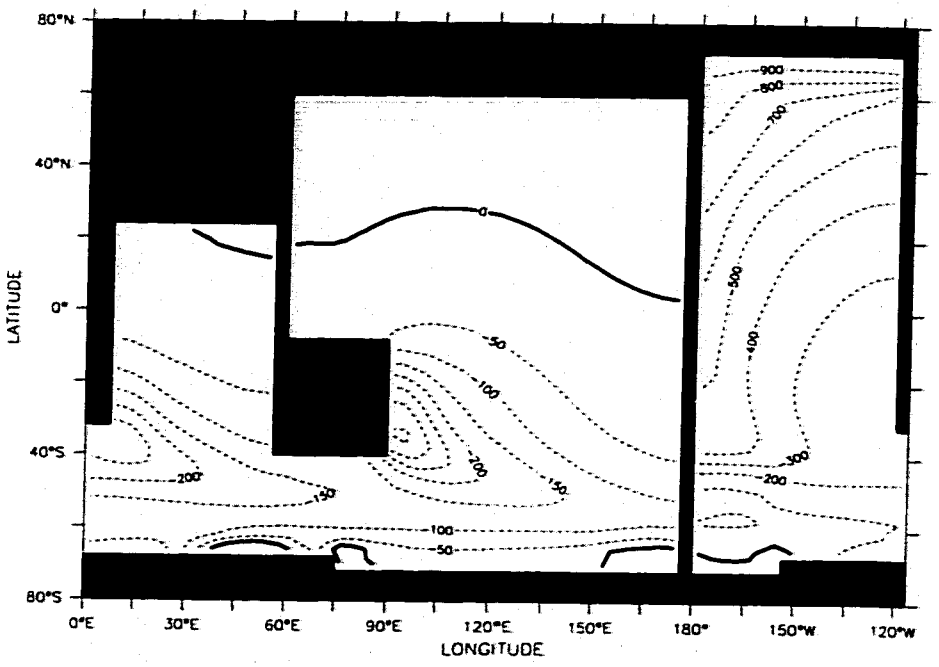

FIGURE 11 : The change in age at 2687 meters due to the production of NADW (Control Experiment - No-NADW Experiment). The contour interval is 100 years in the Atlantic sector and 50 years in the Indian and Pacific sectors.

It is informative to present the age differences caused by NADW formation. Figure 11 shows the differences due to the presence of NADW (the Control Experiment minus the No-NADW Experiment). At 2687 meters [the same level as Figure 6, immediately below the Drake Passage sill], the ventilating effects of NADW are most dramatic in the North Atlantic. In the No-NADW case, water at this depth is ventilated slowly from the south and achieves an age of almost 1000

years. The rejuvenating effect of NADW proceeds southward along the western boundary and then into the ACC. CDW at this level is between 100 and 200 years younger when NADW is included. The circulation carries the younger water into the Indian basin where it gradually spreads northward and eastward. The strong bullet of refreshed water along the southeastern coast of Australia is due to a reversal of the current from southward in the No-NADW Experiment to northward in the Control case, which replaces older deep Pacific water with younger CDW at that location. This reversal is an effect of the large change in the density of CDW. In the Control Experiment, CDW is much denser than the deep Pacific water at this level, but the two are nearly identical in the No-NADW Experiment.

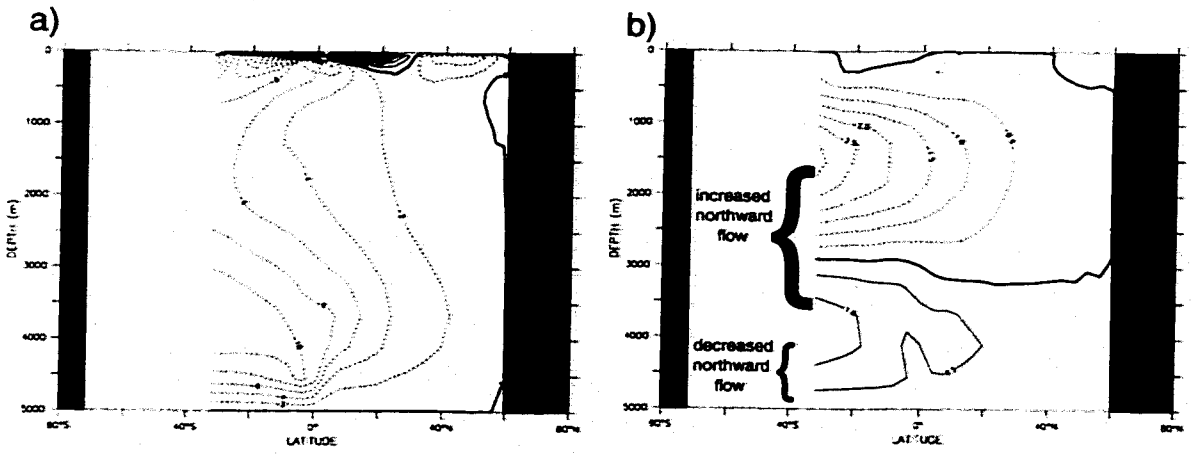

FIGURE 12 : a) No-NADW Experiment, meridional overturning streamfunction for the Indian and Pacific Oceans combined; b) Change in meridional overturning due to NADW production (Nominal Experiment - No-NADW Experiment). Contour interval in a) is 2 Sv and in b) is 0.5 Sv. Solid (dashed) contours denote clockwise (counter-clockwise) circulation. (The streamfunction is undefined south of 32°S.)

4.3 Indo-Pacific Sector

The Indo-Pacific overturning is similar in both experiments. Comparing Figure 7 and Figure 12a shows that the inflow along the bottom is weaker when NADW formation is active [Figure 12b] and less of the bottom flow eventually crosses the equator. It is important to note that the North Pacific (north of about 20°N) is slightly older when NADW production is active, and this is true along the bottom as well, where ages are 0-30 years older north of the equator [Figure 11, Figure 13b]. The ventilation time of the water in this location is determined primarily by the strength of the bottom water influx. The bottom water is of southern origin (AABW and/or CDW) in both experiments, so NADW production can only influence the bottom ages through a dynamical process. The small reduction in the flow of bottom water across the equator in the Pacific and Indian basins causes their deepest waters age slightly. The changes in ventilation times in the Pacific and Indian sectors, due to the formation of NADW, are between -350 and 150 years everywhere.

There is an increased inflow between 1500 and 3500 meters due to NADW formation [Figure 12b], equally divided between the two basins, which increases the total upper-level upwelling by about 2 Sv. Not coincidentally, the Indonesian Throughflow is also 2 Sv stronger in the Control Experiment than in the No-NADW Experiment [Figure 9d]. The link between the strength of the Indonesian Throughflow and the production of NADW has been explored by several studies [Gordon,

et al. (1992), Hirst and Godfrey (1993), Macdonald and Wunsch (1996)] with inconclusive results.

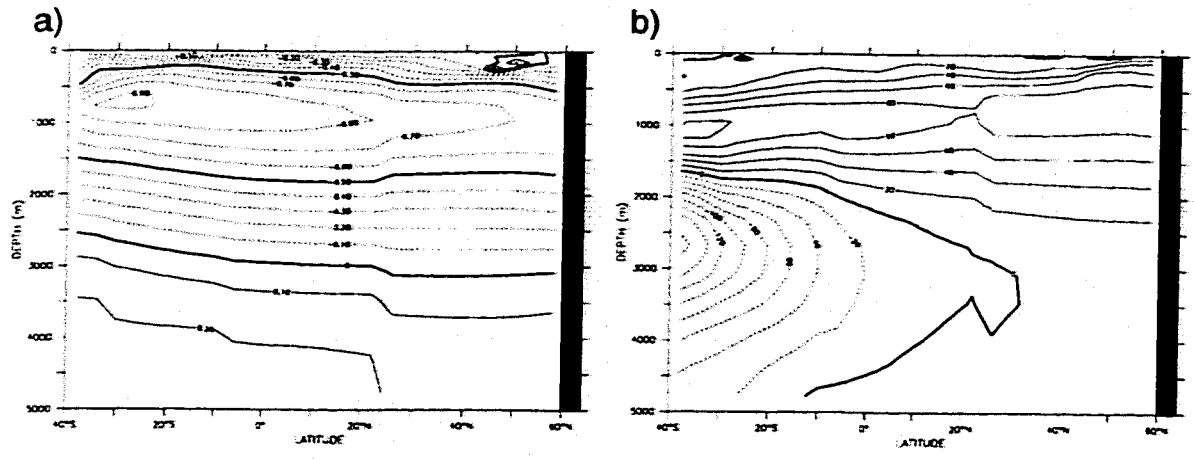

FIGURE 13 : Zonally averaged changes in the Indian and Pacific Oceans due to NADW production (Control Experiment - No-NADW Experiment). a) Change in temperature, contour interval is 0.1°C with the -0.5°C contour darkened. b) Change in idealized age, contour interval is 20 years.

An interesting result is that both the Pacific and Indian Oceans are warmer below 2500 meters and colder above when NADW production is active [Figure 13a], with a decrease of over 0.5°C between 300 and 1500 meters. The warming at depth is due to the incorporation of relatively warm NADW into the CDW, which is advected into the northern basins. The changes to the ACC noted in section 4.1, however, result in less formation of intermediate water, which leaves the upper circumpolar region slightly colder. This cooling is generally not advected northward across 40°S because the main flows at this level are southward [Figure 12b]. The heat balance in the tropical and extratropical Indian and Pacific basins is between the downward diffusion of solar radiation absorbed at

the surface and the upwelling of cold water from below the thermocline; upwelling increases in the model when NADW is present, so the upper level temperature goes down. This subsurface cooling is expressed at the surface, but only weakly due to the surface forcing. The thermal boundary condition restores the model's tropical SST to the same profile in both experiments, but the downward heat flux through the surface is slightly larger in the Control Experiment. If a different thermal boundary condition were implemented, such as the Schopf zero-heat capacity atmosphere [Schopf (1983)], the tropical SST's in the No-NADW Experiment would be noticeably warmer than in the Control Experiment.

This conflicts with the evidence indicating that tropical SST's in the last glacial period were about 5°C colder [Rind and Peteet (1985), Thompson, et al. (1995), Stute, et al. (1995)], despite the absence of NADW formation. This coarse resolution model can not begin to resolve the tropical surface heat budget, but the model results presented here imply that the SST differences observed during the glacial period were the result of atmospheric effects, and not the ocean circulation. Manabe and Stouffer (1988) found that NADW formation caused warming (cooling) over the entire northern (southern) hemisphere, both in the model SST and in the model surface air temperature. It seems clear that the coupled model allows SST anomalies to be redistributed via the atmosphere throughout the model domain, which is not possible here.

It is notable that the thermal structure and the age structure of the upper Pacific and Indian Oceans are determined by the same factors. While NADW production causes the deep Indian and Pacific Oceans to become younger below about 2000 meters due to the rejuvenated CDW (with its NADW component) which flows in at depth [Figure 13b], the increased upwelling in the upper ocean (above 2500 meters) causes the ages there to increase. This change is in agreement with the δ°C evidence reported in Duplessy and Labeyrie (1994) which indicated that Pacific intermediate waters between 1000 and 2600 meters were more ventilated (younger) during the last glaciation. The largest cooling of the upper equatorial Indian and Pacific Oceans occurs over the same depths as the increase in ages.

TABLE 3. Key Sectional Thermohaline Component Transports for the No-NADW Expt. (Positive transport denotes eastward or northward flow. All transports in Sv.)

Location	Surface	Intermediate	Deep	Bottom
Drake Passage (E,W)	---	168.2	66.9	---
Atlantic Basin at 30°S (N,S)	-2.0	1.6	-2.7	3.1
Atlantic Basin at 0° (N,S)	0.1	-0.5	0.4	---
Atlantic Basin at 30°N (N,S)	1.8	-2.1	0.3	---
South of Africa (model 0°E) (E,W)	4.3	147.6	86.3	-3.1
Agulhas Leakage, N of 42°S (E,W)	-4.0	-8.2	0.3	---
Indian Basin at 30°S (N,S)	-14.9	-6.2	0.9	---
South of Australia (model 60°E) (E,W)	13.2	152.3	102.1	-12.3
Pacific Basin at 30°S (N,S)	9.0	5.2	6.0	---
Indonesian Throughflow (E,W)	-12.6	-7.6	---	---
Pacific Basin at 0° (N,S)	-3.7	-0.2	3.9	---
Globally-Averaged Temperature (°C)	14.4	5.7	1.6	0.1
Globally-Averaged Salinity (‰)	34.72	34.51	34.58	34.71
Percent of Total Ocean Volume	8.4%	32.5%	56.5%	2.6%

4.4 Thermohaline Composite for the No-NADW Experiment

The analysis performed on the Control Experiment in Section 3.4 was also carried out for the No-NADW Experiment. Although the globally averaged salinity drops from 34.72‰ in the Control run to 34.60‰ in the No-NADW run, and the average σ_0 decreases from 27.46 to 27.35 kg-m^{-3}, the same four density ranges were used for comparison. Table 3 gives volume transports for each water mass across the various sections, and Figure 14 is the corresponding schematic and should be compared to Figure 8.

An obvious change is the sharp reduction in bottom water formation from 20.8 Sv to 12.3 Sv and the total absence of water with σ_0 greater than 27.8 kg-m° north of the equator [Figure 14d]. Although there is no net production in the Atlantic sector of the Southern Ocean, convection in the Weddell Sea (south of 68°S) does convert just under 10 Sv of deep to bottom water but all of it upwells south of 30°S. All the water located on the bottom is still southern in origin [Figure 14c], but most is now less than 27.8 kg-m°. Due to the non-linearity in the equation of state for sea water, the changes in salinity have a much greater effect on the density at low temperatures than do changes in the temperature. Without the conduit created by convection in the North Atlantic, the salinity throughout the world ocean decreases and the low temperature of water along the bottom away from the coast of Antarctica is no longer sufficient for those waters to be classified as 'bottom water' based on the potential density.

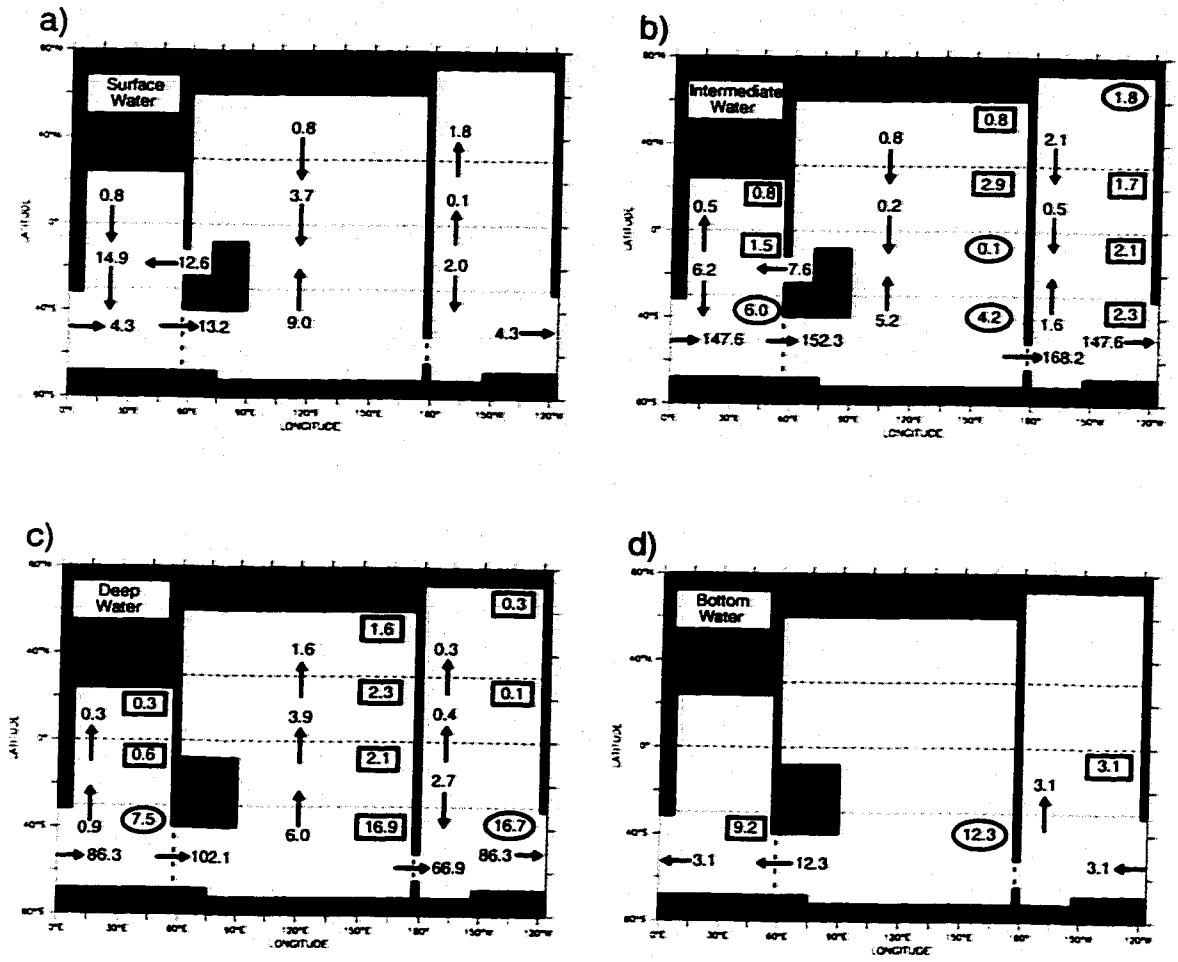

FIGURE 14 : This figure shows the balance for each water mass type in the No-NADW Experiment for each of the three oceans, for the latitude bands 80°-30°S, 30°S-0°, 0°-30°N, and 30°-80°N. Arrows indicate direction of net flow and the net volume fluxes in Sv are noted. The figures outlined in circles (rectangles) indicate downwelling (upwelling) through the top of each box, *i.e.* exchange with the above water mass. The four figures show: a) Surface Water; b) Intermediate Water; c) Deep Water; and d) Bottom Water.

The biggest change is in the volume of intermediate water [compare Table 2 & Table 3]; the net conversion of surface to intermediate water, south of 30°S, is greater by about 2.1 Sv when NADW is absent. This is largely due to the increase in the ACC transport and the resulting horizontal convergence at the western coasts of Australia and South America. The depth of convection in the Southern

Ocean between 60°S and 40°S is about 20% deeper, and the stratification there and throughout the rest of the world ocean is notably weaker above 1400 meters without the influence of NADW. The 27.5 kg-m^{-3} isopycnal surface is deeper everywhere when NADW is absent, ranging from about 500 meters deeper in the Pacific and Indian Oceans to 900 meters or more in the Atlantic. Most of the change in intermediate water is due to the replacement of diffusively warmed, high-salinity upper NADW by low-salinity AAIW. The global salinity drops by about 0.1‰ and the largest decrease occurs around the depth of the 27.5 kg-m^{-3} isopycnal surface in the Control run, causing upper deep water to be reclassified as lower intermediate water. There is still intermediate water formation in the North Atlantic [Figure 14b], but it's effects south of the equator are small or non-existent.

Most of the changes in net transport between Figure 14c,d and Figure 8c,d in the Indian and Pacific Oceans are due to an increase in the broad southward flows (the deep outflow discussed earlier), while the total northward flows in the deep western boundary currents remain fairly constant. The increased deep outflow is also revealed in the reduced upper level upwelling.

The change in the strength of the Agulhas Leakage between the two runs is used to estimate the percentage of upper water compensating for NADW outflow which has travelled through the Indian sector, as was done by CG95. Their Agulhas Leakage is 3.7 Sv weaker when NADW is absent and nearly all of the reduction occurs in the intermediate water. The westward flow of intermediate water in

the present study actually increases by 0.4 Sv when NADW is removed but the surface flow is reduced by 4.5 Sv for a net reduction of 4.1 Sv. Some of these differences are due to the criteria used to differentiate between intermediate and surface water; CG95 levels have a lower depth of 1250 meters for intermediate water and when their criteria are applied to the current study, much of the westward flowing intermediate water is reclassified as deep water. The ratio of the change in the Agulhas Leakage to the upper (surface and intermediate) return flow into the Atlantic is 36% in CG95, and 52% here.

5.0 Summary and Conclusions

A simplified cartoon depicting the major aspects of the model's thermohaline circulation is presented in Figure 15. NADW formation causes several distinct changes in the world ocean's structure and circulation patterns, but the production of Antarctic Bottom Water in the model is not dependent on NADW production. Vertical motion in the high-latitude Southern Ocean is divided into three main regions: downwelling across the Atlantic sector and in a narrow band in the Pacific immediately west of the Antarctic Peninsula, and broad upwelling in the southern Indian and southwestern Pacific sectors. The flow of bottom water across 60°S is divided into the same three regimes; newly downwelled water (AABW) flows northward across the Atlantic and in the far-eastern Pacific, while older (and warmer) circumpolar water flows southward to feed the broad upwelling in the southern Indo-Pacific sector. This feature is robust in both experiments, and is a

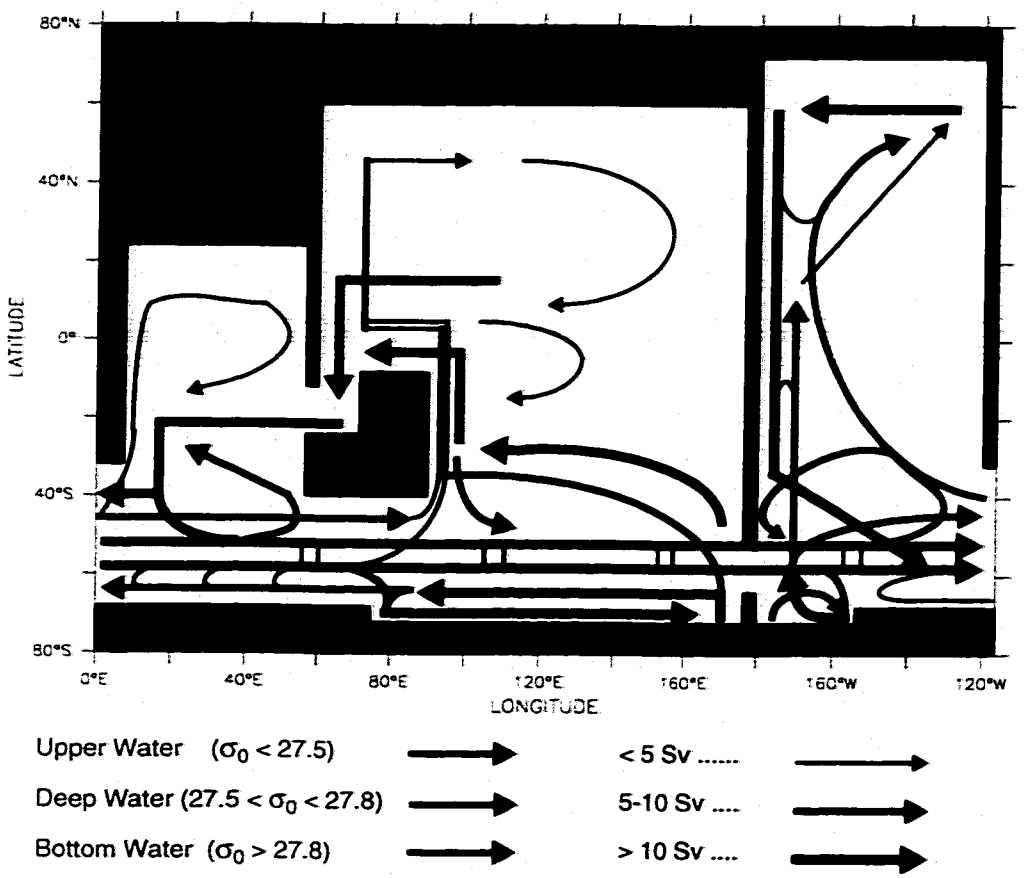

FIGURE 15 : Cartoon of the model's conveyor belt circulation for the Control Experiment. The colors describe flows in terms of density ranges and location in the water column; red arrows indicate the combined surface and intermediate flows, green arrows indicate deep flow, and blue arrows indicate bottom flow. Note that the flow depicted by the blue arrows adjacent to Antarctica indicate an eastward surface flow of roughly the same density as the flow depicted by the westward blue arrows next to them.

strong indication that NADW formation alone does not drive the model's global thermohaline overturning. The strength of AABW formation and the northward flow of bottom water across 60°S are affected, however, by the transport in the ACC and NADW formation influences the Southern Ocean through this intermediary.

In the No-NADW Experiment, all three northern basins behave quite similarly and the THC is fairly simple. Nearly all sub-surface water mass production occurs in the Southern Ocean. The densest water is formed near Antarctica, sinks to the bottom and flows northward into each basin, where it warms diffusively and upwells slowly. In the Atlantic Ocean, all of the bottom water exits southward, rejoining the ACC as upper deep water. In the Indian and Pacific Oceans, some bottom water is recirculated and rejoins the ACC, but most continues to warm, becoming intermediate and then surface water. Low-salinity intermediate water of southern origin also fills the upper levels of the three northern basins; all three have an equatorial salinity minimum located between 1000 and 2000 meters depth. The Pacific and Atlantic both have low-salinity surface water at their northern extreme, but only the northern Atlantic is cold enough for the low-salinity water at the surface to sink into the water column. This weak North Atlantic Intermediate Water formation moderates the deep Atlantic ages slightly and increases the local stratification, preventing the upwelling of bottom water to the surface. The age structure of the three northern basins in the No-NADW Experiment all have their oldest water between 2000 and 3000 meters along the northern wall.

In the Control Experiment, the higher restoring salinity increases the convective mixing in the high-latitude North Atlantic, which overturns nearly 16 Sv down to 3500 meters causing a restructuring of the Atlantic branch of the THC. The upper-level flow (above 1000 meters) in the Gulf Stream at 30°N in the western

Atlantic increases by about 13 Sv, all of which eventually sink and return southward in the deep western boundary current. Despite the prescribed increase in surface salinity, the net precipitation north of 50°N at equilibrium in the Control Experiment is less than in the No-NADW Experiment; the extra surface salt is delivered by the enhanced Gulf Stream, not by the restoring boundary condition. The northward heat transport in the Atlantic basin increases by over 0.35 PW, all of which is released to the atmosphere north of 40°N, providing an additional 26 Wm° of heating over the northern Atlantic. A net of 14 Sv of NADW flows southward across 30°S, out of the basin. This outflow is replaced by 6 Sv of southern bottom water and 8 Sv of upper water. The upper level compensation in this study is evenly divided between the warm- and cold-water routes as is indicated in Figure 15.

The high-latitude convection in the North Atlantic provides a pathway for tropical heat and salt into the deep ocean. The deep outflow from the northern sinking region advects a large quantity of salt southward which leads to an increased density at the northern edge of the ACC and a decreased density gradient across the ACC. This reduces the baroclinic component of the flow through the JEBAR term in the vorticity equation, and thereby reduces the total transport through the Drake Passage. The net effect of NADW on the high-latitude Southern Ocean overturning is to decrease both the downwelling and the upwelling in the Indo-Pacific sector; downwelling decreases due to reduced horizontal conver-

gence at the northwestern tip of the Antarctic Peninsula, and upwelling decreases due to reduced convergence along the bottom in the central Ross Sea. The northward flow of bottom water across 60°S is decreased when NADW present, and this decrease is largely confined to the far-eastern Pacific region (less Antarctic downwelling and less northward flow).

In both of the model experiments presented here, the Indian and Pacific basins are upwelling regions. There is, however, no *a priori* reason why this should be so. If the atmospheric circulation were to change in a way that altered the net hydrological cycle, it could be possible for the northern Pacific to form intermediate (as it already does in reality in the Sea of Okhotsk) or deep water and thus alter its branch of the thermohaline circulation. These experiments have shown that changing the Atlantic circulation has only a small effect on the meridional circulations in the Pacific and Indian Oceans. Rather than a single, unified "conveyor belt", the global THC seems more modular; each high-latitude basin functions quasi-independently, responding to its own heat and salinity balance. New sub-surface water masses spread out from their formation regions and compete for space in the water column according to their relative density, mediated through intense mixing in the circumpolar region. Further study is needed to establish the nature of the relationship and the effects of sub-surface water mass creation in the different regions of the global ocean.

NADW formation reduces the ventilation time of the deep Atlantic by over 900 years at the northern boundary. The age reduction due to this water mass decreases as it flows southward; water at 30°S and 2500 meters depth is between 250 and 500 years younger in the Control Experiment than in the No-NADW Experiment. Outside of the Atlantic basin, the effect of NADW on the ventilation time of the deep ocean decreases dramatically after NADW enters the ACC. The low age signal of NADW is blended into the Circumpolar Deep Water and is then advected into the Indian and Pacific basins. Dynamically, the reduced northward flow of water from the circumpolar region below 4000 meters, which accompanies NADW production, causes those northern areas ventilated by bottom water to age, especially in the North Pacific. The decreased deep outflow (roughly between 1500 and 3500 meters) from the Indian and Pacific Oceans in the Control Experiment leads to increased upper-level upwelling which alters the upper-level age balance. The heat balance and the age balance in the upper ocean are governed by the same factors; the downward diffusion of surface tracers becomes less effective due to the enhanced upwelling, leading to both increased ages and decreased temperatures. Most of the model's deep ocean, outside of the Atlantic basin, experiences less than a 10% change in its age due to NADW production.

The deep Pacific and Indian basins are ventilated by a combination of AABW, CDW and NADW flowing in from the south. The model's CDW is made up of the denser components of a recirculated mixture of all the sub-surface water

masses present in the Southern Ocean. When CDW includes the NADW component, its density increases due to its higher salinity, but its movement throughout the model ocean is only slightly affected. Denser CDW does increase the stratification in the upper Southern Ocean and reduces the formation of southern subpolar intermediate water (AAIW). Globally, NADW production causes the entire ocean to become denser with the largest increase occurring at about 1200 meters depth. This effect causes an increase in the stratification above this level, and a decrease in the stratification below. The increase in upper level stratification reduces the downward diffusion of surface properties and leads to generally colder and less ventilated upper waters.

The age structure of the model ocean derived from the passive age tracer is dependent on the number and strength of sub-surface water mass formation regions and can serve as a useful tool for comparing different ocean modelling efforts. The ventilation time-scales derived from this tracer are highly dependent on the vertical diffusivity employed; further refinements to the models as well as additional observational study will narrow our uncertainties about the overturning time-scale of the world ocean.

The two experiments highlight a critical distinction which is generally lacking in the discussion of the global circulation. Most of the upwelling in the model (the upward vertical movement of water parcels) occurs in the Southern Ocean, while most of the positive buoyancy forcing associated with the THC (converting the

denser sub-surface water masses back into lighter ones) occur in the tropics. The latter is primarily associated with the downward diffusion of heat and this process is strongest near the equator.

Chapter 2

Thermohaline Adjustment and Advection in an OGCM

6.0 Introduction

The observational evidence, [^{13}C, ^{14}C, and ^{18}O, from deep-sea sediments and ice cores], indicates that water masses in the abyssal ocean, most notably in the Atlantic, have undergone dramatic changes in structure over the last few glacial cycles [Roemmich and Wunsch, 1984; Boyle & Keigwin, 1987; Bond, et al., 1993; Duplessy, et al., 1988]. This variability has been linked to the thermohaline circulation (THC) [Broecker, et al., 1985; Gordon, 1986; Broecker, 1991]. The conventional picture of the THC as a vast, yet slow-moving, conveyor belt gives the impression that changes in one region can only affect other regions on the 1000yr advective time-scale. Severinghaus, et al. (1998), however, reported that ice cores from Greenland show that local air temperatures rose by as much as 5-10°C in "several decades or less" during the warming at the end of the Younger Dryas cold period (~12 kya). It has been suggested that the cause of this rapid warming was the re-initiation of convection in the North Atlantic, the renewed production of North Atlantic Deep Water (NADW), and the increased northward heat transport that accompanies it [Broecker and Denton, 1989]. Observations of convection in the GIN and Labrador Seas have shown it to be quite unsteady in time [Dickson,

et al., 1996, Marshall, et al., 1998], and observations of the variability in the total production and outflow of NADW are patchy at best [Dickson, et al., 1990; Dickson and Brown, 1994; Bacon, 1998, Dickson, et al., 1999].

This is the most recent in a hierarchy of model simulations designed to study the oceanic baroclinic adjustment process in response to a lower layer mass source. Stommel and Arons (1960a, SA60 hereafter) examined the structure of the deep circulation using a simple, two-layer model in which uniform upwelling of the layer interface balanced the mass source. Uniform upwelling is unrealistic, however, so Kawase (1987, K87 hereafter) parameterized the upwelling as a damping term in the continuity equation, which led to a much better simulation of the observed oceanic structure. K87 addressed the basic questions of baroclinic adjustment and spin-up of the velocity field in a two-layer, sector model, and was the first study to describe the boundary layer pathway taken by the initial adjustment wave: equatorward on the western boundary, eastward at the equator and poleward on the eastern boundary (see Figure 16), a cyclonic sense in both hemispheres with the wall to the right (left) of the signal's motion in the northern (southern) hemisphere.

Cane (1989, C89 hereafter) solved the steady-state equations for the same two-layer system employed by K87, and recently, Huang, et al. (submitted, HCNG hereafter) applied the two-layer solution of C89 in a real world domain to determine the steady-state thermocline displacement that results from 10 Sv of NADW

formation. The disadvantage of using a two-layer model to study baroclinic adjustment is that only the first baroclinic mode can be represented. This mode generally travels the fastest and has the largest amplitude, but the significance of other modes need not be arbitrarily ruled out. In an OGCM, higher-order modes can be expressed, although the damping increases proportionally to the fourth power of the mode number [Gill, 1982; K87], thus restricting their influence to the boundaries.

This study is a quasi-continuously stratified (20 layer) analog of the previous studies (SA60, K87, C89, HCNG); it will explore the transient response to the initiation of deep water formation in an OGCM, and is the first to do so. Winton (1996) and Greatbach and Peterson (1996) both discussed the propagation of baroclinic waves in a "square" domain associated with decadal variability in the overturning, but their focus was on the boundary layer effects. Karcher and Lippert (1994) used a high-spatial resolution two-layer model to examine the effects of realistic bottom topography on the spin-up and spin-down of the North Atlantic deep circulation and the interface displacement. Their domain only extended to 25°S, however, so the quasi-steady state they discuss is only applicable to the North Atlantic and their results would be modified slightly if the entire world ocean were included. Goodman (1998, G98 hereafter) compared the steady-state differences between model runs with and without NADW production, but did not explore the transition between the two equilibria. Other studies, e.g. Bryan (1986a,b), McDer-

mott (1996), have looked at the effects of changing boundary conditions (freshwater flux, windstress, etc.), but none have described the detailed response of the models' velocity and pressure fields during the spin-up phase as in the previous studies in this series.

In addition to an analysis of the baroclinic adjustment, the distinction between adjustment and advection, in terms of time scales and spatial patterns, will be explored with the help of passive tracers. Several studies have suggested that anthropogenic warming could lead to a collapse of the North Atlantic overturning [Manabe and Stouffer, 1994; Sarmiento, et al., 1998], so the question of the spin-down, or the baroclinic response to the interruption of deep water formation is also briefly addressed.

It is found that the model does not allow an instantaneous change in the convectively driven mass flux, either increasing or decreasing. In both cases, the overturning takes several decades to reach approximate equilibrium. The northward heat transport in the Atlantic increases with the overturning and continues to increase for about a decade after the overturning has leveled off. The oceans north of Drake Passage are connected via boundary layer paths and all locations begin to feel the effects of any large change in the stratification within 20 years, *i.e.* the stratification is altered on the adjustment time-scale and not the advective time-scale.

The pattern of advection is fundamentally different from the adjustment pattern and the North Pacific is not informed of changes in the North Atlantic via advective processes for almost 1000 years, consistent with the ^{14}C-derived ages of the water there [Andrée, 1986]. The majority of the passive tracer convected into the deep North Atlantic is removed from the domain near Antarctica, south of 60°S. Adjustments to the onset and cessation of deep water formation follow the conventional boundary layer path, and are nearly identical. The Drake Passage Effect [Gill and Bryan, 1971;Toggweiler and Samuels, 1995] isolates the high-latitude Southern Ocean; the ACC transport only changes in response to NADW production as the density gradient across the current does, on the order of centuries.

In the following analysis: section 2 will describe the model and the passive tracers employed, and some differences between this model and G98 will be noted. Section 3 will describe the fast part of the baroclinic adjustment, both spatial and temporal, during the Spin-up experiment. Section 4 will examine the difference between the adjustment and advection in the model. Section 5 will present time-series at key locations during the Spin-up run and differences between Spin-up and Spin-down will be noted. Section 6 includes a summary and discussion.

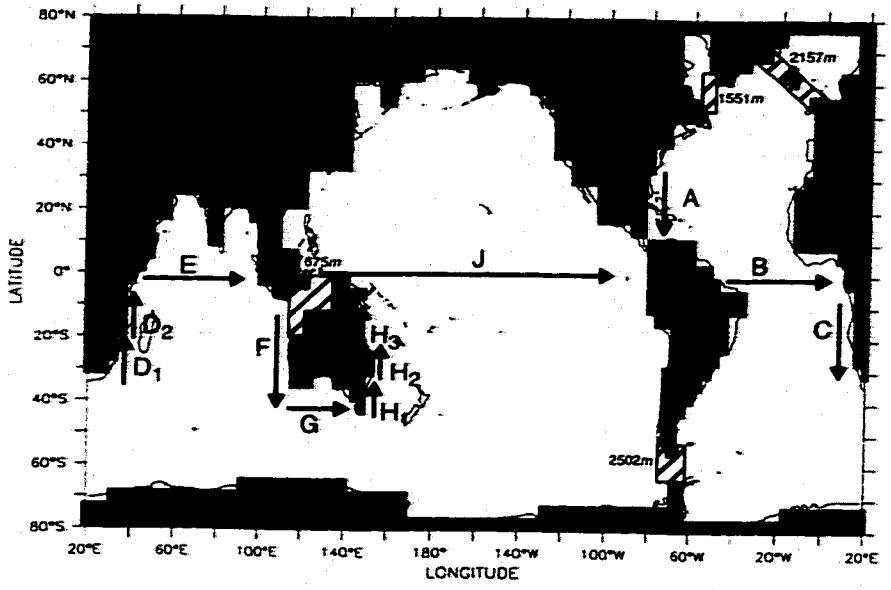

FIGURE 16 : The model domain is unshaded and the contour line is the global sea level. The bottom is at 5000m except in the hatched areas where the depth is noted. The arrows and letters indicate segments of the boundary layer path taken by the adjustment that will be referred to in the text. The locations for each segment are given in Table 4.

7.0 The Model

These experiments were performed with the Modular Ocean Model (MOM1.0) from GFDL [Pacanowski, et al., 1991]. The grid resolution is 4° by 4°, and there are 20 levels of increasing depth from 50m at the surface to 449m at the bottom, comprising 5000m in total. The global coastline was interpolated onto the model grid, and the bottom is flat everywhere, except in the Drake Passage, the marginal polar Atlantic Seas, and the Indonesian archipelago. The bathymetry and sill depths at these locations are indicated in Figure 16.

This study grew out of G98 which was carried out in an idealized domain under restoring boundary conditions on both temperature and salinity, taken from

the 30m level of the Levitus (1982) climate atlas. All of the experiments presented here were also carried out in the domain used in G98 and the transient response as NADW production is initiated or curtailed was unaffected by the choice of model domain. The forcing used here is generally the same as in G98, although the newer Levitus, et al. (1994a,b) climatology has been substituted. All forcing is annually-averaged; there is no seasonal cycle imposed in the model.

The restoring boundary conditions used here are the 1-D zonal averages for each individual basin north of 40°S, and the 1-D global zonal average south of there. The global average is used over the Southern Ocean since the mixing there is large and the properties are fairly uniform, especially given the model resolution and idealized bathymetry. As in G98, the restoring salinity near Antarctica is smoothly increased from climatology at 60°S to 35psu at the southern extreme. To differentiate the forcing between the Labrador and GIN Seas, the Labrador Sea restoring values are reduced by 5°C and 1.5ppt, roughly equal to the observed differences. A comparison experiment in which the model was restored to the 2-D fields (at 30m) from Levitus, et al. (1994a,b) was run, and again, the results presented here did not depend on the nature of the background forcing.

The momentum forcing is taken from the zonally and annually averaged wind stress of Hellerman and Rosenstein (1983), applied uniformly at all longitudes. There is no meridional momentum forcing. The model employs no-slip

boundary conditions at the walls, free-slip conditions at the bottom, and Cartesian mixing with the same values as in G98.

The steady states of the model with and without NADW in the new domain are quite similar to the results from G98. The transport in the ACC, at the Drake Passage, is reduced by ~33% [from 205 Sv to 142 Sv in the NADW run (1 Sv = 10^6 m^3s^{-1})] when the domain is expanded from 240° to 360°. The ACC transport is ~10% stronger in the current configuration when NADW production is curtailed (155 Sv), whereas the increase was ~14% in the idealized domain. The wind imparts momentum to the ACC which is balanced by topographic form drag [Munk and Palmén, 1951; Gille, 1997]. In the model, the form drag is generally too weak due to the idealized bathymetry and the net transport is overestimated. As the area over which lateral diffusion of momentum can act increases, the net transport becomes smaller. The sill depth in the Indonesian archipelago in the current domain is about 500m shallower than G98 and the Throughflow is ~4 Sv weaker (18 Sv here). The other significant change from G98 is that in these runs, the region of NADW formation is restricted to a smaller area in the GIN Sea, but the net overturning is a bit stronger (19 Sv here, versus 16 Sv there).

In order to compare the differences between the wave adjustment due to a deep water source and advection of the deep water mass, a passive water mass tracer that was used by Cox (1989) and Stocker, et al. (1992) was incorporated into the model. Water mass tracers are akin to colored dyes (and will occasionally

be referred to as *colors*), which tag the water at the surface and are then advected with the current. For a parcel at the surface, the local color is restored to 100% on the same time scale [$\tau=(50day)^{-1}$] as the temperature and salinity. When the parcel returns to the surface in a different area, the new color is added and the others are removed. If the entire surface area is divided into non-overlapping regions, then the sum of all the tracer fractions in any water parcel is 1 at equilibrium. If part of the ocean's surface is not included in any of the specified tracer regions, then the uncolored fraction represents contact with this area — for steady-state calculations, one area is computationally free.

Water mass tracers can be used in two different ways: as noted above, when the colors are included in the spin-up phase of a model run, they indicate the fraction of water at any location from each of the surface regions and can be compared to observations of tracer properties for the relevant water mass; when the tracers are added at a later time, they indicate where the surface water from the region has penetrated. Both types of experiments have been realized and results will be described as needed.

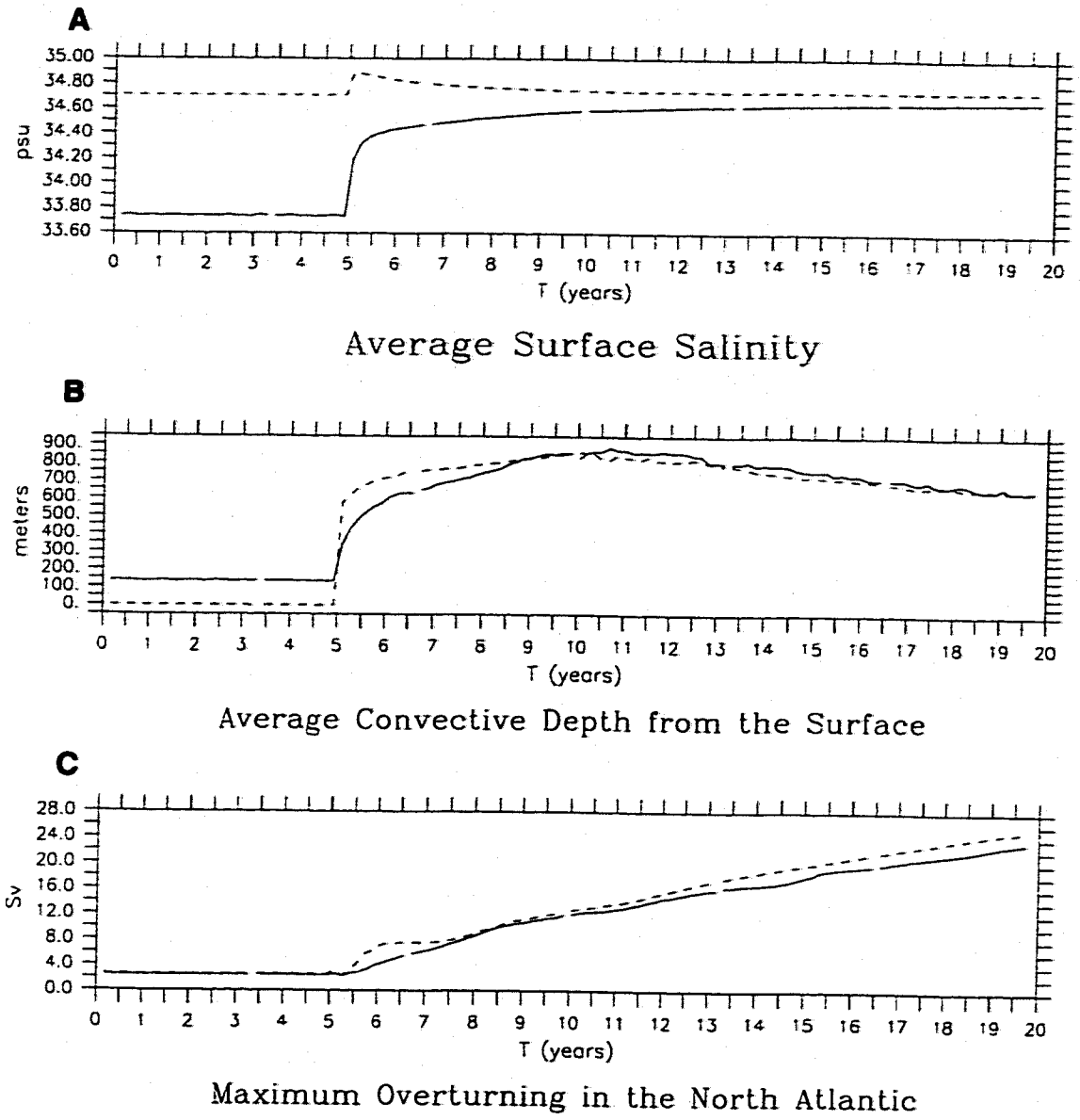

FIGURE 17 : North Atlantic properties for the Spin-up experiment (solid) and the no convection experiment (dashed). A) Surface Salinity; B) Convective Depth from the surface; C) Maximum of the overturning stream function. The North Atlantic surface salinity and convective depth are averaged north of 48°N only.

8.0 Spin-up Experiment: Baroclinic Adjustment

The initial state for the Spin-up experiment is the steady state of the No-NADW run, in which the model was forced with the artificial fresh water anomaly imposed on the North Atlantic north of 40°N. The internal clock is reset to 1 Jan, Year 0 and the model is restarted, still with the anomalous forcing. On the first day of year 5, the artificial freshening is removed from the restoring boundary condition. The restoring time constant for the salinity forcing is $(50\ \text{days})^{-1}$, so the North Atlantic surface salinity rises quickly: 75% of the total change occurs within the first four months [Figure 17a, solid line]. The additional salinity destabilizes the water column; convection increases rapidly in both depth and areal extent and mass is added to the lower ocean [Figure 17b, solid line].

The dashed curves in Figure 17a-c are the results of a parallel experiment: instead of adding a fresh water anomaly to the boundary condition, convection was suppressed north of 40°N in the Atlantic. This eliminates the formation of NADW at the cost of allowing an unrealistic, locally unstable stratification. Convection is then permitted at year 5, and the model responds immediately since the stratification is already unstable. Other than some minor differences in the Atlantic, both runs follow the same sequence of events as NADW production begins.

8.1 Theory

The baroclinic response to a lower layer mass source has been examined in numerous studies [SA60, K87, C89, HCNG, etc.]. In all of these studies, a mass source into the lower layer is initiated and continuity ensures that the response provides a mass sink and therefore upwelling. SA60, K87, and C89 prescribed the deep water formation as a source in the northern part of the basin along the western boundary; in HCNG and this study, the source is in the North Atlantic. The spin-up phase will be compared with SA60 and K87, and the steady state will be compared to HCNG.

After the initiation of the mass source, a "signal" is created consisting of upwelling through the "interface" (at ~2000m), flow toward the source region in the "upper layer", and flow away from the source region in the "lower layer". The lower-layer flow *always* heads west until it hits the boundary and then proceeds in a cyclonic sense with the wall on the right (left) of the signal's motion in the northern (southern) hemisphere. As noted in SA60 and K87, the signal propagates away from the forcing region as a series of coastal and equatorial Kelvin waves. At the western wall, the signal turns southward (segment A, Figure 16) until it hits the equator, where it turns eastward (segment B). At the eastern boundary, the signal splits and heads both northward (not shown) and southward (segment C).

In the single-basin domains of SA60 and K87, the eastern and southern boundaries are connected which directs the signal westward along the southern

wall (wall on the left in the southern hemisphere). The global bathymetry in HCNG and the present study directs the signal eastward south of Africa (again, wall on the left) and then northward into the Indian Ocean (segment D, Figure 16). Next, the signal crosses the Indian basin along the equator (segment E). At this point there are two possible paths on which the signal can progress, either through the Indonesian archipelago or around Australia. The real bathymetry around Indonesia includes many deep, but narrow, channels which may allow a large signal to pass through, although the narrowness of the channels may increase the local dissipation and thus reduce the signal's amplitude. This model has a wide and shallow (12° and 675m) Indonesian passage, but this is typical of coarse resolution models [England, 1993; Hirst and Godfrey, 1993]. The signal can clearly continue southward along the western coast of Australia (segment F), eastward along its southern coast (segment G) and then equatorward along its eastern flank (segment H). This latter route is the one preferred by this model configuration. Arriving at the equator in the Pacific Ocean, the signal continues eastward (segment J) and again splits at the eastern boundary (not shown).

In each of the previous studies, the mass source was initiated at full strength, whereas here it takes a while to ramp up [Figure 17c]. This distinction is important; there is no consistent way to create a large instantaneous mass flux. In this experiment, the model has less than 10 Sv of overturning for at least 3 years

after the change in the boundary condition. At this time, the initial signal is nearly at the southern tip of Africa, as will be discussed shortly.

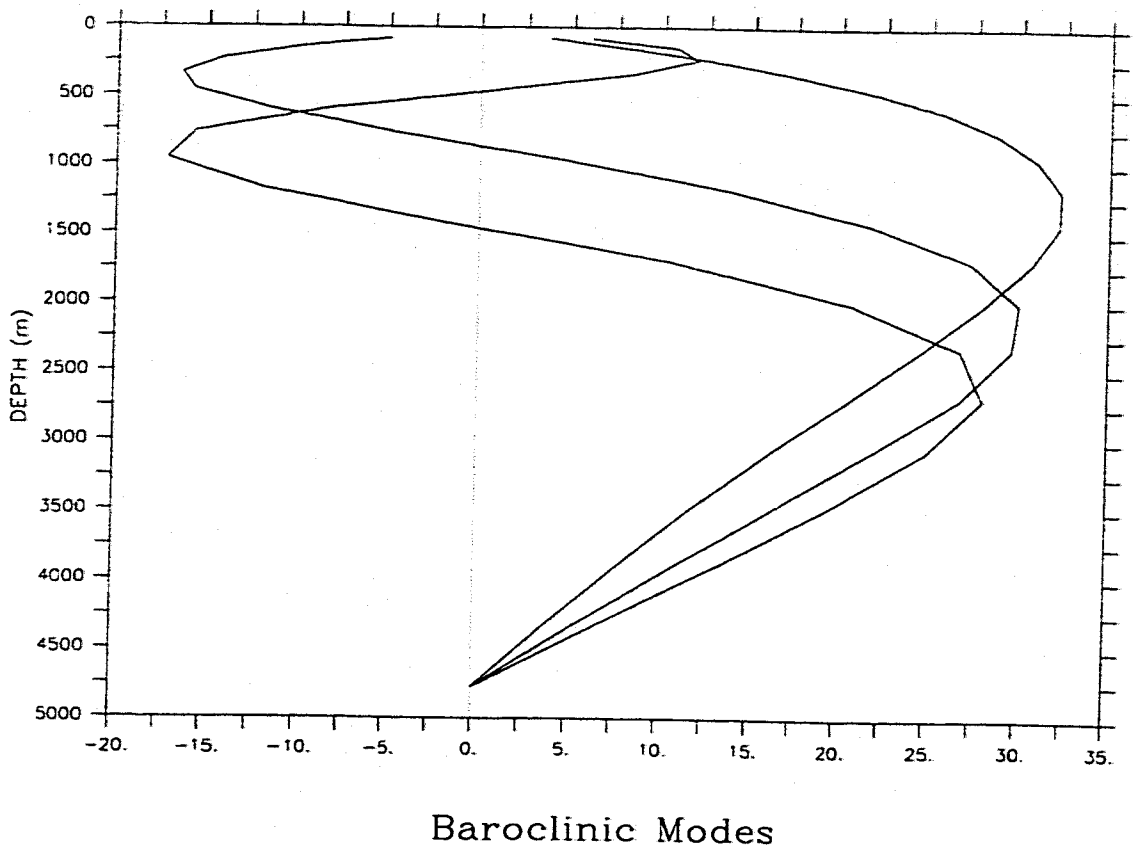

FIGURE 18 :The first 3 baroclinic modes for the vertical velocity, calculated from the model's globally-averaged stratification (using the method of Gill, 1982).

The wave speed for a coastal Kelvin wave travelling meridionally in a GCM was calculated in McDermott (1996, Appendix). The no-slip boundary condition at the wall and the assumption of geostrophic flow offshore allows the numerical boundary wave speed to be calculated. This speed is given by $c_1^2/f\Delta x$, where c_1 is the wave speed of the first baroclinic mode, f is the local Coriolis force and Δx is

the cross-flow dimension of the grid box [McDermott, 1996]. The mean wave speed, c_1, is calculated from the modeled stratification [Figure 18] to be about 2.5 ms^{-1} and the corresponding numerical boundary wave speed is about 0.23 ms^{-1} at roughly 40° latitude.

Once the boundary currents are set up in the wake of the initial wave, long Rossby waves are formed along the eastern boundary that propagate into the interior. K87 determined that the structure of the response depended on a non-dimensional parameter (δ), the ratio of the damping time scale to the transit time for long Rossby waves to cross the basin. For a continuously stratified ocean:

$$\delta = \frac{N^2}{A_v \beta L_B^3 m^4} \qquad (1)$$

where N is the buoyancy frequency, A_V is the vertical viscosity, L_B is the width of the basin and m is the vertical wavenumber. Under strong damping ($\delta \ll 1$), the lower layer response is confined to the boundaries (coastal and equatorial). For weak damping ($\delta \gg 1$), the Rossby waves flow freely into the basin and allow the entire area to participate in the upwelling, approximating the SA60 solution. The vertical wavenumber (m) is proportional to the baroclinic mode number; δ for the higher-order modes decreases as m^4, implying that these higher-order modes are strongly damped and confined to the boundaries. For this experiment, $\delta \sim O(250)$ for the first baroclinic mode and is thus in the weakly damped regime (see

Figure 20 and Figure 21). Readers interested in the analytical solution for the first baroclinic mode in the real world domain should refer to HCNG.

8.2 Model Results

The increased upwelling due to the baroclinic adjustment leads to changes in the local density profile; the vertical density gradient is negative everywhere, so positive vertical velocity anomalies create positive density anomalies at a given depth. These changes lead to both dynamic height anomalies and changes in the thickness of the 0-2000 db layer (1db = 10^4 Pa). Accordingly, thickness changes will be used as a marker for the signal's progress.

A plot of the thickness change in the 0-2000 db layer, along the coastal and equatorial boundary path in Figure 16, versus time is shown in Figure 19 (the precise locations of the segments are given in Table 4). These thickness anomalies are calculated by determining the change in the depth of the 2000 db surface; the 0db surface is assumed to be constant. Due to the experimental procedure (there is an unrealistic, globally-integrated, non-zero freshwater flux added during the transient phase), the salinity increases steadily at almost all locations, so the thickness anomalies will include the effects of the increasing salinity as well as the changing stratification. In order to remove the direct salinity effect, the initial salinity in the column is used for the purposes of calculating the density anomaly. The calculated density (and thickness) anomalies, therefore, are only due to the net changes in the heat content of the water column. The differences between the full

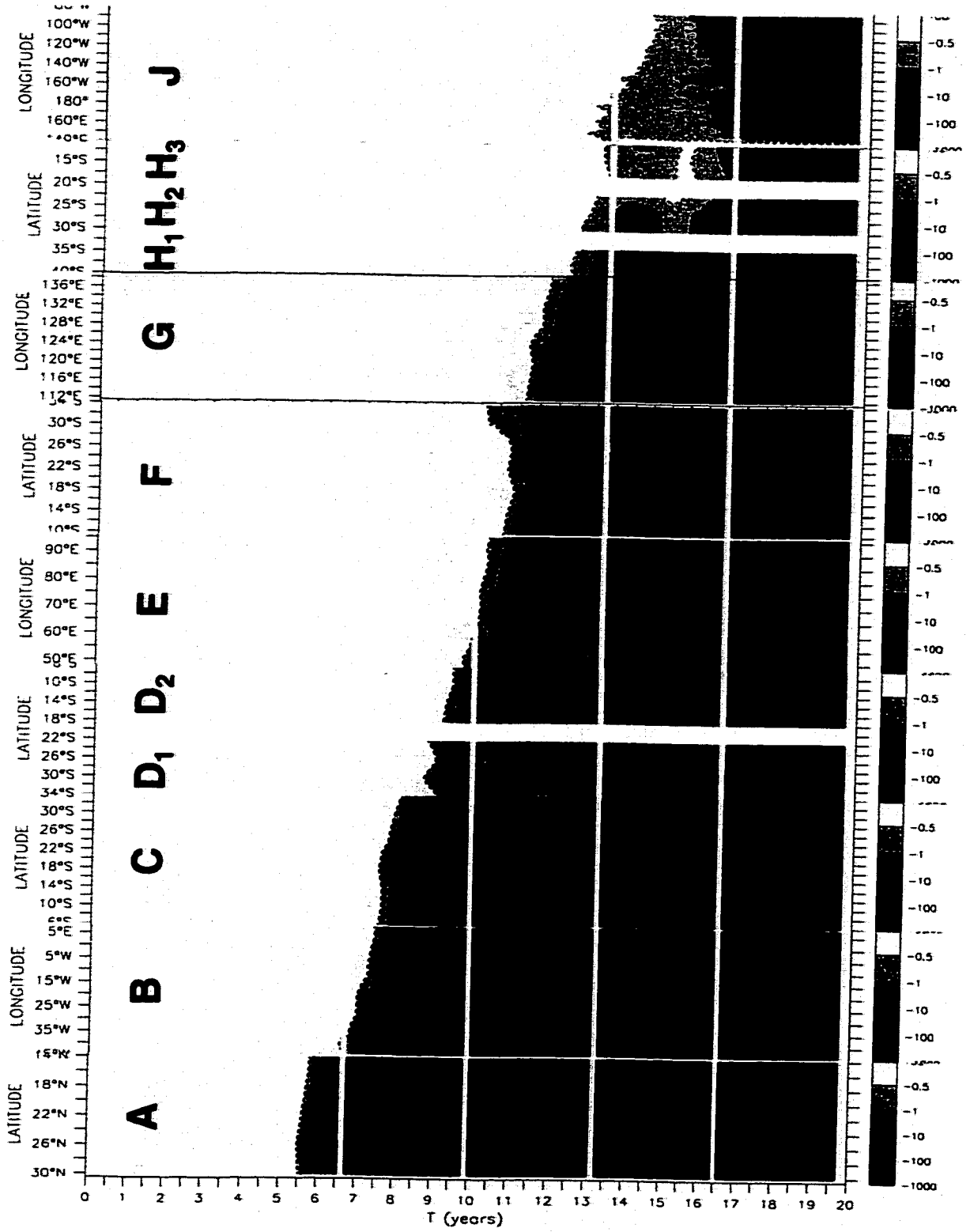

FIGURE 19 :Time series of the thickness anomaly in the 0-2000db layer in (mm) along the boundary wave path given in Figure 16. Contour lines at -0.5mm and -1mm.

change in density and that due to temperature alone are small in the early years and do not effect the timing of the anomalies presented in Figure 19 or Figure 20: Time of Arrival for Initial Signal (signal = 0.5mm decrease in the 0-2000db thickness), shading as indicated, contour lines at each year from 0 to 21.. In later years, the spatial pattern of the anomalies, including the full salinity change or not, is quite similar although local amplitudes are obviously different.

The -0.5mm contour is above the upper bound of the numerical noise in the model, so its arrival is a good indication of the progressing wave. The magnitude of the thickness anomaly reaches -0.5mm at each location within a few months of the calculated arrival time. The apparent discontinuity between panels A and B in Figure 19 is due to the distance between the sections, as is the offset between panels C and D and panels G and H. The slope of the -0.5mm contour in panel J is larger than in the other panels because the greater width of the Pacific basin has been compressed more than in the other panels. There is a weak indication that some of the signal leaks through the Indonesian Passage into the equatorial Pacific (from panel E to panel J, above sill depth and not shown), but the majority of the response takes the circum-Australian route. As noted, the sill in the model's Indonesian passage is at 675m, whereas in the real ocean, there are deep channels between the various islands which may permit the communication of a larger signal than is seen here.

TABLE 4. Various sections referred to and indicated in the text (see Figure 16 and Figure 19).

		LOCATION	
SECTION	**LETTER**	**LONGITUDE(S)**	**LATITUDE(S)**
Western North Atlantic	A	80°W	30°N -14°N
Equatorial Atlantic	B	44°W - 14°E	0°N
Eastern South Atlantic	C	12°E	6°S - 34°S
Western South Indian	D_1	36°E	34°S - 22°S
Western South Indian	D_2	40°E	18°S - 6°S
Equatorial Indian	E	48°E - 96°E	0°N
Eastern South Indian	F	112°E	10°S - 34°S
South of Australia	G	112°E - 140°E	38°S
Western South Pacific	H_1	152°E	40°S - 34°S
Western South Pacific	H_2	156°E	30°S - 22°S
Western South Pacific	H_3	148°E	18°S - 10°S
Equatorial Pacific	J	124°E - 84°W	0°N

While the -0.5mm contour indicates the initial signal, the arrival of the -1mm contour signifies that the adjustment is well underway. This contour is nearly parallel to the -0.5mm contour in panels A-G, although the rate of thickness decrease from -0.5mm to -1mm seems to slow farther downstream from the forcing anomaly. The marked deviation of the -1mm contour in the panels H_2 and H_3 occur because the Kelvin wave hugs the coast and the coastline is irregular here (see also Figure 20). As noted above, the meridional boundary wave speed in the model is about an order of magnitude slower than the theoretical result, given the noted assumptions; this implies that the time scales presented here are likely an upper maximum for the response in the real ocean.

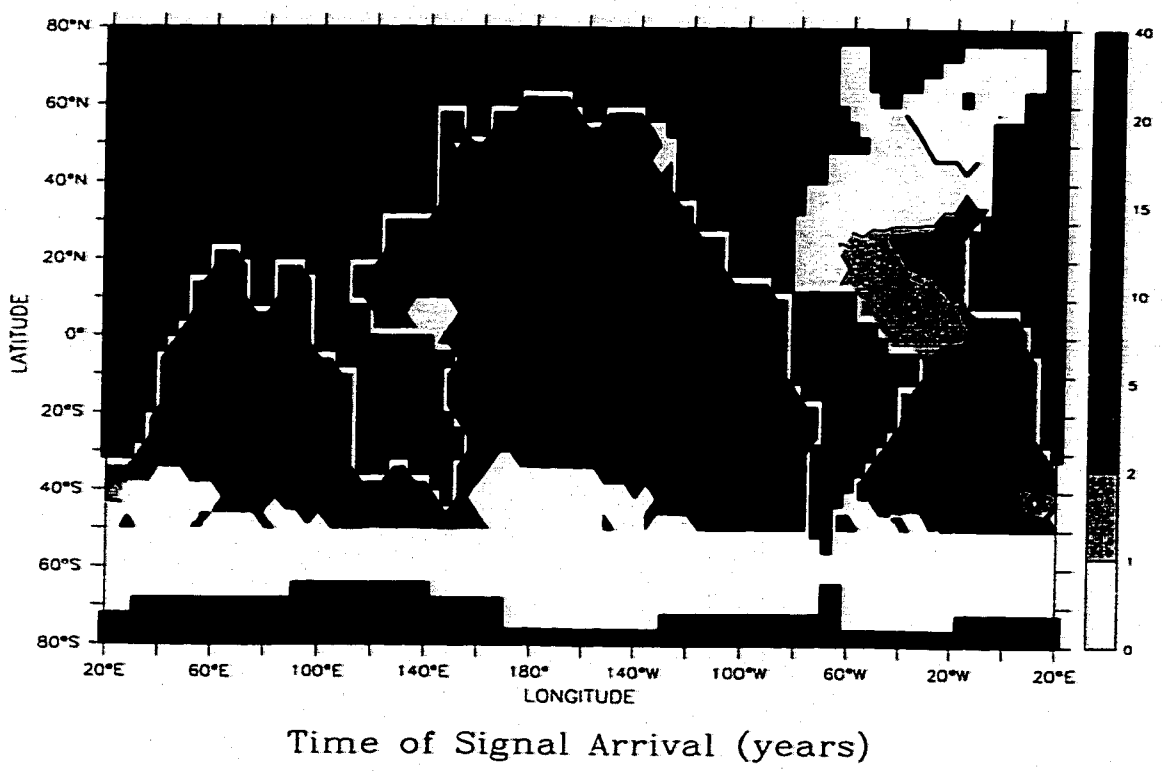

FIGURE 20 :Time of Arrival for Initial Signal (signal = 0.5mm decrease in the 0-2000db thickness), shading as indicated, contour lines at each year from 0 to 21.

The boundary current has run its course by year 15 (model year 20, Figure 20) and nearly all locations north of the ACC are informed of the change within 20 years (Figure 21c). By the third year of the spin-up, a curious feature has begun to develop at 60°W, 30°N (Figure 21a,b,c). The initial response here is a thickness decrease (Figure 20), but after about 2.5 years the thickness anomaly in this region turns positive. Steepening of the pressure gradient at 2000m is in agreement with the "thermal wind" balance across the boundary current as the baroclinic velocity increases, although the mechanism which causes this increase is unclear.

The area north of 40°N in the Atlantic is only weakly shaded in Figure 20 as this is the forcing region and there is virtually no lag between the change and the arrival of the signal. The spatial patterns of the response in the North Pacific and the southern Indian and Pacific basins can be described by the classical wave theory analyses [Cane and Sarachik, 1977; Moore and Philander, 1976]; the signal moves quickly along the eastern boundary and then long Rossby waves are shed from there. The phase speeds of these long waves are greatest near the equator and slow appreciably poleward of about 15°, accounting for the slower arrival at the poleward western corner of each basin. Note that since the Pacific is entirely bounded in the north, the boundary layer signal heads westward along the northern wall and the signal arrives sooner than at more southward, interior locations. The timing along the edge of the ACC in Figure 20 is ragged due mainly to the method by which the time of signal's arrival is interpolated and should not be given too much emphasis here, but this region will be described shortly in terms of the similar structure seen in Figure 21d.

In Figure 20 and Figure 21a (shading), it seems that the signal travels between the Indian and Pacific basins both north and south of Australia; there is no reason for the signal to choose one path over the other. The upper part of the baroclinic adjustment is "pulling" water toward the North Atlantic, so when the signal arrives at the western end of the Indonesian Throughflow, the westward transport through the IT begins to increase [see Figure 28]. In Figure 21, the shading

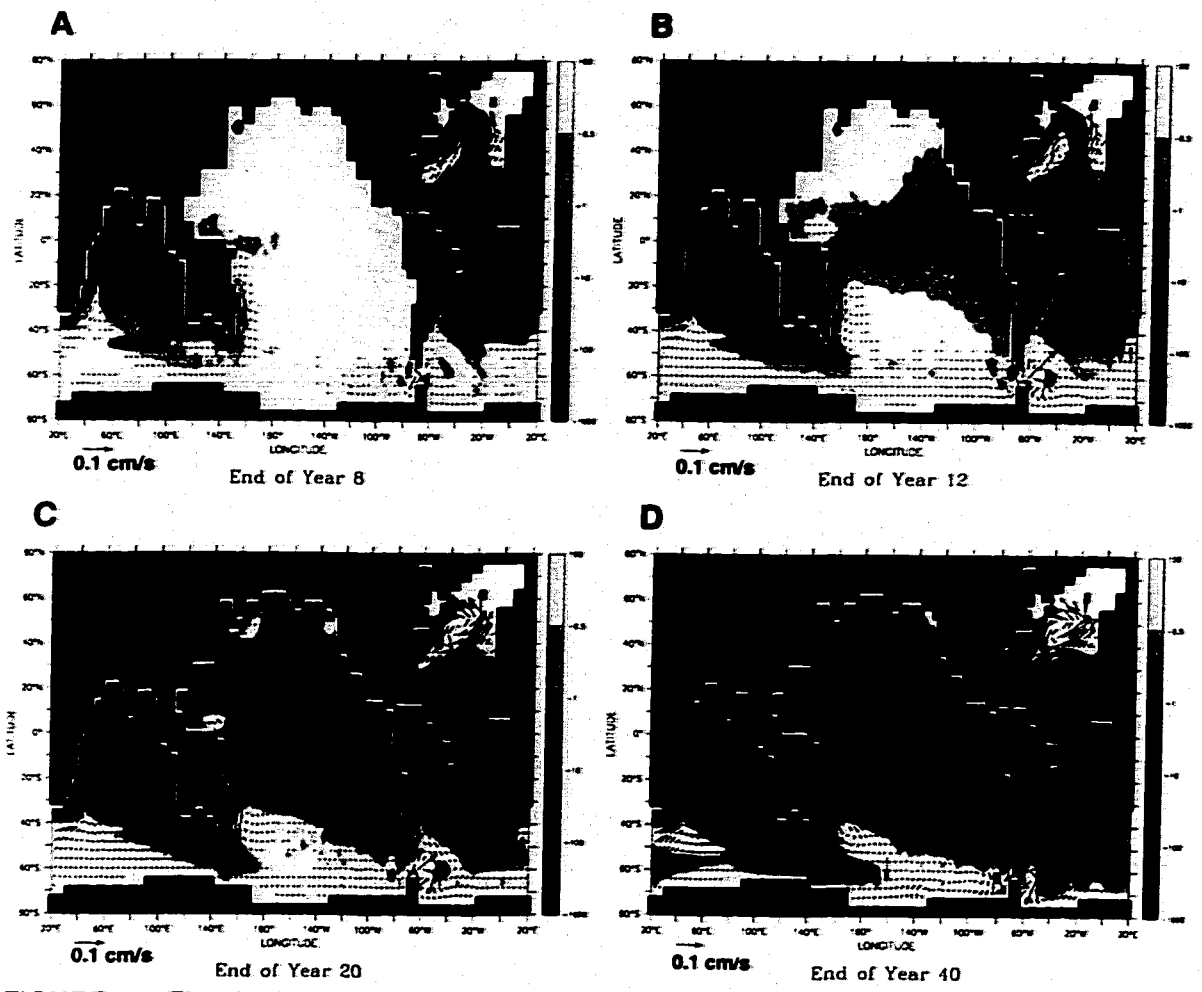

FIGURE 21 :The thickness anomaly between 0 and 2000db (in mm) is shaded, and the average velocity anomalies below 2000m are vectored (vectors over 0.15 cm/s and those north of 60°N omitted for clarity).

indicates the change of the 2000db surface which is not present in the model's Indonesia, and the velocity anomalies are averaged between 2000m and 5000m, so there are no vectors printed in this region. The upwelling part of the signal likely has to take the long way around Australia before reconnecting with the upper layer flow in the western Pacific.

The high-latitude Southern Ocean is separated from the northern basins (and the adjustment wave) by the Drake Passage Effect [Toggweiler and Samuels, 1995]; the absence of meridional boundaries prohibits the creation of zonal pressure gradients above the level of the bottom topography (2500m here), which in turn, prevents the existence of geostrophically-balanced meridional flow above the topography. The Southern Ocean is only affected on the advective and diffusive time-scales as the density gradients across it are slowly altered, and this will be discussed more thoroughly in the next section. The zone along the northern edge of the ACC has a distinct structure (Figure 21d). Southeast of both Africa (at 40°E, 45°S) and Australia (at 170°E, 45°S) the initial responses are positive thickness anomalies. As in the Atlantic (at 60°W, 30°N), these locations are close to an increasing western boundary current, and the increasing thickness is consistent with the "thermal wind" balance across the boundary current. Note that the circulation vectors are moving cyclonically around these points, also consistent with a developing low pressure anomaly.

Many studies have discussed the advection of properties from the North Atlantic and have mentioned the 1000 year advective time scale. Advection in the model will be thoroughly discussed in the next section, but it is worth reiterating here that adjustment is much faster than advection, especially given the fact that meridionally travelling Kelvin waves in the mid-latitudes are close to an order of magnitude slower in the model than they are in the real ocean. The times given in

Figure 20 are for the arrival of the -0.5mm thickness anomaly which is quite small (but noticeable). After 40 years (Figure 21d), the thickness has decreased by more than 10 mm at nearly all locations, except the northern Atlantic where the water column becomes significantly warmer and therefore exerts less pressure. The deep western boundary current in the Atlantic basin at year 40 crosses the equator and is very reminiscent of the simulation in SA60 and the weakly damped cases in K87.

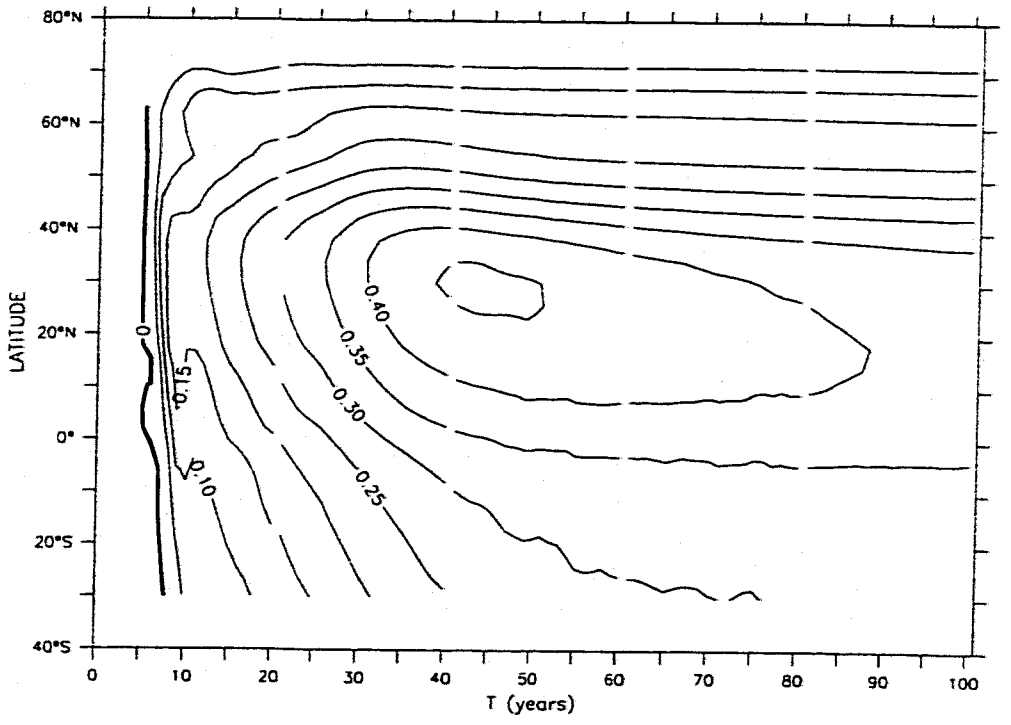

FIGURE 22 : Increase in the northward heat transport by the Atlantic Ocean in PW (1 PW = 10^{15} W). Contour interval is 0.05 PW.

Increased overturning in the North Atlantic greatly enhances the poleward heat transport in the basin. Figure 22 shows the change in northward heat transport in petawatts (1 PW = 10^{15} W) for the Atlantic only as a function of latitude and time. The extra heat flux out of the ocean increases rapidly for the first 40 years and the levels off (see also Figure 27c). At 40°N, this flux amounts to an additional 25-30 Wm^{-2} of heating for the atmosphere over the area of the North Atlantic, and it is likely that the model is underestimating the extra heat transport for the same magnitude of overturning [Bryan, 1987]. Without the assistance of a coupled model, it is impossible to tell whether this change can account for the dramatic warming of 5-10°C in ~30 years over Greenland during the transition out of the Younger Dryas as is seen in the ice-core record [Severinghaus, et al., 1998]. The oceanic response in the coupled model of Manabe and Stouffer (1988) is quite similar to the present study and they reported a steady-state difference in the surface air temperature of 6-10°C over the GIN Sea region. While most of the warming they identify was due to the increased heat transport, they cite additional warming due to 1) the effects of decreased sea ice on the air-sea interaction; and 2) the net absorption of incoming solar radiation due to decreased albedo.

The steady-state thickness anomaly between 0 and 2000db will now be discussed and the steady-state "interface" displacement will be compared with the analytical solution of HCNG. The steady-state thickness anomalies are shown in Figure 23: Steady-state thickness anomaly in the 0-2000db layer in mm (due to

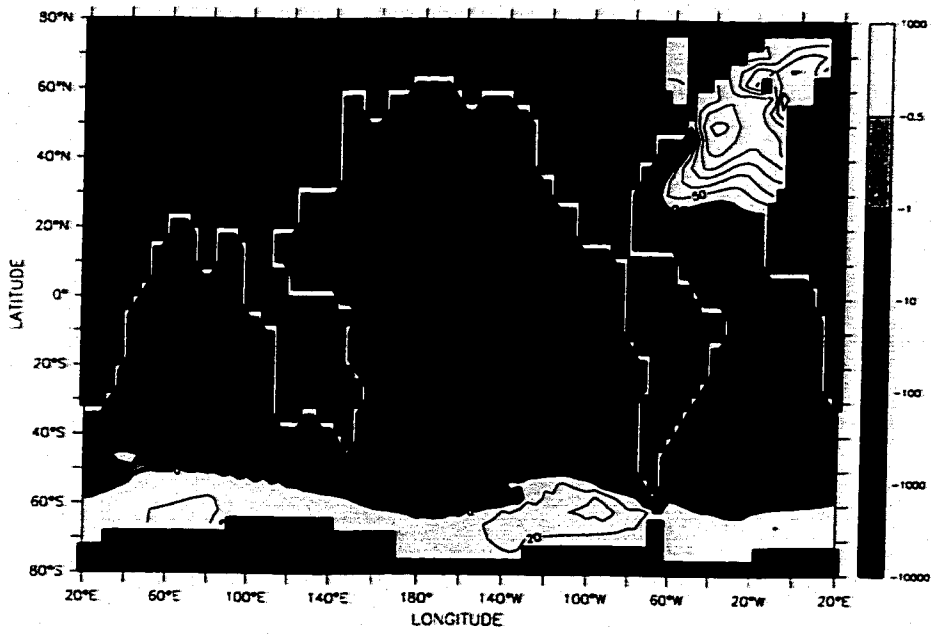

Steady State 0—2000db Thickness Change

FIGURE 23 : Steady-state thickness anomaly in the 0-2000db layer in mm (due to temperature/heat content only); contour interval is 20mm in the Indian and Pacific, and 50mm in the Atlantic.

temperature/heat content only); contour interval is 20mm in the Indian and Pacific, and 50mm in the Atlantic.. As noted earlier, the experimental procedure causes the globally-averaged salinity within the model to increase steadily. The anomalies in this figure have been adjusted to remove the direct effect of the salinity increase; the change in layer thickness is due to temperature changes only (decreasing the average water column temperature by 1°C reduces the 0-2000db thickness by about 300mm). The thickness in the northern Atlantic increases as the water column is significantly warmer with NADW production than without. The thickness increase in the high-latitude Southern Ocean is also consistent with the weakening of the ACC and the increased presence of the relatively warm NADW

in the circumpolar region. Note the local minimum in the high-latitude, southeastern Pacific: as will be discussed shortly (see Figure 26b), this is the same location where most of the NADW passive tracer re-emerges at the surface. The tropics (20°S-20°N) of each basin experience a net decrease on the order of 100-300mm with the Atlantic undergoing the largest change and the Pacific, the smallest.

The steady state displacement of the isotherms in the Atlantic at 30°W are shown in Figure 24a. The displacement in the tropics is upward above 1500m (due to cooling) and downward below there (due to warming). The water in the North Atlantic is significantly warmer below 500m. The upper layer cools due to the increased vertical advection, while the lower layer warms as the relatively warmer NADW replaces the AABW and CDW originally present. In order to compare these results to those of HCNG, it was necessary to determine which level in the OGCM would be most characteristic of the interface in the two-layer model. By definition, the maximum displacement in a two-layer model occurs at the interface, so the displacement at the level of maximal response in the model's tropical Atlantic (at 764m) is compared to the HCNG "open Indonesian Throughflow" results at 300m. Figure 24b shows the steady-state, upward displacement through which the isotherms have moved during the spin-up. The water in the North Atlantic at this level is now warmer so the displacement there is negative (downward). The largest displacement is along the Brazilian coast at the equator due to its proximity to the forcing region and the zonal barrier which enhances the local conver-

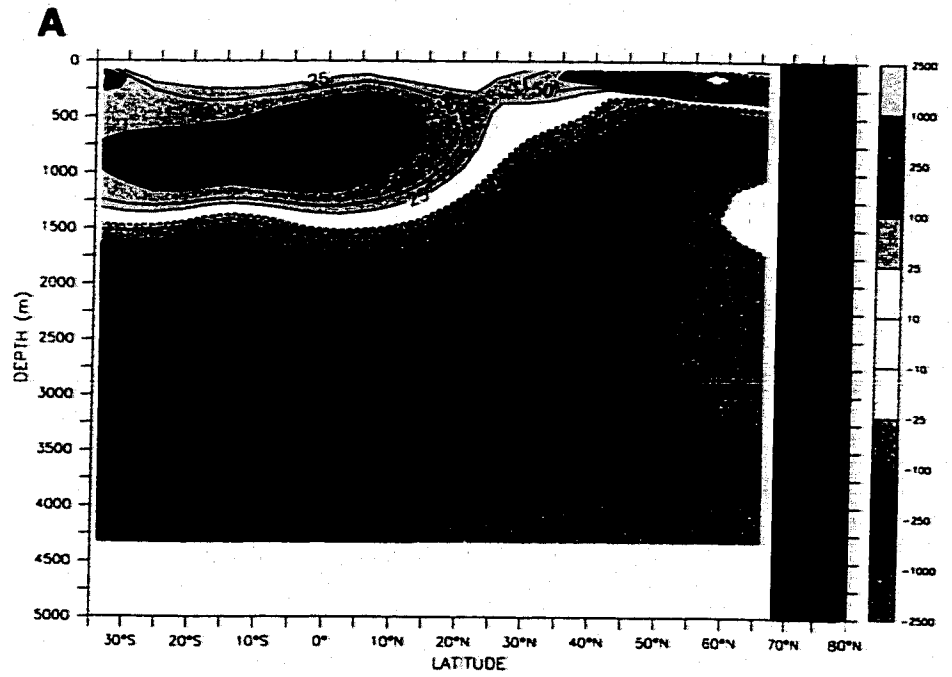

Steady–State Isotherm Displacement at 30W

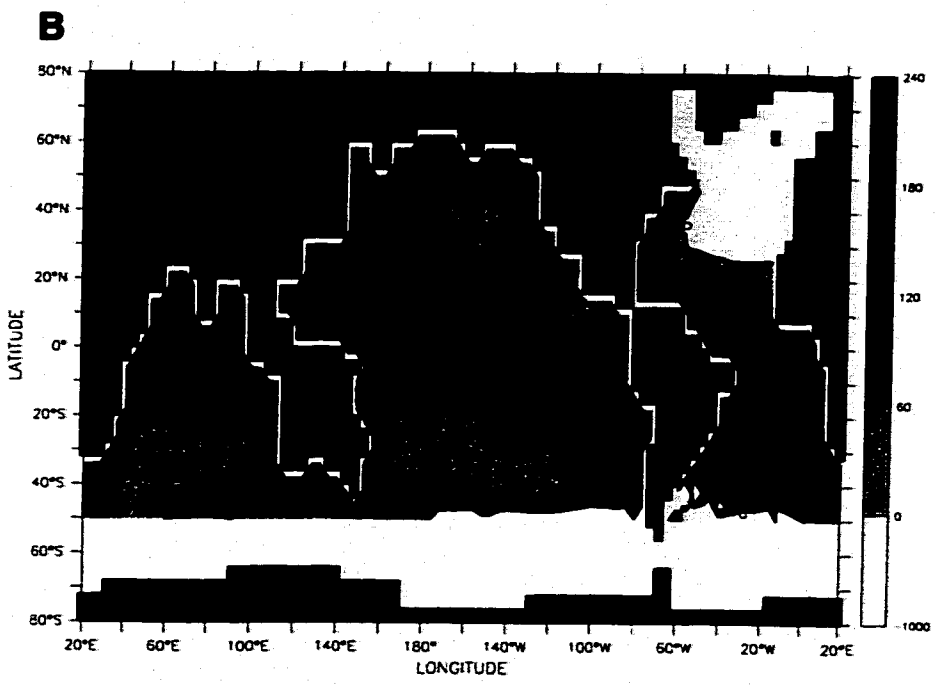

Upward Displacement of Isotherms

FIGURE 24 : a) Displacement of isotherms in meters in the Atlantic at 30°W at steady state, relative to the initial state; b)Upward displacement of the isotherms in meters at steady state, defined as the vertical movement of the isotherms to 764m: the shading south of 50°S is omitted for clarity and the contour interval is 5m in the Indian and Pacific basins and 20m in the Atlantic.

gence and upwelling. In the Indian, the displacement is nearly uniform north of the southern tip of Indonesia (8°S) which is nearly identical to the response in HCNG. In the Pacific, the displacement in the equatorial region is larger than in mid-latitudes and the weakest responses are in the anti-cyclonic gyres. It must be noted that due to the thermal relaxation boundary condition, SST in the model is held nearly fixed. As the upwelling increases, however, the model does have to add more heat in the tropics (~0.4 Wm^{-2}) to keep the surface at the same temperature, a sign of cooling.

The spatially-averaged displacements of the isotherms in the tropics (20°S - 20°N) at steady-state at this level are compared to the analytical solution given in HCNG. There is a 128m displacement in the Atlantic, a 80m displacement in the Indian, and a 67m displacement in the Pacific. These values are almost exactly 20% over the predicted values for each basin (HCNG reports 106m, 67m, and 54m for the Atlantic, Indian and Pacific, respectively). The net overturning increase is 65% larger here (16.5 Sv vs. 10 Sv), but the net outflow across 50°N is nearly identical (9.9 Sv). The 20% difference in the response may be tied to this model's weaker friction parameter, the coarser resolution (4° vs. 1°), the more poorly-defined interface and/or the diffusivity in the model. The diffusivity here, while comparable at the surface (0.3 vs. 0.36 cm^2s^{-1}), has a larger value of 0.5 cm^2s^{-1} at the depth of maximum displacement.

Another experiment was run in which the anomaly in the restoring boundary condition for salinity is reduced by one half: that is, from the No-NADW steady state, 0.5 psu of the 1 psu anomaly are added back and the flow development is tracked for a century (called the Half-on run). A century is not enough to even approach steady state, so the analytical solution in HCNG does not apply, but the results at this time will be compared to the Spin-up experiment. After 100 years of the Half-on run, the overturning in the North Atlantic was 8.3 Sv and the outflow across 50°N was 4.2 Sv. These values were 20.9 Sv and 10.9 Sv, respectively, in the Spin-up run after 100 years, so the 0.5 psu anomaly accounted for ~40% of the increase. The displacements at 1200m (the level of maximum response at this time in both Half-on and Spin-up) in the Atlantic, Indian, and Pacific measure 78 m, 25 m, and 16 m, respectively for the Half-on run and 179 m, 67 m, and 43 m in the Spin-up run, again a 40% response.

9.0 Advection vs. Adjustment

The preceding section discussed how a change in stratification is communicated from one region to another via baroclinic adjustment waves. Adjustment, however, does not transfer water mass properties to remote locations. In order to determine where the newly-formed NADW (and its climatologically important components) goes, a passive tracer is continuously added to the surface of the North Atlantic north of 60°N after the change in boundary condition. This tracer is convected into the deep ocean and then advected with the newly formed water mass

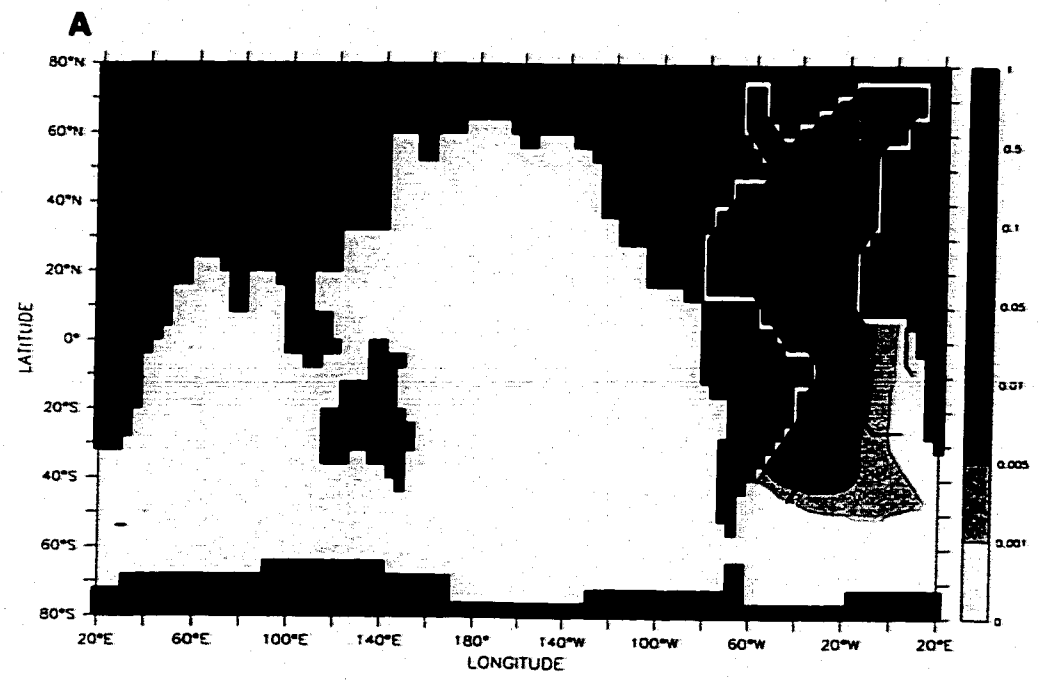

After 100 Years

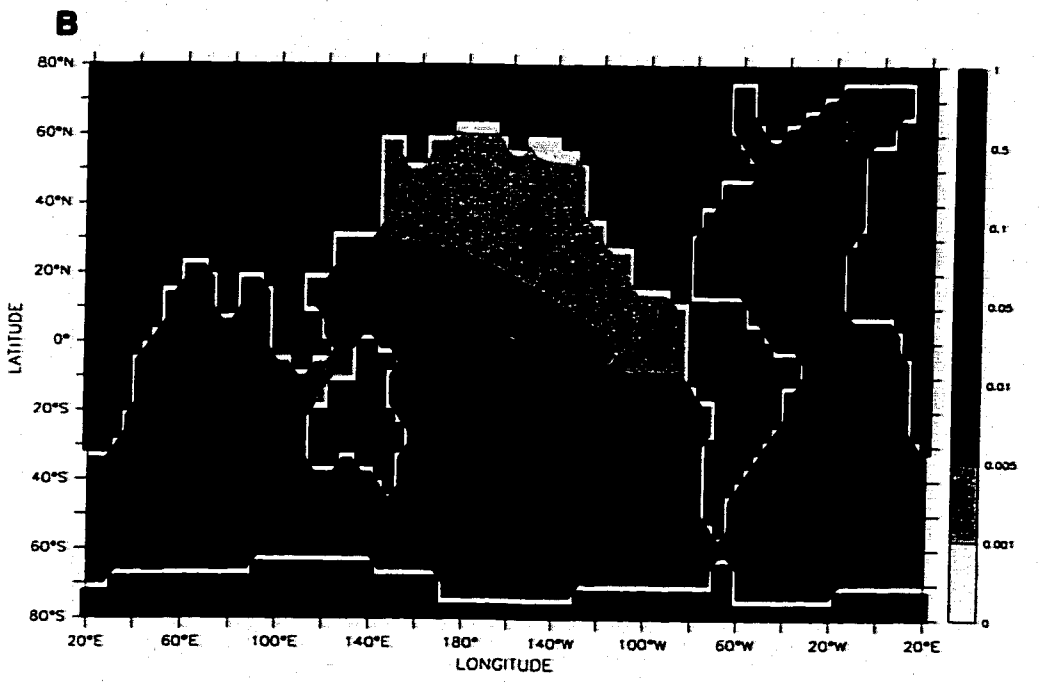

After 500 Years

FIGURE 25 : Maximum fraction of the water column tagged with the North Atlantic tracer (shading) and depth of the maximum (contours). Contour lines at 500m, 1000m, 1500m, 1750m, 2000m, 2500m, 3000m, and 4000m; the 2000m contour is darkened. A) After 100 years; B) after 500 years.

as it spreads throughout the world ocean. Figure 25a shows the maximum amount of NADW tracer in the water column after 100 years which indicates the penetration of the core of the NADW mass. Comparing this figure to Figure 21a-d reveals the wide disparity between the adjustment and advective time scales, as well as their spatial structures.

Advection does not follow the boundary layer path since the flow regime is already near the final state by the time the tracer has achieved a measurable level. Virtually no NADW tracer has left the Atlantic basin by year 100 although the global adjustment to the new stratification is over 80% completed (defined as the ratio of the isotherm displacement to the steady-state difference) at all sites north of the ACC, and is completed in the Atlantic. As the NADW enters the ACC it begins to descend in the water column as it is slightly denser (saltier) than the water present at that level.

The picture after 500 years (Figure 25b) is even clearer. Some NADW tracer has reached nearly all parts of the world ocean, although the maximal amount in the northern Pacific is between 1 and 5 parts per thousand at this time. The tongue of tracer in the Southern Ocean is as expected; the maximum at the African coast is quickly advected downstream by the fast moving ACC. The tracer slowly diffuses its way to the south; the contours in Figure 25b indicate that south of 40°S and west of Tasmania, the tracer maximum is always above 2500m and so is subject to the Drake Passage Effect. The tracer is advected northward

slightly more quickly in the equatorward western boundary currents along Africa and Australia, but in general, the front seems to diffuse uniformly northward. One notable exception is in the North Pacific, north of the 4000m contour along the equator and north of New Guinea. Here the maximum of the NADW tracer is in the deepest grid box (at 4776m) and moves a bit more quickly as the bottom boundary currents are stronger due to the absence of bottom friction in the model.

Figure 26a shows the maximum concentration of the NADW tracer 1000 years after the onset of NADW production. This is also the approximate e-folding time for the NADW tracer in the northern North Pacific; the concentration at the northern extreme is ~35% of its steady state value. Comparing the depths of the NADW maximum in Figure 25b and Figure 26a shows that there is little change in its relative place in the water column, although there is a slight deepening over time in the Southern Ocean from the Australian Bight (~130°E) to the Drake Passage. It is reassuring that the general location of the NADW core in the water column agrees well with the observational evidence [Reid, 1989].

The flux of the NADW tracer into or out of the water column and the local convective depth are shown in Figure 26b. In areas where the flux is negative, these fluxes can be thought of as the replacement of 100% NADW-colored water with an equivalent volume of uncolored water. The only location where the tracer is being added (shading) is north of 60°N in the Atlantic. Tracer that remains at the surface south of there is removed quickly [$\tau=(50\text{day})^{-1}$]. A fraction of the tracer

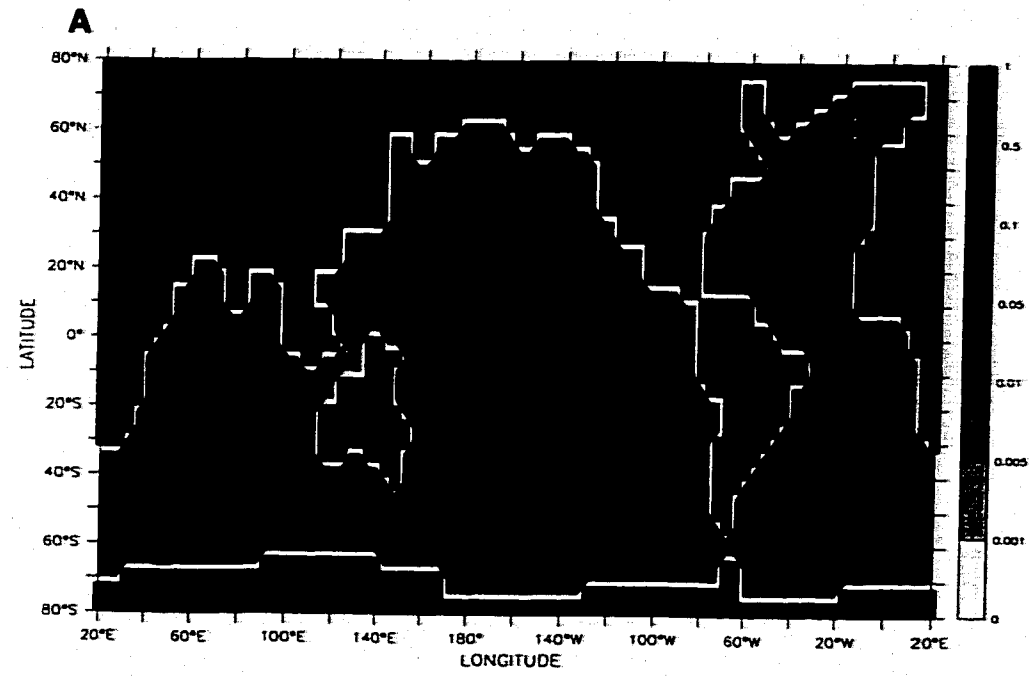

After 1000 Years

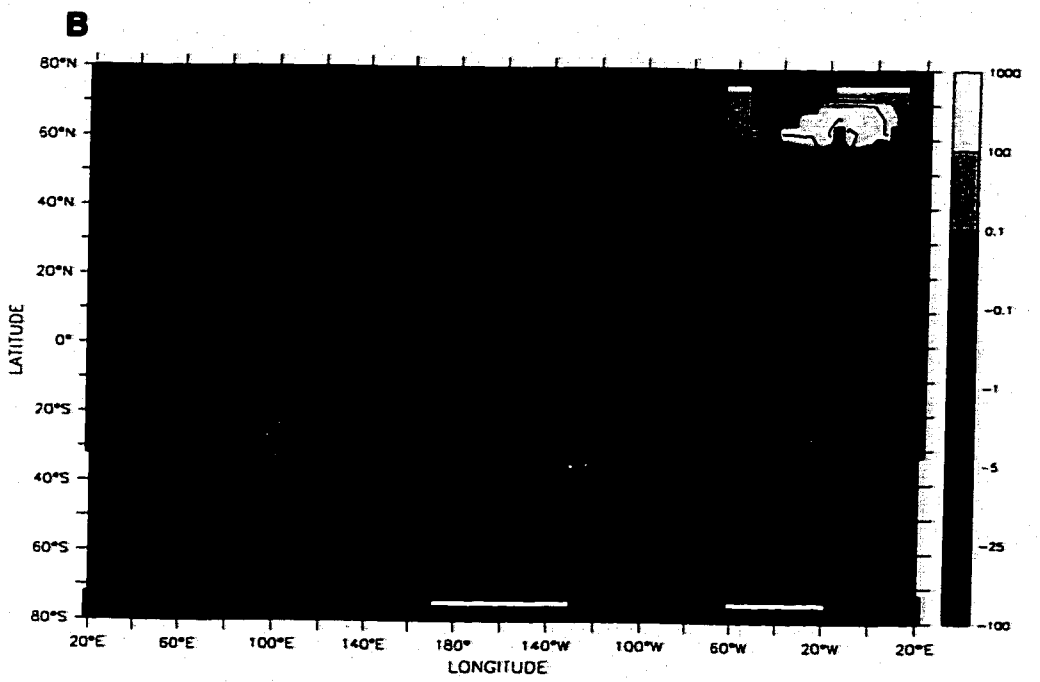

Flux of NADW Tracer at the Surface

FIGURE 26 : A) Maximum fraction of the water column tagged with the North Atlantic tracer (shading) and depth of the maximum (contours) at 1000 yrs. Contour lines at 500 m, 1000 m, 1500 m, 1750 m, 2000 m, 2500 m, 3000 m, and 4000 m; the 2000 m contour is darkened. B) Flux of NADW tracer at the surface in 1000 m^3s^{-1} at 1000yrs (shading). The local depth of surface convection (contours), contours at 50 m, 250 m, 500 m, 1000 m, 2500 m, and 4000 m. The 500 m contour is darkened.

upwells locally in the tropical Atlantic (~9%), but most of the tracer is carried into the deep ocean and is not re-exposed to the surface until it is adjacent to the coast of Antarctica. The largest fluxes of NADW tracer out of the ocean are in the Pacific sector of the high-latitude Southern Ocean. The lower layer velocities (see Figure 21d) advect the tracer into the convecting regions (Figure 26b, contours) in the model's Ross Sea. Of the 8.8 Sv of NADW tracer added north of 60°N, 3.3 Sv or 38% are removed south of 60°S. If only the net color addition north of 20°N is considered (6.2 Sv) to remove the effect of the local gyre recirculation, then the amount removed near Antarctica is over 50% of the total.

There is a direct relationship between the tracer flux contours and the convective depth contours throughout most of the Southern Ocean, especially southeast of Africa in the Agulhas retroflection region where mixing is strong, and in the swath from south of Australia to the southern tip of South America where mode waters are formed [McCartney, 1977]. Most of the remaining tracer is removed in the equatorial upwelling regions in the Indian and Pacific basins and there is a very small fraction removed in the northwest corner of the Pacific.

To sum up, the advective time-scales of NADW spreading in the model are much slower than the baroclinic adjustment time-scales due to the onset of convection in the North Atlantic. The "interface" between the "upper" and "lower" layers responds on the quicker adjustment time-scale. Much of the passive tracer input into the North Atlantic convection region does not reemerge at the surface

until it is adjacent to the coast of Antarctica. The e-folding time for changes in the average Southern Ocean stratification is a few hundred years and the e-folding time for the advection of North Atlantic properties into the extreme North Pacific is about 1000 years.

TABLE 5. Various locations of the time series referred to in the text.

NAME	LOCATION or DEFINITION
North Atlantic Overturning	Maximum of the overturning stream function, north of 50°N
Gulf Stream	80°- 68°W, 28°N, 0 - 1058m
Deep Western Boundary Current	80°- 68°W, 28°N, 1290 - 3266m
Tropical Atlantic Upwelling	Atlantic Ocean, 20°S - 20°N, 1000m
Atlantic Outflow	Maximum of the overturning stream function at 30°S
Agulhas Leakage	26°E, 42°- 34°S, 0 - 1000m
Tropical Indian Upwelling	Indian Ocean, 20°S - 20°N, 1000m
Indonesian Throughflow	120°E, 18°- 6°S, 0 - 675m
Tropical Pacific Upwelling	Pacific Ocean, 20°S - 20°N, 1000m

10.0 Time Series at Significant Locations

This section will show the evolution of the transport at various locations as the system responds to the North Atlantic overturning. All of the figures in this section will indicate the change in transport at the stated location, relative to the initial steady-state circulation (without NADW). Table 5 gives the locations where the time series were recorded.

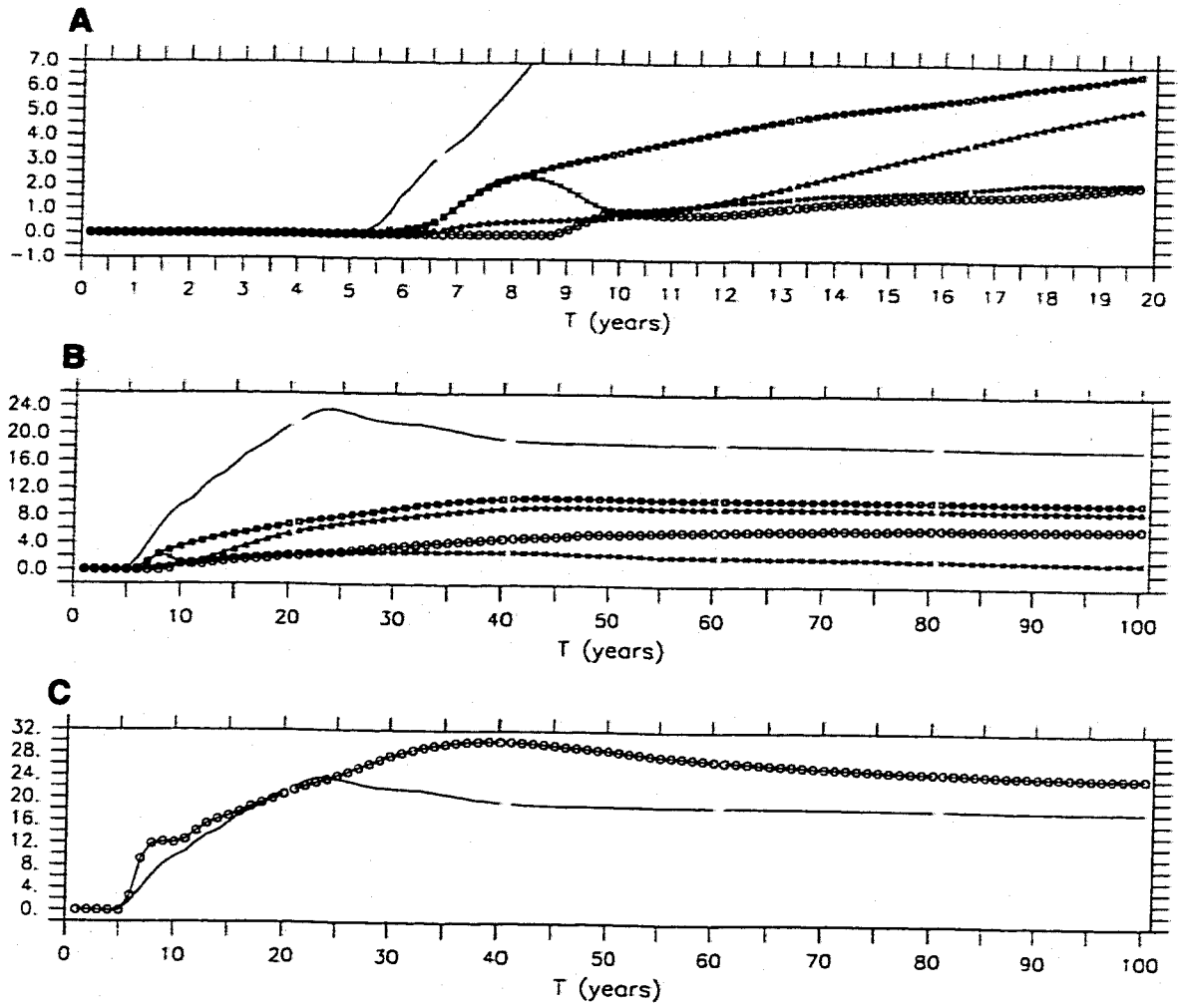

FIGURE 27 : See Table 5 for the precise location of each time series. A) Changes over the first 20 years in Sv of the Atlantic's maximum overturning (no symbol), northward flowing Gulf Stream (squares), southward flowing deep western boundary current (triangles), tropical upwelling at 1000m (crosses), and outflow at 30°S (circles); B) as in A but over the first 100 years; C) the change in heat released north of 40°N over the Atlantic in Wm^{-2} (circles), overturning in Sv (no symbol).

10.1 Spin-up

As shown in Figure 17a-c, the surface salinity and the volume of water mixed by convection increase at an exponential rate, while the overturning circulation increases more linearly in time. Figure 27a shows that the increased transport in the Gulf Stream (squares) and the deep western boundary current (DWBC, trian-

gles) both trail the increase in overturning (no symbol). This implies that the convectively mixed water is supplied and upwelled locally (north of 28°N) at first. The signal's path marks the parts of the ocean that have become involved in the adjustment. For the first 3 years after the forcing change (between model years 6 and 8), the increased flow in the Gulf Stream is supplied entirely by increased upwelling between 20°S and 20°N in the Atlantic. Tropical upwelling peaks at 2.4 Sv and then gradually weakens to a value of 1.9 Sv after 100 years [Figure 27b].

The long-term differences between the changes to the Gulf Stream transport and the DWBC transport [Figure 27b] are an artifact; the region over which the transport is calculated is fixed and only captures the core of the DWBC, which deepens slightly over the first century. The barotropic vorticity at this latitude, however, does not change; it is determined solely by the wind stress, because there is no topography to interact with the baroclinic transport and all northward mass transport in the upper layer must be balanced by a southward transport in the lower layer [Holland, 1973; Mertz and Wright, 1992]. Nearly 2/3 of the transport in the DWBC at 28°N reaches the southern extreme of the basin at 30°S and flows into the ACC (circles).

The excess heat released to the atmosphere north of 40°N over the Atlantic is shown in Figure 27c; the Atlantic's extra northward heat transport at 40°N attains a maximum of 0.4 PW, which, when divided by the area of the Atlantic north of 40°N, yields a release of just over 30 Wm^{-2}. The heat transport and

release increases linearly with the overturning, but continues to increase for over a decade after the overturning reaches its maximum. If the Atlantic's "conveyor" circulation were to shut down, the loss of this heat transport would be one of the first major indicators.

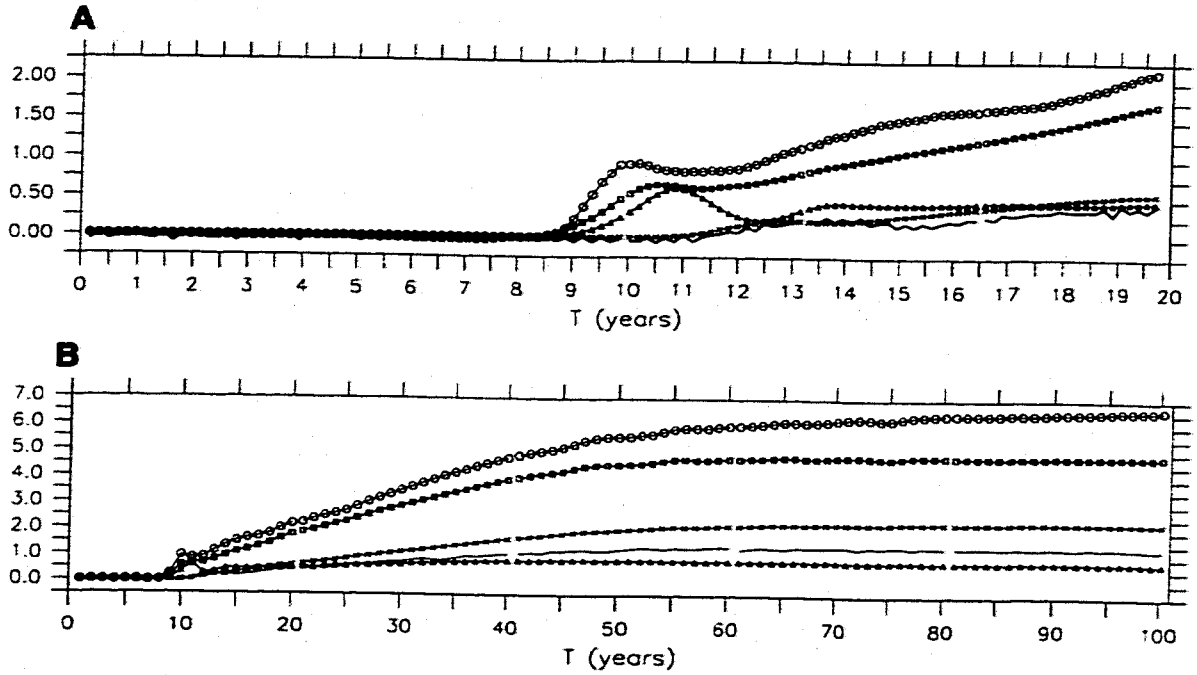

FIGURE 28 : Changes in Sv of the Atlantic outflow (circles), westward flowing Agulhas Leakage (squares), Indian Ocean tropical upwelling at 1000m (triangles), westward Indonesian throughflow (crosses), Pacific Ocean tropical upwelling at 1000m (no symbol); a) the first 20 years, and b) the first 100 years.

Questions remain about the source of the inflow water needed to balance the export of NADW from the basin, often referred to as the "*warm-*" or "*cold-*" water route debate [Gordon, 1986; Gordon, et al., 1992; Rintoul, 1991]. As the outflow of NADW across 30°S increases (Figure 28a,b, circles), transport in the Agulhas Leakage (Figure 28a,b; squares; defined here as the westward flow in

the model above 1000 m, south of Africa) tracks it quite closely: the classical picture of the warm-water route. It must be noted that in nature, the majority of the westward transport in the Agulhas Leakage is likely in the form of baroclinic eddies [Gordon, 1986; Gordon, et al., 1992] which are not resolved in this model. This region, however, is directly in the path of the baroclinic adjustment signal, so it is not surprising that the modeled response there is sizable. In the idealized 3-basin domain used in G98, the Agulhas Leakage seemed to account for about half of the inflow, partly as Indian Ocean surface water and partly as Antarctic Intermediate Water (AAIW) that had been slightly modified by a circuit through the Indian Ocean. In this experiment, the Agulhas Leakage transport could replace 65% of the water which flows out of the Atlantic at depth. It should be noted that the "leaked" water between the surface and ~400 m is entrained into the southward flowing western boundary current, while the water between 400 m and 1000 m eventually flows northward across the equator in the Atlantic.

The increased transport in the Agulhas Leakage is initially supplied by increased upwelling in the tropical Indian Ocean, but this upwelling levels off after about a decade while the flow through the Indonesian Passage continues to increase. At steady state, the westward Indonesian Throughflow is about 2 Sv stronger when NADW is being formed. The increase in the Throughflow is about half of the increase in the Agulhas Leakage which supports the warm-water route, but also indicates that the Leakage water must have an additional source, proba-

bly recycled AAIW. The Pacific Ocean upwelling curve is nearly identical to the Indonesian Throughflow curve for the first 15 years; this implies that the increased deep flow into the Pacific is balanced by outflow through the Indonesian Passage. After 100 years, there is a greater volume of upwelling in the Pacific than in the Indian due to the larger area in the Pacific.

10.2 Spin-down vs. Spin-up

The modern climate includes NADW formation, but many studies have shown that this process is sensitive to the fresh water balance in the North Atlantic [Bryan, 1986b; Huang, 1993; Rahmstorf, 1995]. Several coupled modeling studies have indicated that one possible result of atmospheric warming is an increased hydrological cycle which may alter this balance [Bryan and Spelman, 1985; Cai, et al., 1997]. This raises a few questions: If the rate of NADW formation will change (or is changing), how could we tell? Where should we expect to see changes and when should we see them?

The following experiment was performed to address these questions: starting from the equilibrium of the model run with NADW production, a negative salinity anomaly is imposed into the restoring boundary condition at year 5, the exact opposite of the Spin-up experiment. All other forcing parameters remain the same. Rahmstorf (1995) and McDermott (1996) performed experiments in which the salinity of the North Atlantic is slowly changed, both up and down, and determined that there was some hysteresis involved. This behavior is not seen here; those

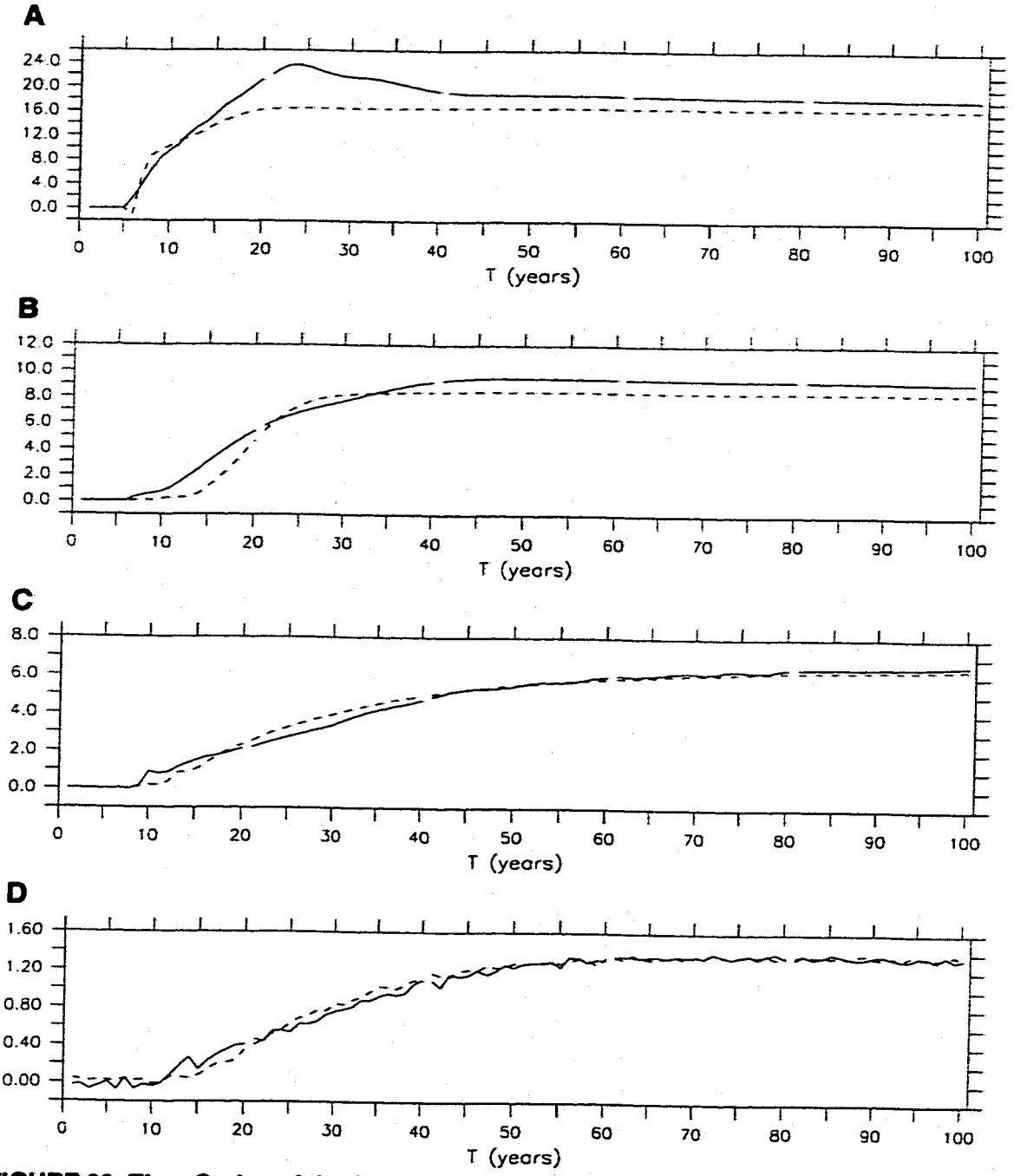

FIGURE 29 :Time Series of the Spin-up and Spin-down experiments. In each figure, the solid line is the result of the Spin-up run, and the dashed line is the result of the Spin-down run, inverted for comparison. All units are in Sv. A) change in the maximum North Atlantic Overturning, B) change in the Deep Western Boundary Current at 28°N, C) change in the outflow from the Atlantic at 30°S, D) change in the Pacific tropical upwelling, 20°S-20°N at 1000m.

studies used mixed boundary conditions (restoring temperature and a fixed salinity flux), which effectively decouples the salinity flux from the advection. The restoring boundary condition for salinity in the Spin-down run guarantees that final state will be the same as the No-NADW equilibrium.

As with the Spin-up experiment, the circulation responds quickly to the forcing change and convection in the GIN Sea region disappears within a few months. The boundary layer path taken by the adjustment is exactly the same as the previous run, so it will not be restated here. Figure 29 shows the comparison between the Spin-down and Spin-up experiments over the first century, the solid line is the change as NADW starts, and the dotted line is the change as NADW is eliminated, but flipped so that both series are positive. Figure 29a shows the change in the NA overturning: the circulation actually increases a small amount, but then decreases at a faster rate than it increased. The halocline over the sinking region forms quickly so the stratification is capped at the top and the overturning just stops, whereas in the Spin-up case, the new dense water has to "cut" through the existing stratification. Unlike the Spin-up run, the circulation does not overshoot its equilibrium value.

The deep western boundary current starts to increase sooner than it starts to decrease [Figure 29b]. The pool of dense water under the sinking region takes a few years to dissipate, so the deep flow continues even though the convection has stopped. Once the DWBC does feel the change in the forcing, the flow

decreases rapidly; by model year 25 (two decades after the change), the DWBC in the Spin-down experiment is close to its steady state value, while it increases for the first 35 years of the Spin-up run. As noted before, the barotropic circulation remains constant, so the evolution of the Gulf Stream mirrors the DWBC.

The lag seen in the DWBC response is also seen in the time series of the outflow at 30°S [Figure 29c]. The increase in outflow begins at about model year 9 in the Spin-up run, but the decrease doesn't begin until model year 12 in the Spin-down case. As with the other time series, the rate of decrease is quicker than the rate of increase, but after model year 45, the two curves are almost identical. When the adjustment reaches the Pacific basin [Figure 29d], there is only a slight hint of the initial lag and the quicker decrease. The trend seen in these figures is that the system responds more similarly to increased and decreased deep water formation farther downstream from the forcing region.

11.0 Summary and Discussion

This is the most recent in a series of experiments using numerical models to study the oceanic baroclinic adjustment to a deep water source. Stommel & Arons (1960), Kawase (1987), Cane (1989), and Huang, et al. (submitted) all used a simple two-layer model to study the spin-up process and/or the steady state interface displacement due to deep water production. Two layers, however, can only capture the first baroclinic mode, and while this mode generally has the largest

amplitude and travels the fastest, there is no reason to rule out the effects of other modes arbitrarily, especially on longer time-scales.

McDermott (1997) explored the baroclinic response in an OGCM to a changed wind stress over the Southern Ocean. As in this study, he compared the response in cases with and without convection in the North Atlantic, and noted that the model did exhibit some higher order effects. His study, however, was focused on an upper layer disturbance forced at the free surface, while this study examines a source to the lower layer through an internal interface. The main purpose, here, is to investigate the baroclinic response to a lower-layer mass source from a physical oceanographic perspective. This study allowed me to address some other questions including the spatial and transient differences between adjustment and advection, and the relevance of baroclinic adjustment to climate studies.

The initial condition for this experiment was the steady-state circulation in the model with the NADW production artificially eliminated. This state was chosen to explore the baroclinic adjustment associated with deep water formation in North Atlantic, in the presence of a background circulation. It is unlikely that the pre-existing circulation affected the initial baroclinic boundary wave propagation which is directed more by the domain than the stratification. There may be some non-linear effects in the subsequent development of the response, but the goal was to

eliminate as many other factors as possible, in order to isolate the adjustment process in an environment that more closely approximates the real ocean.

The transient part of the baroclinic adjustment in the OGCM is quite similar to the two-layer models; the boundary layer path, the pressure perturbations at the interface, the upper-layer thickness and the spin-up of the lower-layer velocity field are all comparable. The response in the OGCM is insensitive to the choice of model domain (idealized or realistic), the background forcing (Levitus, 1982; Levitus, et al., 1994a,b; zonally-averaged or full fields), and the method by which deep water formation is initiated or curtailed (salinity anomaly or suppressed convection). The fastest "signal" by which the baroclinic adjustment is communicated consists of upwelling through the "interface" accompanied by flow toward the source region in the upper layer, and flow away from the source in the lower layer.

A coastal and equatorial boundary layer path connects all three ocean basins north of the ACC. The initial deep water pulse, a mass source to the lower layer, creates a series of upwelling Kelvin waves which propagate as follows: equatorward on western boundaries, eastward at the equator and then poleward on eastern boundaries, a cyclonic sense in both hemispheres. The upwelling Kelvin waves lead to the creation of long baroclinic upwelling Rossby waves along the eastern boundaries. These waves then propagate into the ocean's interior, allowing more of the interface to play a role in balancing the mass source and sink. The upwelling anomaly is spread out quickly and all locations north of the

ACC are affected in less than 20 years after the initial pulse. The change in upwelling, and therefore the change in stratification, is spread throughout the world ocean on the adjustment time-scale.

One noticeable difference between the response of the OGCM and the two-layer model is that there is no consistent way to create a very large, instantaneous mass source to the lower layer in the OGCM. The previous studies all initiate their deep water source at full strength, whereas in this study the North Atlantic overturning takes several years to reach a significant size, and several decades until it approaches its new equilibrium value. This implies that the oceanic response exhibits some "inertia" as it responds to large changes in the deep water formation rate, and this is true for both increased and decreased overturning.

Coincident with the increase in overturning, the northward heat transport in the Atlantic increases linearly in time and continues to increase for 10-15 years after the overturning has stabilized (at about year 20). As much as 0.5 PW of heat are transported northward of 20°N and over 0.4 PW reach 40°N, equivalent to an extra 30 Wm^{-2} of heat released over the North Atlantic north of 40°N. Observations of the heat transport in the Atlantic put it closer to 1 PW [Trenberth and Solomon, 1994], but most coarse resolution OGCMs underestimate this, due to the overly diffuse thermocline structure [Bryan, 1987]. It is quite possible that the true heat transport could be twice as big as the model response for the same level of overturning. Whether this amount of heat release can be solely responsible for

the dramatic warming at the end of the Younger Dryas cold period (5-10°C in 20 years, Severinghaus, et al., 1998) is unclear. These results are similar to the oceanic component of the coupled GCM experiment by Manabe and Stouffer (1988) in which they observed a warming of 6-10°C over the GIN Sea region for the same heat transport (~0.4 PW or 30 Wm^{-2}).

A "communication time" of 20 years to the North Pacific, the most remote part of the world ocean from the North Atlantic, is much faster than usually cited in the literature. Bryan (1986a) cites some observational changes to the deep water properties in the North Atlantic during the 20 years between large-scale surveys [Brewer, et al., 1983; Roemmich and Wunsch, 1984] and linked these to thermohaline variability. These changes, however, were local and Bryan (1986a) did not address how quickly or where a remote change might occur. Bryan also describes a reorganization of the model's THC within 50 years. Several authors have discussed internal variability in stand-alone OGCM experiments with roughly 20, 50, or 300 year cycles [Mikolajewicz and Maier-Reimer, 1990; Weaver & Sarachik, 1991; Weaver, et al., 1991; Weaver, et al., 1993; Greatbatch and Zhang, 1995; Drijfhout, et al., 1996; Huck, et al., 1999], but a non-local communication time on the order of decades has yet to be examined.

It must be acknowledged that the parameterization of convection in the model is necessarily too simplistic to capture the finer structure of open-ocean convection, but this is not crucial as this study focused on the effects resulting

from the process of deep water formation and not the process itself. Also, the time-scales presented are dependent on the model's resolution and friction parameterization. These caveats aside, the basic adjustment process in the OGCM is quite robust: deep water formation in the North Atlantic causes the model's upper-layer isotherms to shoal throughout the world ocean, north of the ACC. Although sea surface temperatures (SSTs) are tightly held to the restoring boundary condition, the model had to add more heat to keep the SSTs constant during the Spin-up run. This implies that with increased NADW production, the thermocline has risen and the SSTs have cooled under the fixed thermal forcing. The magnitude of the tropical response is still an open question, but it seems at least plausible that changes in the North Atlantic could have noticeable effects on the strength, timing, and low-frequency variability of ENSO and other tropical phenomena which rely on the upwelling of sub-thermocline water [Battisti, 1988]. If so, a future decrease in the rate of NADW formation and the associated decreased upwelling could affect these major climatic processes, shifting the balance toward one extreme and changing the mean state. The effects of multi-decadal variability in the production of NADW on the oceanic structure will be examined in future work.

The patterns of adjustment and advection in the OGCM are quite different spatially as well as temporally. Advection does not follow the boundary layer path described above; a passive tracer reveals that NADW travels down the eastern

coast of the Americas where it joins the ACC after about a century, at which time the adjustment is 80% completed globally (defined as the ratio of the change in isotherm depth to the steady-state difference). The NADW tracer is quickly advected zonally by the strong currents there and is gradually mixed into the model's circumpolar water and spreads southward. Over 50% of the tracer incorporated into NADW is removed from the system near Antarctica, south of 60°S. The tracer seems to spread northward from the ACC more diffusively with slightly enhanced advection along the southwestern boundaries of the Indian and Pacific and along the equator. The e-folding time of the NADW tracer in the model North Pacifc is just over 1000 years. The model successfully reproduces the path and the depth of the NADW maximum, especially in areas of the Southern Ocean where mode and intermediate waters are formed [McCartney, 1977, Reid, 1989].

This model simulation supports the warm-water route theory, in which the export of deep water from the Atlantic is balanced primarily by flow from the Indian Ocean westward around the southern tip of Africa (called the Agulhas Leakage) and into the Benguela current along West Africa. This balance is likely in the form of baroclinic eddies which are not resolved by this model, but the Agulhas Leakage is directly in the boundary wave path taken by the adjustment signal so baroclinic changes in the flow (westward above and eastward below) there are not unexpected.

The differences between the onset and cessation of deep water formation are compared and are found to be remarkably similar, although the ocean seems to exhibit some "inertia" here as well: deep water production begins to increase sooner but at a slower rate than it decreases. This timing difference is also seen in the strength of the deep western boundary current, and the differences become much weaker farther downstream: in the Pacific, the responses to the initiation and cessation of NADW formation are identical.

Fluctuations in the strength of the North Atlantic overturning and the poleward heat transport are well documented on millennial, centennial, and decadal time scales. These changes have had a large effect on the climate over Europe and Greenland and it has been suggested that many of the large-scale reorganizations of the entire climate system over the glacial-interglacial cycle are intimately tied to the state of the North Atlantic circulation [Broecker, 1988; Manabe and Stouffer, 1988; Charles and Fairbanks, 1992]. More recently, evidence has emerged from ice cores in Greenland and Antarctica as well as deep-sea sediments which seem to indicate that during global climate reorganizations, changes begin near Antarctica several millennia before changes appear in the northern hemisphere [Sowers and Bender, 1995; Bard, et al., 1997; Petit, et al., 1999].

The implication of this evidence is that the Southern Ocean, with its strong wind forcing, ice formation and weak stratification, is playing a (or the) major role in the maintenance of the world ocean's structure. As noted in Goodman (1998),

the global THC seems to be quite modular with each high-latitude basin responding to its own forcing. As the Southern Ocean is the source for all of the world's bottom water and much of the intermediate water, there will be no full understanding of the THC and its role in the global climate until we can explain and reproduce the physical mechanisms (open-ocean mixing, shelf processes, effect of sea-ice on the freshwater balance, etc.) at work there.

Chapter 3

Forced Variability of NADW Production in an OGCM

12.0 Introduction

The thermohaline circulation in the world ocean is driven by heating, cooling, freshening and salinification around the globe. Deep water is formed in the northern North Atlantic as warm water is carried north by the Gulf Stream and then evaporated and cooled substantially at high-latitudes. This process is generally regarded as the first step in the density-driven overturning of the global ocean: the thermohaline circulation (THC) which has been likened to a great conveyor belt. Convection in the GIN Sea region, north of the Greenland-Scotland ridge creates a pool of cool, salty water which then overflows through various fissures and is entrained into the southward flowing deep western boundary current as the core of the NADW mass. This overflow has been shown to vary on inter-annual time-scales [Dickson and Brown, 1994], possibly linked to the NAO [Dickson, et al., 1999], but as yet, we do not understand the cause of this short-term variability.

Also, the $\delta^{18}O$ fractionation from ice cores and ocean sediments shows that the formation of NADW has varied on centennial to millenial time-scales in the past [Bond, et al., 1993]. This longer-term variability has been linked to global variability throughout the climate system over the course of the last few glacial-

interglacial cycles [Charles and Fairbanks, 1992; Lowell, et al., 1995; Guo, et al., 1998]. Whether the connection between thermohaline variability in the Atlantic and global changes in remote regions of the ocean is transmitted through the ocean or the atmosphere is unclear and needs further exploration. Sowers and Bender (1995) showed that as the globe emerged from the last glacial period, and again at the end of the Younger Dryas, changes to the air temperature proxies in the Antarctic ice cores lead those from Greenland by 2000-3000 years. It has yet to be explained how a thermohaline circulation, driven by Atlantic processes, can cause changes near Antarctica first, although Broecker (1998) recently proposed that there exists a "seesaw" relationship between deep water production in the northern and southern hemispheres.

This study is the third in a series by the author designed to assess the role of NADW production in the global THC. The first explored the different steady states of the model with and without NADW formation [Goodman, 1998, G98 hereafter] and the second explored the transition from each state to the other [Goodman, in review; Part II, hereafter]. Here, an OGCM is used to examine how, and to what extent, variability in the formation rate of NADW is communicated to the rest of the world ocean. Several modelling studies have examined internal variability in the rate of NADW production [Mikolajewicz and Maier-Reimer, 1990; Delworth, et al, 1995, 1997; Weaver, 1995, Huck, et al., 1999], but this experiment does not fall into that category. In this study, the variability is imposed as an external forcing

into the restoring boundary condition on the salinity over the North Atlantic. It must be noted that the external causes responsible for the variability of NADW production will not be explored here, but the results will permit a speculative assessment of their likely character. The implied rates of freshwater input and removal imposed on the model are generally larger than any of the proxy evidence indicates. These experiments can then be considered an upper bound on the possible effects which NADW production can cause around the globe.

Results indicate that there are significant changes in the Atlantic basin as the formation rate of NADW is varied, the largest of which is the northward heat transport which varies by almost 0.4PW at 40°N in as little as 30 years. Changes in the mid-depth stratification are felt throughout the Atlantic and to a lesser extent in the Southern Ocean. Overall, the impact of NADW variability is quite small in the Indian and Pacific basins. All locations in the model vary with the same period as the imposed forcing, although in some runs, higher order frequencies are seen. Section two will discuss the model and the methods employed and section three will present the results from the various model runs. Section four will give a discussion of the results and their implications for the "conveyor-belt" hypothesis and the probable role of NADW variability in the global climate, and section five will present some conclusions.

13.0 Methods

13.1 Model

These experiments were performed in and ocean-only general circulation model, the Modular Ocean Model (MOM1.0) from GFDL [Pacanowski, et al., 1991]; no atmospheric, sea-ice or land surface model is included. The grid resolution is 4° by 4° and the domain covers 360° longitudinally and extends from 80°S to 80°N, so there is no Arctic Ocean present in this simulation. There are 20 levels of increasing thickness from 50m at the surface to 449m at the bottom, comprising 5000m in total. The global coastline was interpolated onto the model grid, and the bottom is flat everywhere, except in the Drake Passage, the marginal polar Atlantic seas, and the Indonesian archipelago. The bathymetry and sill depths at these locations are indicated in Figure 30. The bathymetry, while highly idealized, is nonetheless important as bottom topography provides a mechanism by which changes in the stratification can lead to changes in the baroclinic flow. As will be shown, these changes are not insubstantial near Iceland and Indonesia.

The forcings employed are restoring boundary conditions on both temperature and salinity, taken from Levitus, et al. (1994a,b) climatology. There is no seasonal cycle imposed in the model; all forcing is annually-averaged. The restoring boundary conditions used here are the 1-D zonal averages for each individual basin north of 40°S, and the 1-D global zonal average south of there. The global

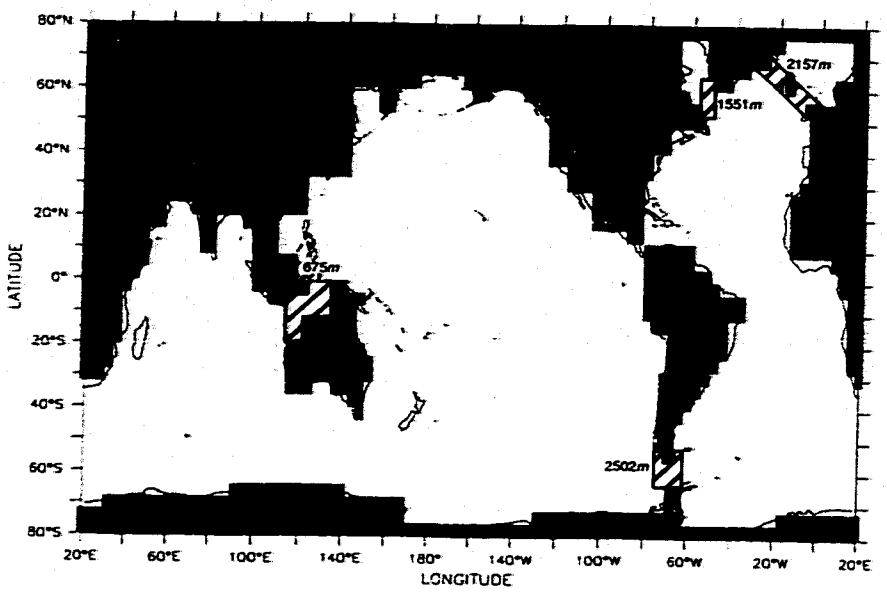

FIGURE 30 :Model Domain is the unshaded area. The hatched areas are locations where the bottom is less than 5000m deep. The contour line is the global sea-level.

average is applied over the Southern Ocean since the mixing there is large and the properties are fairly uniform, especially given the model resolution and idealized bathymetry. As in G98, the restoring salinity near Antarctica is smoothly increased from climatology at 60°S to 35 psu at the southern extreme. To differentiate the forcing between the Labrador and GIN Seas, the Labrador Sea restoring values are reduced by 5°C and 1.5 ppt, roughly equal to the observed differences. The momentum forcing is taken from the zonally and annually averaged wind stress of Hellerman and Rosenstein (1983), applied uniformly at all longitudes. There is no meridional momentum forcing. The model employs no-slip boundary conditions at the walls, free-slip conditions at the bottom, and Cartesian mixing with the same values as in G98.

The model is initiated at rest with a uniform salinity and temperature. The variable forcing is applied during the spinup and all of the long-term drift is dissipated after about 8000 model years. At that point the model is oscillating smoothly about its long-term average "steady" state.

13.2 Experiments

Variability is imposed on the model by adding a salinity anomaly to the targeted restoring salinity north of 40°N in the Atlantic Ocean. The target restoring salinity is varied by adding an anomaly of variable magnitude with a sinusoidal period of 10, 25, or 50 years according to the following formula:

$$(\text{Levitus} - 0.3\ \text{psu}) + \text{AMP}^{*}\cos(2^{*}\pi^{*}\text{model\_year}/\tau) \qquad \text{(EQ 1)}$$

where τ = 10, 25, or 50 years, and AMP is the magnitude of the salinity anomaly, either 0.5 psu or 1.0 psu. The offset of 0.3 psu was included so that the targeted salinity in most runs would not be excessively higher than the observed salinity; when AMP is 0.5 psu the salinity forcing varies from 0.8 psu below the Levitus value to 0.2 psu above. As was shown in G98, a negative salinity anomaly at the surface in the North Atlantic suppresses convection and the formation of NADW.

The different time-scales and magnitudes were used in order to assess the maximal response of the system to large and fast changes in the forcing. When the amplitude of the anomaly is 1.0 psu, the target salinity is outside the observed range of salinities from measurements and proxies, but this experiment is

included to provide an upper maximum on the effect which variability in the North Atlantic can have on the rest of the globe. The magnitude of the implied fresh water fluxes in the simulations will be compared to both observed evaporation minus precipitation rates as well as reconstructed changes in the ice volume during the last glacial period. Four experiments were conducted and are listed in Table 1.

TABLE 6. Experimental Runs

Name	Period (years)	Amplitude (psu)
Experiment 50a	50	0.5
Experiment 25a	25	0.5
Experiment 10a	10	0.5
Experiment 50b	50	1.0

Changes in the strength of the flow at the various choke points of the "conveyor," (the overturning at 50°N, the Gulf Stream transport, the outflow of NADW across 30°S, the Agulhas Leakage, and the Indonesian Throughflow) will be presented. Also, changes in the stratification around the globe will be compared to assess whether NADW variability is a possible source of the wide-spread changes seen in the historical record.

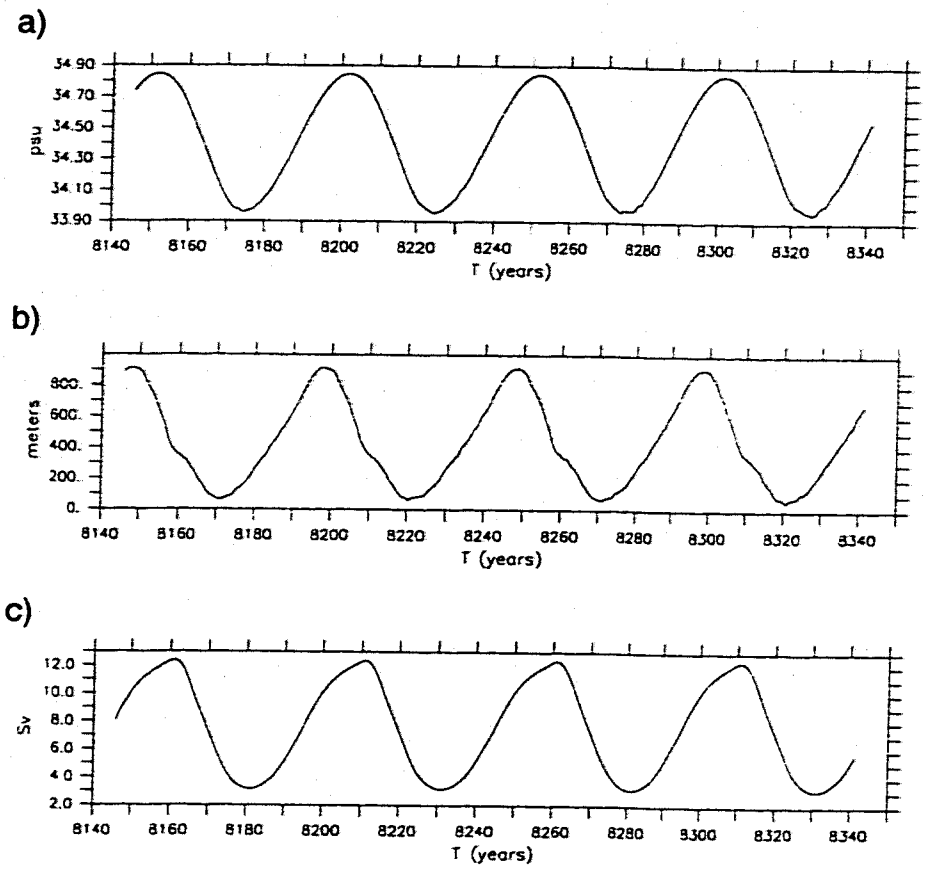

FIGURE 31 :Experiment 50a: a) sea surface salinity in the North Atlantic; b) average convective depth in the North Atlantic; c) maximum overturning at 50°N in the Atlantic.

14.0 Results

14.1 Experiment 50a

The North Atlantic's average salinity, average convective depth and overturning at 50°N from Experiment 50a are shown in Figure 31a,b, and c, respectively. Note how all three model features respond with the same frequency as the external forcing: each peak is 50 years apart. As expected, the surface salinity varies by about 1psu over the course of a cycle. The average convective depth

ranges from a maximum of 910 meters to a low of about 60 meters, but is never eliminated entirely due to the continuous advection of salt from the south. The overturning at this 50°N peaks at about 12.5 Sv and is a minimum of 3 Sv.

The maximum and minimum Atlantic overturning from Experiment 50a are shown in Figure 32a,b. As can be seen, the overturning circulation varies from vigorous to weak. The southern end of the Greenland-Scotland ridge is located at 58°N in the model so overturning north of there is confined to the GIN basin; accordingly, the strength of the outflow from the GIN region will be compared at 50°N. The presence of the sill allows for baroclinic changes in the vertically integrated vorticity balance [Holland (1973), Mertz and Wright (1992)].

Unlike the steady state without NADW production discussed in G98, the upper NA cell always carries some newly formed deep water into the Southern Ocean. This figure is reminiscent of the studies by Rahmstorf (1995) which suggested that the glacial North Atlantic exported the same amount of water to the Southern Ocean, but that the overturning was a bit weaker and much shallower. Fichefet, et al. (1994) reported the same weakening and shoaling of the overturning, but no export of overturned North Atlantic surfcae water to the Southern Ocean during their "glacial" simulation.

Figure 33a shows the variation in transport from the long term mean at various locations along the supposed "conveyor belt." Increased convection leads to increased overturning (downwelling, solid line) which is supplied entirely via the

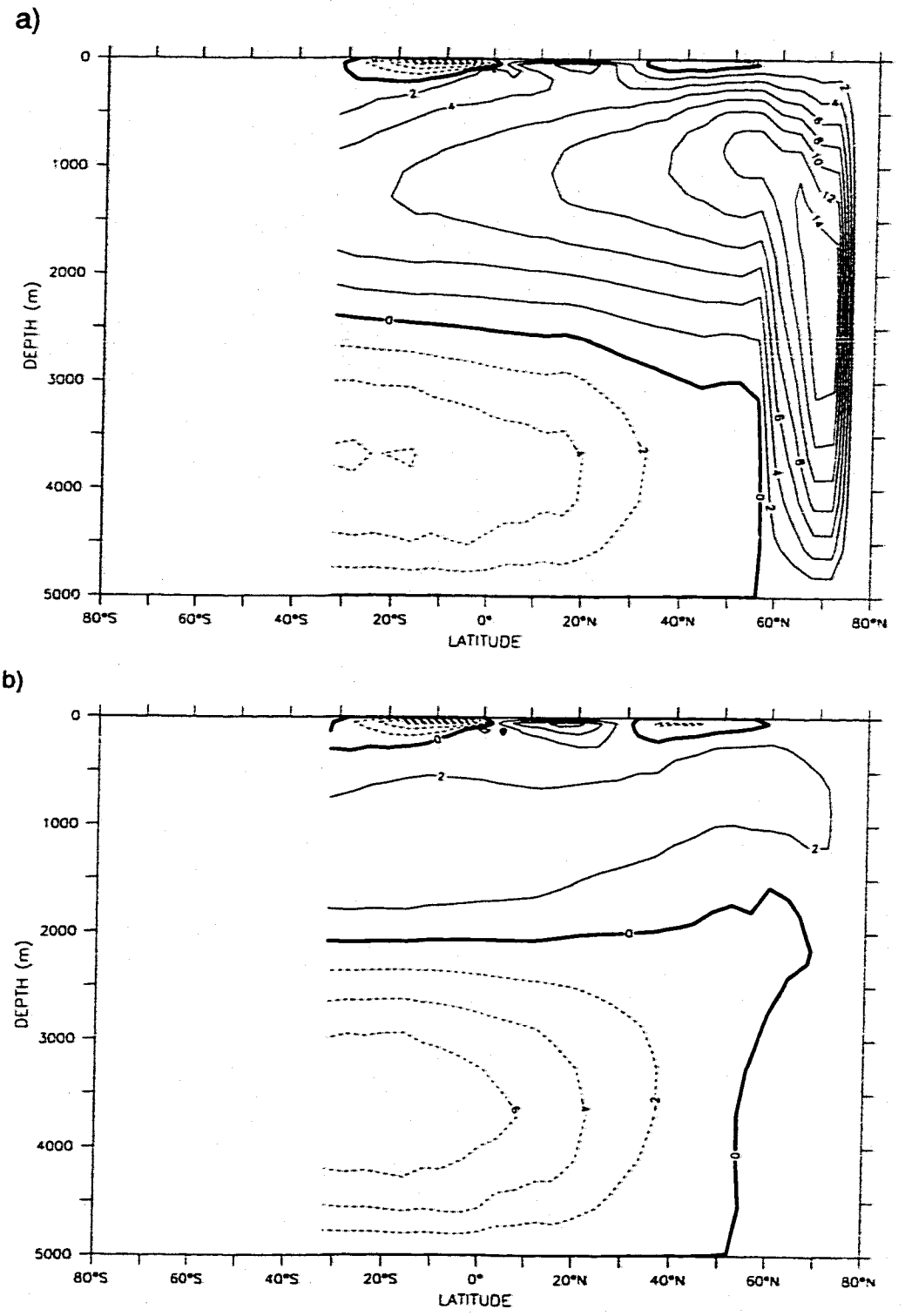

FIGURE 32 : Experiment 50a: a) maximum Atlantic overturning; b) minimum Atlantic overturning.

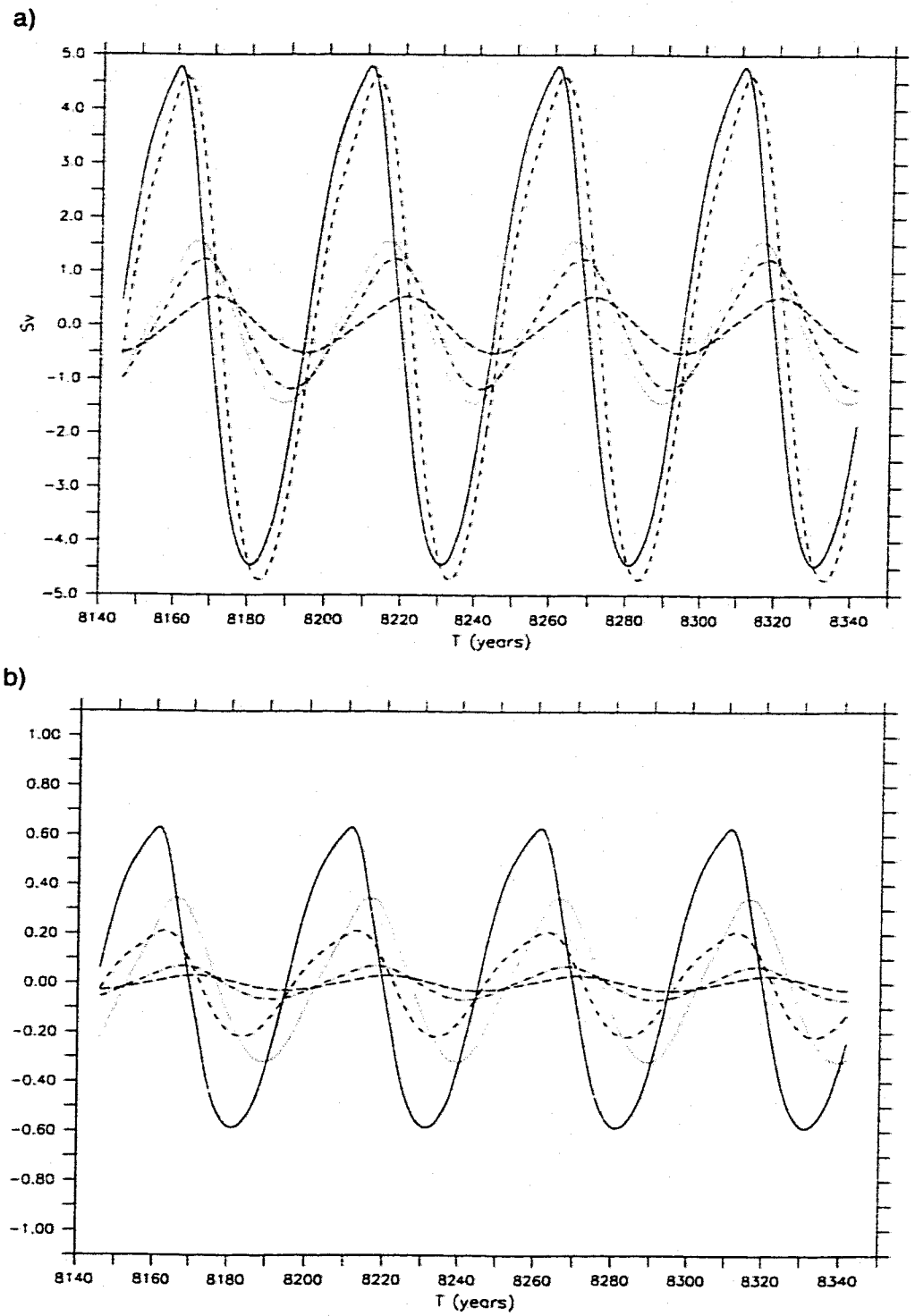

FIGURE 33 :Variation of the transport at various choke points a) in total magnitude (Sv); and b) as a percentage of the mean transport. The choke points are the overturning at 50°N (solid), the Gulf Stram transport at 28°N (short dash), the outflow into the Southern Ocean at 30°S (dotted), the Agulhas Leakage (dash-dot), and the Indonesian Throughflow (long dash).

Gulf Stream current (short dashed line). Variability of the flow out of the Atlantic basin into the Southern Ocean across 30°S (dotted line) is about 40% as large as the variability of the overturning with a lag of approximately 5 years. The outflow variability is mirrored by the nearly identical variability in the Agulhas Leakage (dash-dot line). Lastly, the Indonesian Throughflow (long dashed line) varies by a few Sv, peaking about 10 years after the peak in the overturning. This figure shows the total magnitude of the change at each location, while Figure 33b shows the variation as a fraction of the strength of the transport's average. The overturning at 50°N (solid) changes by about ± 60%, while the larger Gulf Stream (short dash) only varies by about 20%. The outflow at 30°S (dotted) varies by about a third and the Aghulas leakage (dash-dot) and Indonesian Throughflow (long dash) vary by less than 10%. Variability of the transport decreases as the locations become more distant from the North Atlantic and not along the path of the conveyor belt.

The variability in overturning seen in the preceding figures is responsible for large change in the northward transport of heat in the Atlantic basin [Figure 34, shading]. The northward heat transport calculated across a section at 40°N varies from a low of 0.13 PW to a high of 0.51 PW. It is well known that coarse resolution models under estimate the heat transport due to the high values of vertical diffusivity need to maintain stability [Bryan, 1987]. Observations put the northward heat transport in the Atlantic at about 1 PW so the change implied by the model

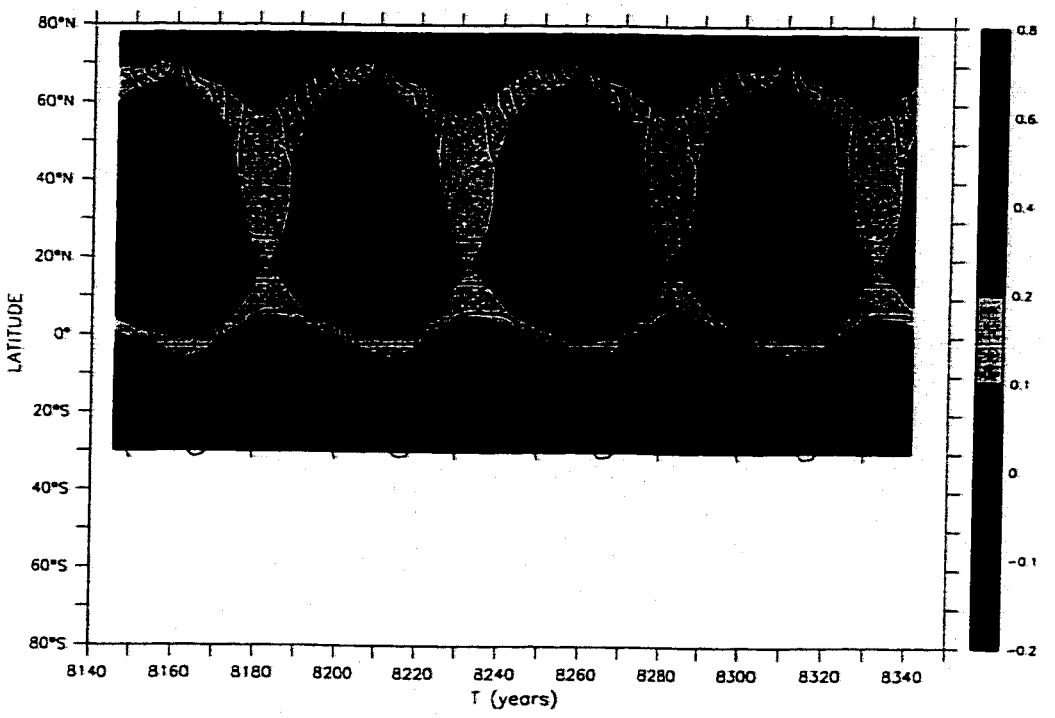

FIGURE 34 :Northward meridional heat transport in the Atlantic in petawatts (shading), and the maximum overturning in Sv (contours).

could be twice as large. The maximum overturning streamfunction is overlaid on the heat transport. Note that the overturning peaks at high latitudes first, slightly before the heat transport at 40°N reaches its maximum. As noted previously, this northernmost overturning is confined by the bottom topography so the peak heat transport at 40°N is synchronous with the peak in overturning at 50°N, not with the highest peak. Also coincident with the maximum overturning, the heat transport south of the equator is northward, in agreement with observations.

Figure 35 shows the heat transport calculated across a section at 50°N (solid) and that it differs from the surface heat flux integrated over the Atlantic, north of 50°N (dashed). These imply that the heat storage within the ocean also

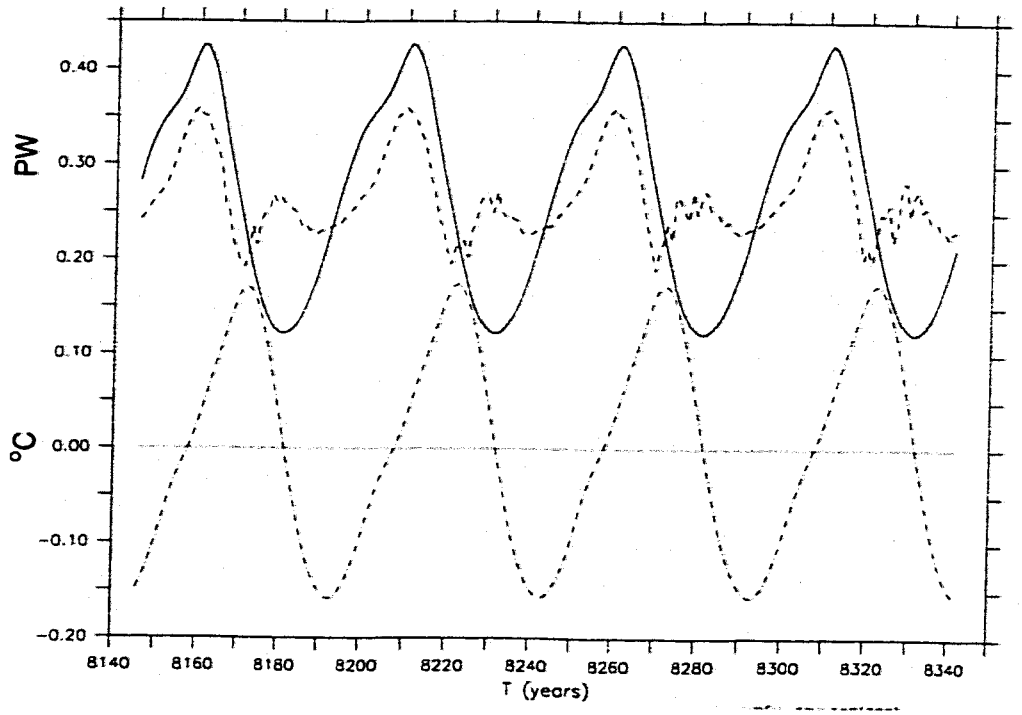

FIGURE 35 : Northward heat transport at 50°N in PW (solid), integrated heat flux out of the North Atlantic north of 50°N in PW (dashed), average temperature anomaly of the entire water column north of 50°N in °C (dash-dot).

varies and this is shown as the temperature anomaly north of 50°N (dash-dot, calculated as the difference from the long-term mean). Note that, as expected, while the heat transport within the ocean is greater (less) than the heat flux out of the ocean, the average temperature is increasing (decreasing). The temperature of the water changes by about 0.3°C averaged from 0 to 5000 m, and there are changes of about 2°C at 250 m.

As the production and transport of NADW increases and decreases, there are changes in the stratification throughout the globe. Figure 36 shows the range of the variation of the stratification at 800 m in parts per thousand. Stratification is

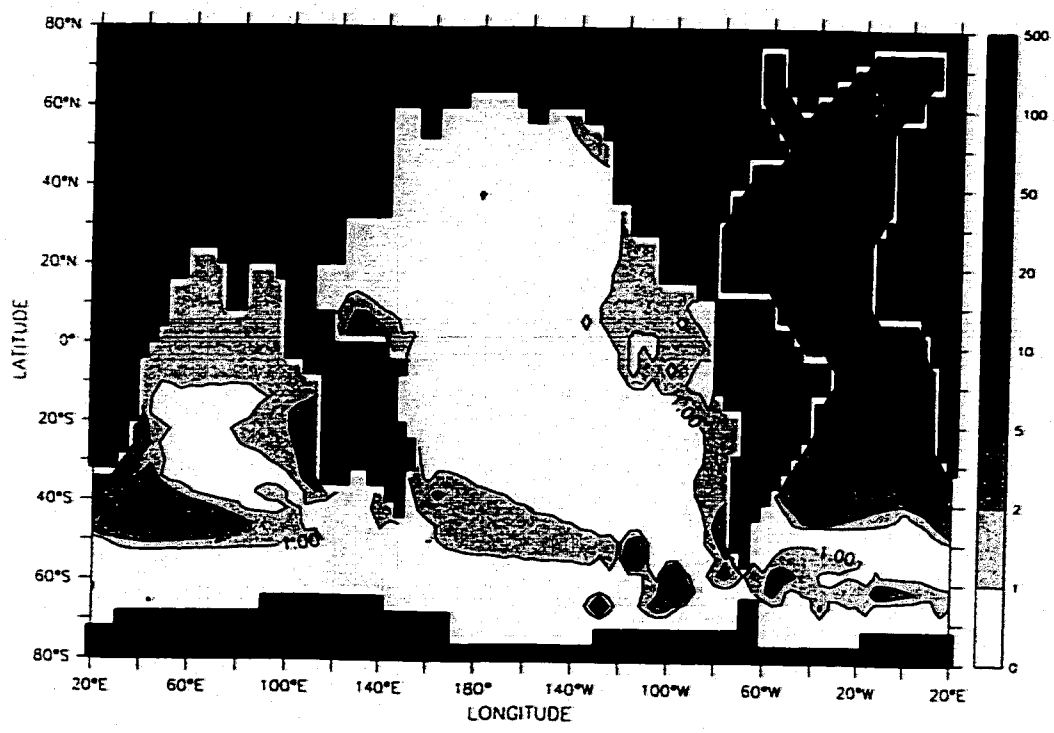

FIGURE 36 : Experiment 50a: Stratification changes at 800 m in parts per thousand.

defined here solely as the vertical density gradient; the range of variation is calculated by subtracting the minimum gradient from the maximum and dividing by the average. All of the major change is in the northern Atlantic, primarily along the path of the western boundary current. There are relatively smaller changes in the mid-latitudes and relatively larger changes near 20°N and 20°S. After NADW joins the ACC, the salt advected with the NADW changes the stratification above the core, especially near 45°S in the southern Indian Ocean. It should also be noted that there are stratification changes in the intermediate water formation regions south of Australia and west of Chile. While the changes in these regions are small,

the stratification in the ACC is generally quite weak [Marshall, et al., 1993] so small changes could affect the overall production of intermediate water.

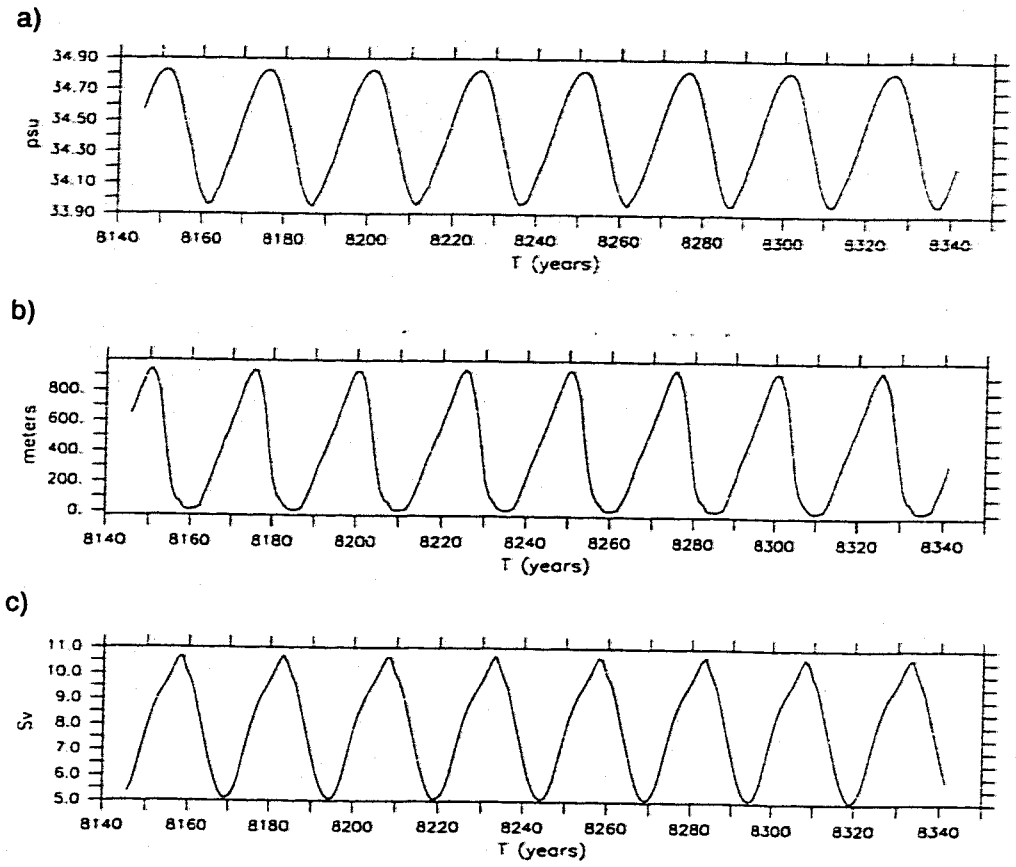

FIGURE 37 :Experiment 25a: a) sea surface salinity in the North Atlantic; b) average convective depth in the North Atlantic; c) maximum overturning at 50°N in the Atlantic.

14.2 Experiment 25a

When the period of oscillation is reduced to 25 years, the salinity, convective depth and overturning at 50°N are quite similar to that for Experiment 50a; the average surface salinity varies from 33.9 to 34.9 psu [Figure 37a], the average convective depth varies between 10 m and 950 m [Figure 37b] and the overturning varies between 5 Sv and 11 Sv [Figure 37c], with the period reduced by a fac-

tor of two as expected. The range of the overturning is smaller as the there is less time when the advection of salt is weak during the same interval that the restoring salinity is at a minimum. That is, the strength of the overturning is determined by both the northward advection of salt and removal of salt through the surface and these are not synchronized as well as in experiment 50a. The overturning reacts on the adjustment time-scale which was determined in Part II to be approximately 25 years, so the 50 year run gives the overturning more time to adjust to the salinity forcing, whereas, here the advection is still increasing after the restoring salinity has started to decrease.

The times of maximal and minimal Atlantic overturning in the 25-year experiment are shown in Figure 38a,b. Note that as in Figure 32b for the 50-year run, the time of minimum still shows overturned water proceding all the way out of the basin across 30°S. Variability in the flow at the choke points in this run is about half of that in the experiment 50a, about means which are nearly identical (not shown). The variability in the heat transport at 40°N in this experiment is also about half of the previous run with extremes of 0.25 PW and 0.42 PW. Figure 39 shows the range of the variability in the stratification for this run as was shown in Figure 36. Changes are of similar magnitude along the western boundary in the North Atlantic, but are much weaker here at all locations in the South Atlantic and minimal to non-existant in the Indian and Pacific basins.

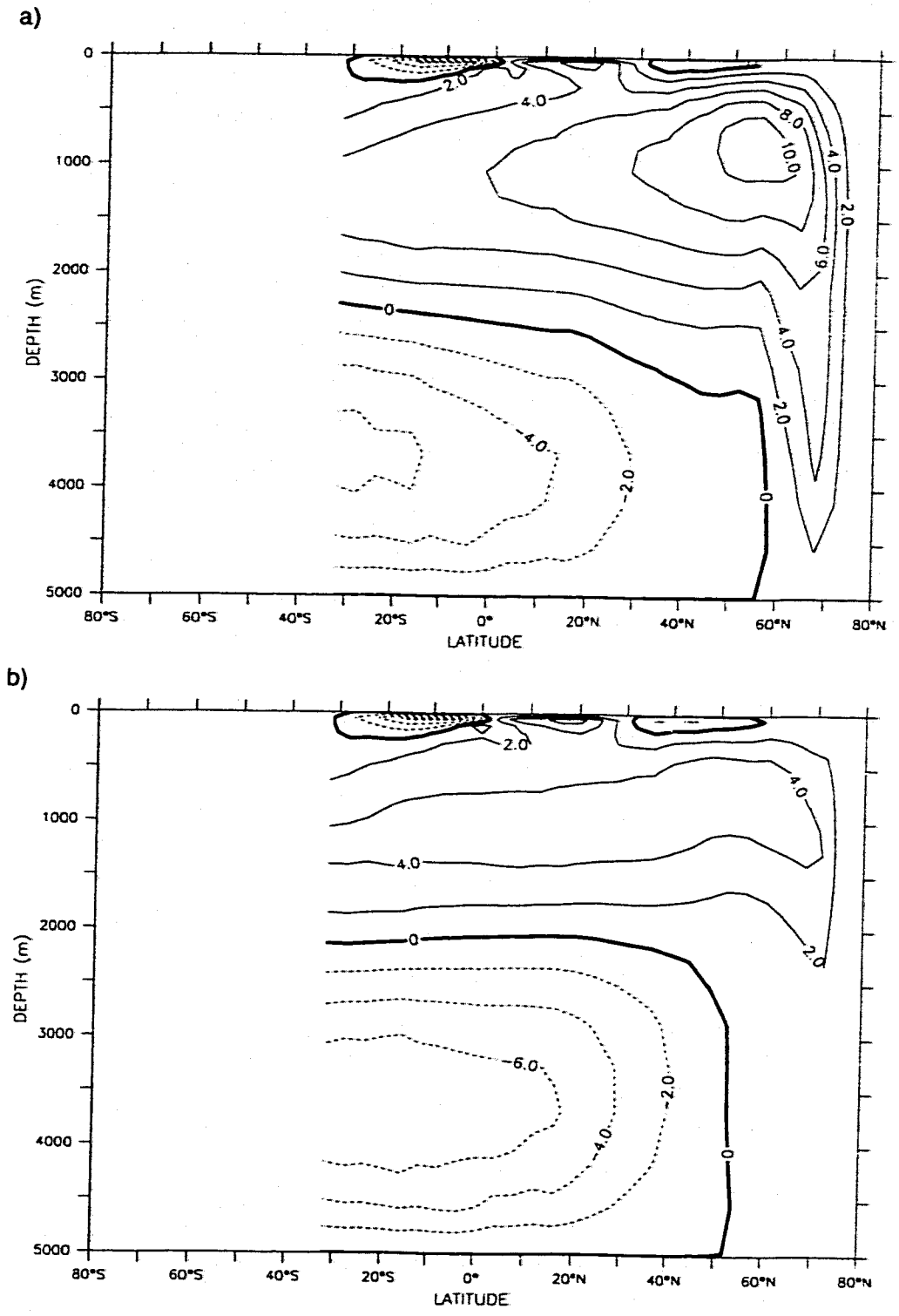

FIGURE 38 :Experiment 25a: a) maximum Atlantic overturning; b) minimum Atlantic overturning.

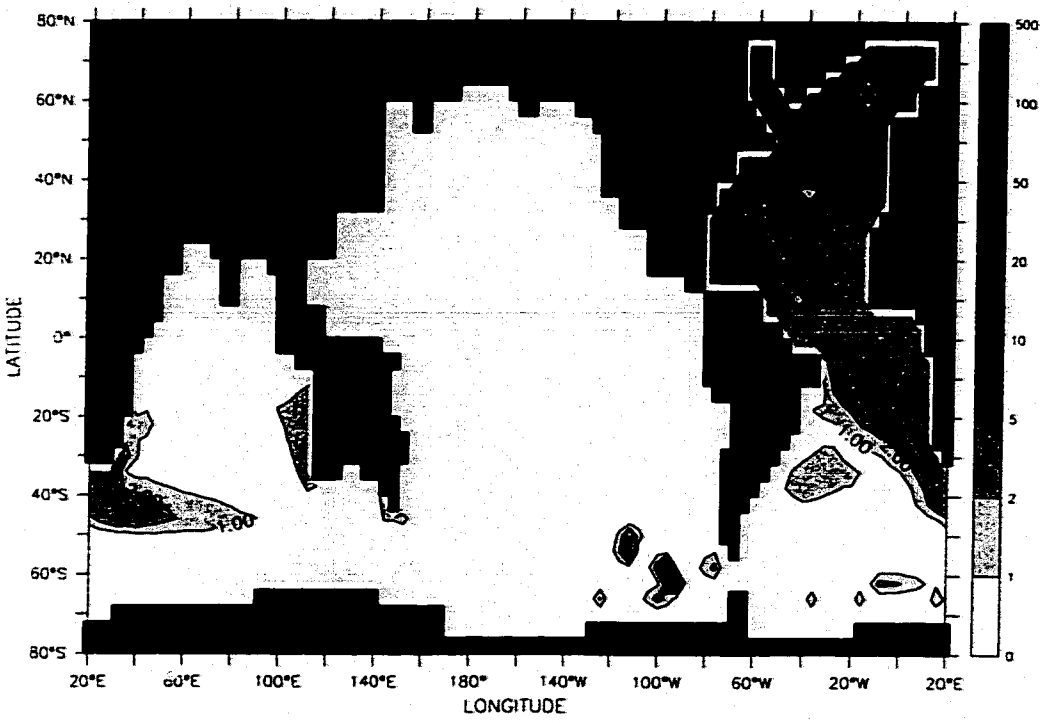

FIGURE 39 :Experiment 25a: Stratification changes at 800m in parts per thousand.

14.3 Experiment 10a

When the period of the salinity forcing is reduced to 10 years, some noteable changes are observed. Note that for about 3 years out of the 10 year cycle, there is no convection from the surface in the North Atlantic [Figure 40b]. During these years, a strong halocline at the surface [Figure 40a] prevents surface convection, but the convergence of surface waters maintains the overturning [Figure 40c]. The rapidly changing salinity boundary condition causes minor changes in the rate of NADW production, although, as indicated previously, the overturning responds on the ~25 year adjustment time scale so the inertia of the system overwhelms the forcing with a period of 10 years.

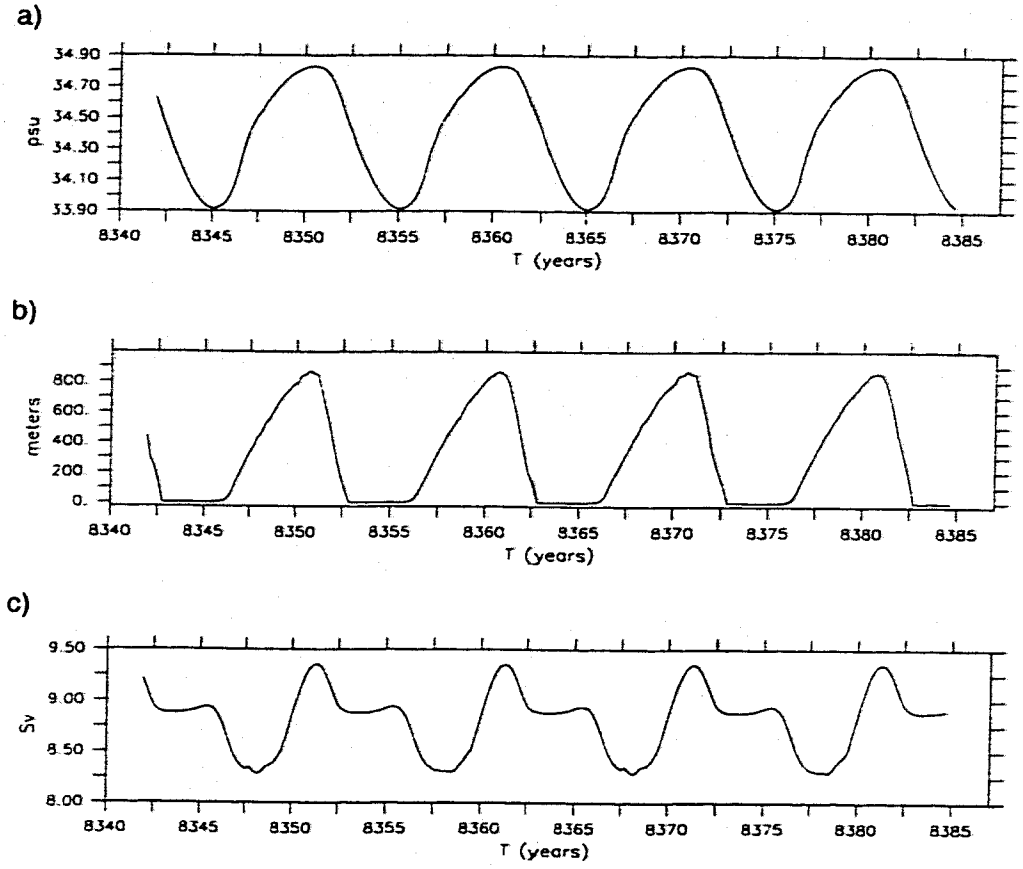

FIGURE 40 :Experiment 10a: a) sea surface salinity in the North Atlantic; b) average convective depth in the North Atlantic; c) maximum overturning at 50°N in the Atlantic.

As in the other two experiments, the maximum and minimum streamfunctions always show the transport of water directly from the overturning region across 30°S. Transports at the choke points vary by less than 7% of their mean values in the Atlantic and less than 2% elsewhere. The northward heat transport is between 0.3 and 0.4 PW and changes in the startification are negligible outside of the northern Atlantic.

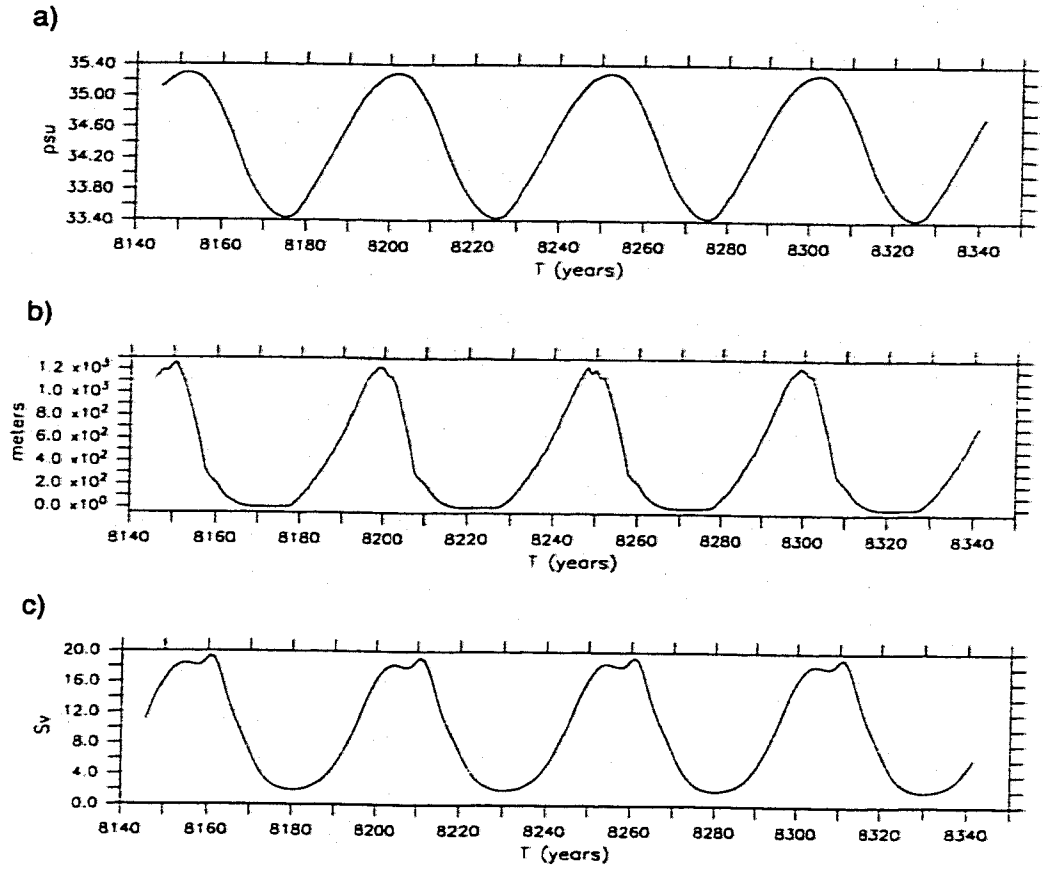

FIGURE 41 :Experiment 50b: a) sea surface salinity in the North Atlantic; b) average convective depth in the North Atlantic; c) maximum overturning at 50°N in the Atlantic.

14.4 Experiment 50b

In order to determine how the amplitude of the variability in the forcing affects the results, an additional experiment was carried out with a 50-year period, but in which the amplitude of the forcing was 1.0 psu compared to 0.5 psu in experiment 50a. From Equation 1, the maximum and minimum salinity restorings were 1.2 psu higher and 0.8 psu lower than the Levitus values [Figure 41a, which lead to greatly enhanced (20 Sv) and severly diminished (2 Sv) overturning [Figure 41c]. Unlike experiments 50a and 25a in which there was always some

convective activity, there is an 8 year period in each 50 year cycle during which surface convection is entirely eliminated [Figure 41b]. Transport anomalies along the conveyor and heat transport anomalies in the Atlantic are about twice as big as in experiment 50a. The stratification at 800 m throughout the world ocean varies by a few parts per thousand [Figure 42] and the 15°C isotherm in the tropical Indian and Pacific changes moves about 20 m over the course of one cycle [Figure 43].

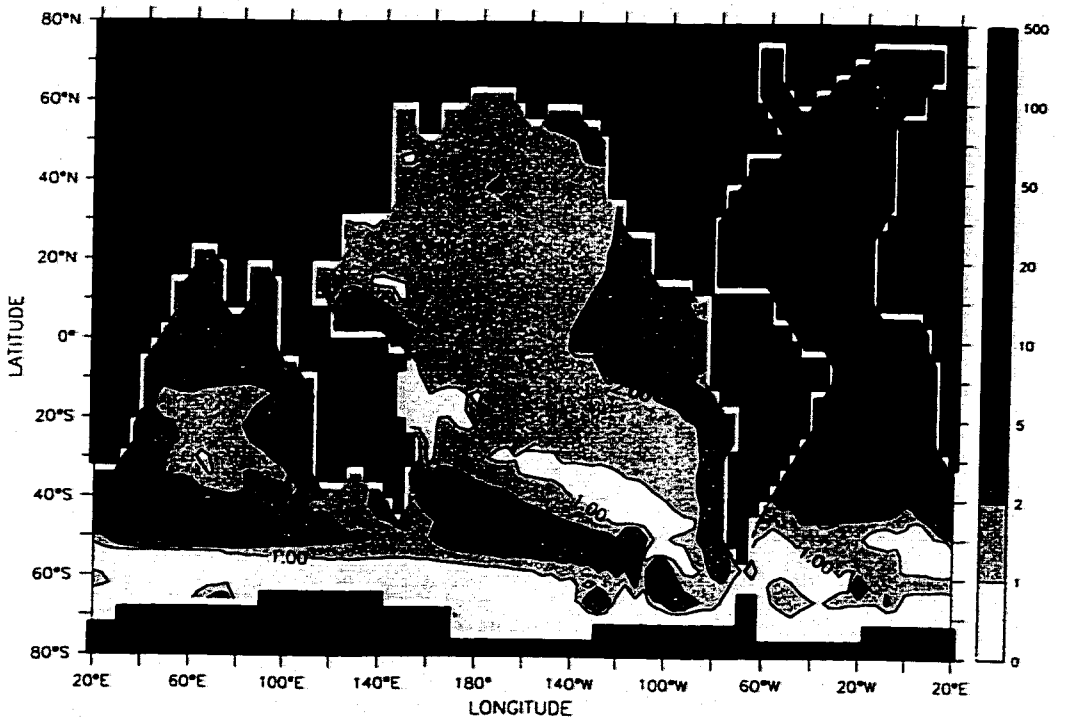

FIGURE 42 :Experiment 50b: Stratification changes at 800m in parts per thousand.

As this is the experiment with the largest response, it is worth comparing the implied rates of freshwater input to the proxy evidence and the observations. The integrated freshwater input over the North Atlantic north of 50°N is shown in

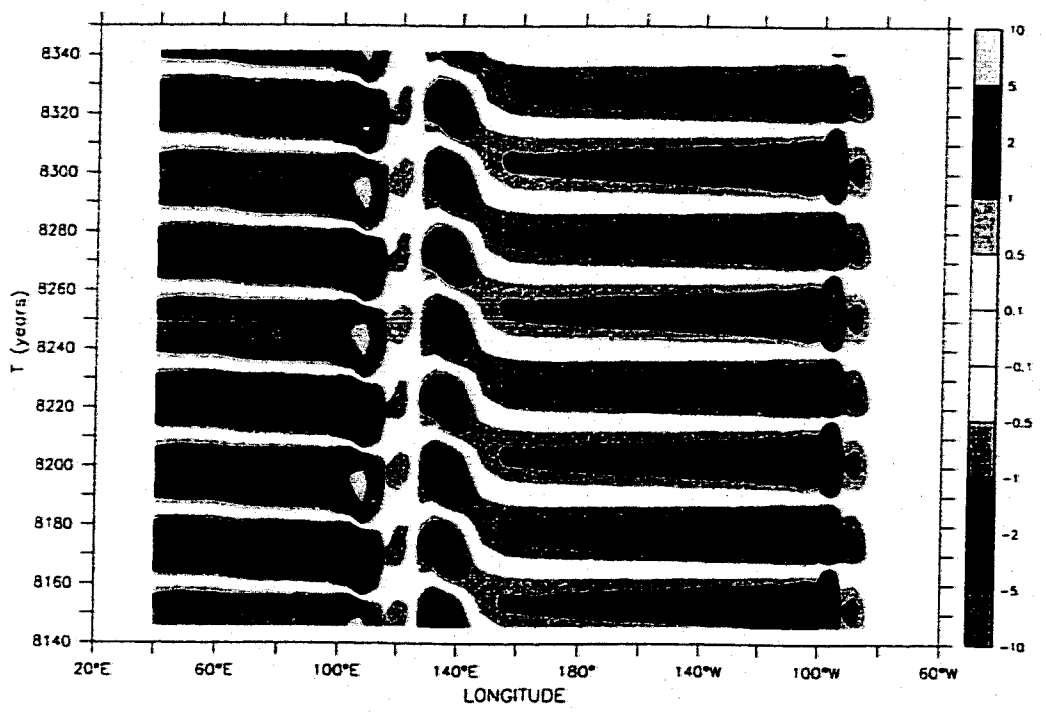

FIGURE 43 :Experiment 50b: Variation in the depth of the 15°C isotherm between 10°S and 10°N in meters.

Figure 44 in equivalent units of km^3 of ice which would have to be transfered to or from land in order to produce the modeled surface salinity. Kwok and Rothrock (1999) estimated that the yearly flux of sea ice through Fram Strait is 2366 km^3yr^{-1}. Teller (1990) estimated that fresh water reaching the North Atlantic due to runoff from the Laurentide Ice Sheet averaged 4000 km^3yr^{-1} during the Younger Dryas, in contrast to 2870 km^3yr^{-1} just before this cold episode and 3440 km^3yr^{-1} just after it. Fairbanks (1989), on the other hand, estimated that a maximum of ~13,000 km^3yr^{-1} of land ice were melted at the peak, equal to an input rate of roughly 0.4 Sv. The rates presented here, while large, are not impossible. A discharge rate of 13,000 km^3yr^{-1} is equivalent to a sea-level rise of ~4 cm per year.

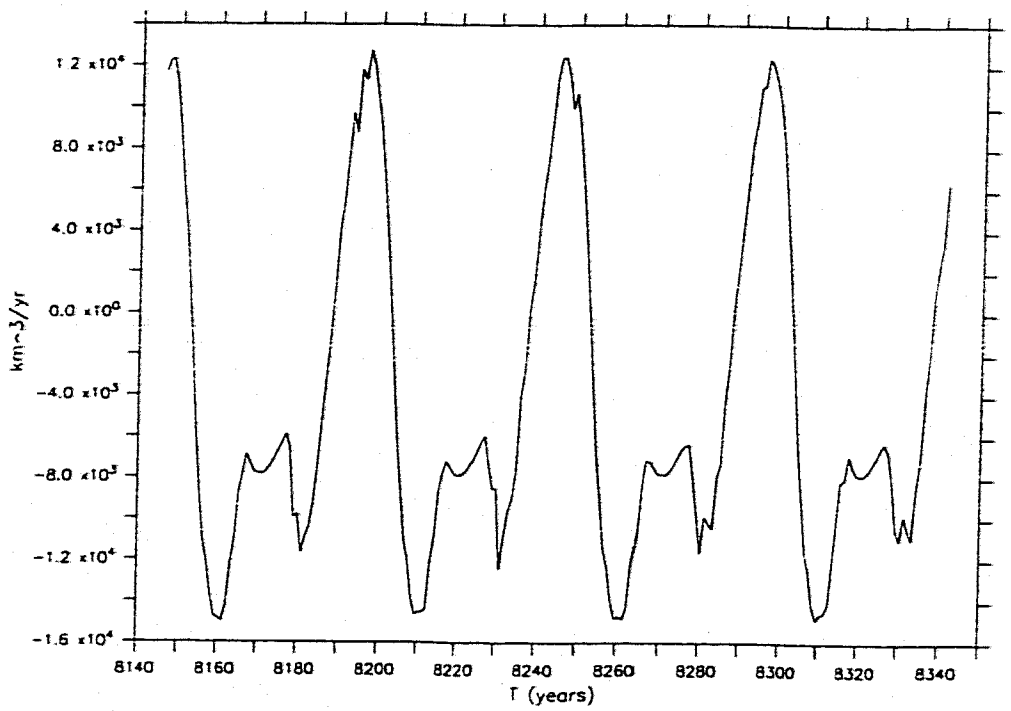

FIGURE 44 :Experiment 50b: Fresh water flux into the North Atlantic, north of 48°N, given as an eqivalent volume of land ice formed (positive) or melted (negative).

15.0 Discussion

Forcing an ocean model with a variable restoring salinity target over the North Atlantic causes the global circulation to oscillate around its long-term mean. The longer the period and the larger the amplitude of the forcing, the greater the changes in transport and stratification. All model parameters vary with the same period as the imposed forcing, although some higher-order frequencies are exhibited when the period of the forcing is shorter than the inherent 25-year time-scale over which the North Atlantic overturning adjusts to changes.

In the Atlantic basin during experiment 50b, the production of NADW increases from 2 Sv to 20 Sv in 30 years as the imposed boundary condition changes. During this same 30 year interval, the heat transport at 40°N increases from 0.07 PW to 0.7 PW and enough heat is released to the atmosphere to easily account for the rapid warming of the Greenland air temperature implied by the $\delta^{18}O$ fractionation in the GRIP ice core.

An increase in the fresh water input to the North Atlantic from either runoff or precipitation can cause the cessation of NADW production, but it is quite unlikely that the reverse is true. About 60% of the change in the average salinity of the North Atlantic during this 30-year interval is due to the imposed fresh water flux, but the remaining 40% is due to increased advection as the overturning increases. Removal of fresh water through the surface (via evaporation) at this rate is unlikely, but a decrease in the runoff into the North Atlantic may contribute, and the increased advection which accompanies the overturning is a positive feedback. This study cannot explain how the North Atlantic overturning is reestablished, but it does indicate that $\delta^{18}O$ record in the ice cores and marine sediments can be explained by the resumption of NADW production.

Changes to the transport, measured at choke points along the supposed conveyor belt, decrease rapidly outside the Atlantic basin. The outflow of NADW across 30°S in experiment 50b (the most extreme case) varies from 3.6 Sv to 10.4 Sv, while the strength of the Agulhas Leakage varies between 16.3 Sv and 21.6

Sv. The variability of the Indonesian Throughflow (the most remote choke point) is only about 6% of its mean value or about 2 Sv. These changes indicate that the conveyor belt metaphor incorrectly implies a one-to-one correspondence between the overturning in the North Atlantic and the transport along the conveyor.

Stratification changes due to variability in the rate of NADW formation are insignificant outside of the Atlantic except for a few regions in the ACC [Figure 42]. These include the location where Antarctic Intermediate Water is formed west of Chile, and the location where Subantarctic Mode Water is formed south of Tasmania (McCartney, 1977). Although the simulated changes in the stratification at 800m are small, it is notable that G98 reported that the fraction of intermediate water (defined as sigma-theta between 26.5 and 27.5 kg-m^{-3}) throughout the world ocean expanded from 21% to 33% when NADW production was eliminated.

16.0 Conclusions

The thermohaline circulation in the world ocean is the product of many different process occurring in many different locations. Likening it to a "Great Conveyor" is too simplistic and generally misleading: it implies that changes in one region will be expressed with the same magnitude at a remote location at a later time; this later time being determined by the advective velocities. There is an adjustment time-scale on the order of 25 years, much shorter than the advective time-scale (100-1000 years), over which changes in the deep water production rate of the

North Atlantic can be communicated to the rest of the Atlantic basin. The Atlantic basin does exhibit some of the characteristics of a "conveyor belt": an increase in the formation rate of NADW draws more surface water northward which increases the northward heat transport and the convergence of water at high-latitudes.

The critical point is that the heat transport responds on the adjustment time-scale, so it it quite possible that a re-initiation of convection in the North Atlantic and the renewed production of NADW are responsible for the rapid warmings seen in the $\delta^{18}O$ records at the end of the last glacial period and the Younger Dryas. Very little change occurs outside of the Atlantic basin in response to NADW variability which implies that the production of NADW cannot be solely responsible for the globally synchronous changes seen at these times: it is most likely that they are transmitted via the atmosphere.

While it seems fairly easy to add enough fresh water to the surface of the North Atlantic to cap the production of NADW via runoff or precipitation, it seems quite unlikely that this production could be re-initiated through atmospheric forcing. In order for the stratification to be eroded enough for convection to resume, it seems more likely that the intermediate and deep water below the surface layer would have to become less dense through heating or freshening, either advective or diffusive.

References

Andrée, M., H. Oeschger, W. Broecker, N. Beavan, M. Klas, A. Mix, G. Bonani, H. J. Hoffman, M. Suter, W. Woelfli, and T.-H. Peng, 1986: Limits on the ventilation rate for the deep ocean over the last 12,000 years, *Climate Dynamics*, **1**, 53-62.

Bard, E., F. Rostek, and C. Sonzogni, 1997: Interhemispheric synchrony of the last deglaciation inferred from alkenone palaeothermometry, *Nature*, **385**, 707-710.

Battisti, D. S., 1988: Dynamics and thermodynamics of a warming event in a coupled tropical atmosphere-ocean model, *J. Atmos. Sci.*, **45**, 2889-2919.

Bond, G., W. Broecker, S. Johnsen, J. McManus, L. Labeyrie, J. Jouzel, and G. Bonani, 1993: Correlations between climate records from North Atlantic sediments and Greeland ice, *Nature*, **365**, 143-147.

Böning, C. W., W. R. Holland, F. O. Bryan, G. Danabasoglu, and J. C. McWilliams, 1995: An overlooked problem in model simulations of the thermohaline circulation and heat transport in the Atlantic Ocean, *J. Climate*, **8**, 515-523.

Boyle, E. A., and L. Keigwin, 1987: North Atlantic thermohaline circulation during the past 20,000 years linked to high-latitude surface temperature, *Nature*, **330**, 35-40.

Brewer, P. G., W. S. Broecker, W. J. Jenkins, P. B. Rhines, C. G. Rooth, J. H. Swift, T. Takahashi, and R. W. Williams, 1983: A climatic freshening of the deep North Atlantic north of 50°N over the past 20 years, *Science*, **222**, 1237-1239.

Broecker, W. S., 1987: The biggest chill, *Natural History Magazine*, **97**, 74-82.

Broecker, W. S., 1988: Chronology of the last deglaciation: implications to the cause of the Younger Dryas event, *Paleoceanography*, **3**, 1-19.

Broecker, W. S., 1991: The great ocean conveyor, *Oceanography*, **4**, 79-89.

Broecker, W. S., 1995: Chaotic Climate, *Scientific American*, **273**, 62-68.

Broecker, W. S., 1998: Paleocean circulation during the last deglaciation: A bipolar seesaw?, *Paleoceanography*, **13**, 119-121.

Broecker, W. S., S. Blanton, W. M. Smethie, Jr., G. Ostlund, 1991: Radiocarbon decay and oxygen utilization in the deep Atlantic Ocean, *Global Biogeochemical Cycles*, **5**, 87-117.

Broecker, W. S., and G. H. Denton, 1989: The role of ocean-atmosphere reorganizations in glacial cycles, *Geochim. Cosmochim. Acta*, **53**, 2465-2501.

Broecker, W. S., S. L. Peacock, S. Walker, R. Weiss, E. Fahrbach, M. Schroeder, U. Mikolajewicz, C. Heinze, R. Key, T.-H. Peng, and S. Rubin, 1998: How much deep water is formed in the Southern Ocean?, *J. Geophys. Res.*, **103**, 15,833-15,843.

Broecker, W. S., T.-H. Peng, S. Trumbore, G. Bonani, W. Wolfli, 1990: The distribution of radiocarbon in the glacial ocean, *Global Biogeochemical Cycles*, **4**, 103-117.

Broecker, W. S., D. M. Peteet, and D. Rind, 1985: Does the ocean-atmosphere system have more than one stable mode of operation?, *Nature*, **315**, 21-26.

Bryan, F., 1986a: Maintenance and variability of the thermohaline circulation, Ph.D. thesis, Program in Atmos. and Oceanic Sci, Princeton Univ., Princeton, NJ, 254pp.

Bryan, F., 1986b: High-latitude salinity effects and interhemispheric thermohaline circulations, *Nature*, **323**, 301-304.

Bryan, F., 1987: Parameter sensitivity of primitive equation ocean general circulation models, *J. Phys. Oceanogr.*, **17**, 970-985.

Bryan, K., and L. J. Lewis, 1979: A water mass model of the world ocean, *J. Geophys. Res.*, **84**, 2503-2517.

Bryan, K., and M. J. Spelman, 1985: The ocean's response to a carbon dioxide-induced warming, *J. Geophys. Res.*, **90**, 11,679-11,688.

Cai, W., and R. J. Greatbatch, 1995: Compensation for the NADW outflow in a global ocean general circulation model, *J. Phys. Oceanogr.*, **25**, 226-241.

Cai W., J. Syktus, H. B. Gordon, and S. O'Farrell, 1997: Response of a global coupled ocean-atmosphere-sea ice climate model to an imposed North Atlantic high-latitude freshening, *J. Climate*, **10**, 929-948.

Cane, M. A., 1989: A mathematical note on Kawase's study of the deep-ocean circulation, *J. Phys. Oceanogr.*, **19**, 548-550.

Cane, M. A., and E. S. Sarachik, 1977: Forced baroclinic ocean motions: II. The linear equatorial bounded case, *J. Marine Research*, **35**, 395-432.

Carmack, E. C., and T. D. Foster, 1975: On the flow of water out of the Weddell Sea, *Deep-Sea Research*, **22**, 711-724.

Charles, C. D., and R. G. Fairbanks, 1992: Evidence from Southern Ocean sediments for the effect of North Atlantic deep-water flux on climate, *Nature*, **355**, 416-419.

Cox, M. D., 1989: An idealized model of the world ocean. Part I: The global-scale water masses, *J. Phys. Oceanogr.*, **19**, 1730-1752.

Delworth, T. L., S. Manabe, and R. J. Stouffer, 1995: North Atlantic interdecadal variability in a coupled model, In: *Natural climate variability on decade-to-century time scales*, National Research Council, et al., National Academy Press, Washington, D. C., 432-441.

Delworth, T. L., S. Manabe, and R. J. Stouffer, 1997: Multidecadal climate variability in the Greenland Sea and surrounding regions: a coupled model simulation, *Geophysical Research Letters*, **24**, 257-260.

Dickson, R. R., and J. Brown, 1994: The production of North Atlantic Deep Water: Sources, rates, and pathways, *J. Geophys. Res.*, **99**, 12,319-12,341.

Dickson, R. R., E. M. Gmitrowicz, and, A. J. Watson, 1990: Deep-water renewal in the northern North Atlantic, *Nature*, **344**, 848-850.

Dickson, R. R., J. Lazier, J. Meinke, P. Rhines, and J. Swift, 1996: Long-term coordinated changes in convective activity of the North Atlantic, *Progress in Oceanography*, **38**, 241-295.

Dickson, R. R., J. Meinke, I. Vassie, J. Jungclaus, and S. Østerhus, 1999: Possible predictability in overflow from the Denmark Strait, *Nature*, **397**, 243-246.

Drijfhout, S., C. Heinze, M. Latif, and E. Maier-Reimer, 1996: Mean circulation and internal variability in an ocean primitive equation model, *J. Phys. Oceanogr.*, **26**, 559-580.

Drijfhout, S. S., E. Maier-Reimer, and U. Mikolajewicz, 1996: Tracing the conveyor belt in the Hamburg large-scale geostrophic ocean general circulation model, *J. Geophys. Res.*, **101**, 22,563-22,575.

Duffy, P. B., and K. Caldeira, 1997: Sensitivity of simulated salinity in a three-dimensional ocean model to upper ocean transport of salt from sea-ice formation, *Geophysical Research Letters*, **24**, 1323-1326.

Duplessy, J.-C., M. Arnold, E. Bard, L. Labeyrie, J. Duprat, and J. Moyes, 1992: Glacial-to-Interglacial Changes in Ocean Circulation, In: *Radiocarbon After Four Decades*, R.E. Taylor, A. Long, R.S. Kra, eds., NATO ASI Series, Springer-Verlag, New York, pp. 62-74.

Duplessy, J.-C., and L. Labeyrie, 1994: Surface and deep water circulation changes during the last climatic cycle, In: *Long-Term Climatic Variations*, J. C. Duplessy, M. T. Spyridakis, eds., NATO ASI Series, Springer-Verlag, Berlin, pp. 277-298.

Duplessy, J.-C., N. J. Shackleton, R. G. Fairbanks, L. Labeyrie, D. Oppo, and N. Kallel, 1988: Deepwater source variations during the last climatic cycle and their impact on the global deep water circulation, *Paleoceanography*, **3**, 343-360.

England, M. H., 1993: Representing the global-scale water masses in ocean general circulation models, *J. Phys. Oceanogr.*, **23**, 1523-1552.

England, M. H., 1995: The age of water and ventilation timescales in a global ocean model, *J. Phys. Oceanogr.*, **25**, 2756-2777.

Fairbanks, R. G., 1989: A 17,000-year glacio-eustatic sea level record: influence of glacial melting rates on the Younger Dryas event and deep-ocean circulation, *Nature*, **342**, 637-642.

Fichefet, T., S. Hovine, and J.-C. Duplessy, 1994: A model study of the Atlantic thermohaline circulation during the last glacial maximum, *Nature*, **372**, 252-255.

Fieux, M., R. Molcard, and A. G. Ilahude, 1996: Geostrophic transport of the Pacific-Indian Oceans throughflow, *J. Geophys. Res.*, **101**, 12,421-12,432.

Foster, T. D., 1995: Abyssal water mass formation off the eastern Wilkes Land coast of Antarctica, *Deep-Sea Research*, **42**, 501-522.

Foster, T. D., and E. C. Carmack, 1976: Frontal zone mixing and Antarctic Bottom Water formation in the southern Weddell Sea, *Deep-Sea Research*, **23**, 301-317.

Gent, P. R., and J. C. McWilliams, 1990: Isopycnal mixing in ocean circulation models, *J. Phys. Oceanogr.*, **20**, 150-155.

Gill, A. E., 1982: *Atmosphere-Ocean Dynamics*, Academic Press, San Diego, CA, 662pp.

Gill, A. E., and K. Bryan, 1971: Effects of geometry on the circulation of a three-dimensional southern hemisphere ocean model, *Deep-Sea Research*, **18**, 685-721.

Gille, S. T., 1997: The Southern Ocean momentum balance: Evidence for topographic effects from numerical model output and altimeter data, *J. Phys. Oceanogr.*, **27**, 2219-2232.

Goodman, P. J., 1998: The role of North Atlantic Deep Water formation in an OGCM's ventilation and thermohaline circulation, *J. Phys. Oceanogr.*, **28**, 1759-1785.

Gordon, A. L., 1986: Interocean exchange of thermocline water, *J. Geophys. Res.*, **91**, 5037-5046.

Gordon, A. L., 1991: The role of the thermohaline circulation in global climate change, *Annual Report 1990-1991*, Lamont-Doherty Earth Observatory, Columbia Univ., Palisades, N. Y., pp. 44-51.

Gordon, A. L., R. F. Weiss, W. M. Smethie, Jr., and M. J. Warner, 1992: Thermocline and intermediate water communication between the South Atlantic and Indian Oceans, *J. Geophys. Res.*, **97**, 7223-7240.

Greatbatch, R. J., and K. A. Peterson, 1996: Interdecadal variability and oceanic thermohaline adjustment, *J. Geophys. Res.*, **101**, 20,467-20,482.

Greatbatch, R. J., and S. Zhang, 1995: An interdecadal oscillation in an idealized ocean basin forced by constant heat flux, *J. Climate*, **8**, 81-91.

Guo, Z., T. Liu, N. Fedoroff, L. Wei, Z. Ding, N. Wu, H. Lu, W. Jiang, and Z. An, 1998: Climate extremes in loess of China coupled with the strength of deep-water formation in the North Atlantic, *Global and Planetary Change*, **18**, 113-128.

Haidvogel, D. B., and F. O. Bryan, 1992: Ocean general circulation modeling, In: *Climate System Modeling*, K. E. Trenberth, ed., Cambridge University Press, Cambridge, 788 pp.

Haney, R. L., 1971: Surface thermal boundary condition for ocean circulation models, *J. Phys. Oceanogr.*, **1**, 241-248.

Hellerman, S., and M. Rosenstein, 1983: Normal monthly wind stress over the world ocean with error estimates, *J. Phys. Oceanogr.*, **13**, 1093-1104.

Hirst, A. C., and J. S. Godfrey, 1993: The role of Indonesian throughflow in a global ocean GCM, *J. Phys. Oceanogr.*, **23**, 1057-1086.

Holland, W. R., 1973: Baroclinic and topographic influences on the transport in western boundary currents, *Geophysical Fluid Dynamics*, **4**, 187-210.

Huang, R. X., 1993: Real freshwater flux as a natural boundary condition for the salinity balance and thermohaline circulation forced by evaporation and precipitation, *J. Phys. Oceanogr.*, **23**, 2428-2446.

Huang, R. X., M. A. Cane, N. Naik, and P. J. Goodman, 1999: Global adjustment of the thermocline in response to deepwater formation, *Geophysical Research Letters*, submitted, June 1999.

Huck, T., A. C. de Verdière, and A. J. Weaver, 1999: Interdecadal variability of the thermohaline circulation in box-ocean models forced by fixed surface fluxes, *J. Phys. Oceanogr.*, **29**, 865-892.

Hughes, T. M. C., and A. Weaver, 1994: Multiple equilibria of an asymmetric two-basin ocean model, *J. Phys. Oceanogr.*, **24**, 619-637.

Karcher, M., and A. Lippert, 1994: Spin-up and breakdown of source-driven deep North Atlantic flow over realistic bottom topography, *J. Geophys. Res.*, **99**, 12,357-12,373.

Kawase, M., 1987: Establishment of deep ocean circulation driven by deep-water production, *J. Phys. Oceanogr.*, **17**, 2294-2317.

Kwok, R., and D. A. Rothrock, Variability of Fram Strait ice flux and North Atlantic Oscillation, *J. Geophys. Res.*, **104**, 5177-5189.

Levitus, S., 1982: Climatological Atlas of the World Ocean, *NOAA Prof. Pap. 13*, U. S. Government Printing Office, Washington, D.C.

Levitus, S., R. Burgett, and T. P. Boyer, 1994a: *World Ocean Atlas, Volume 3: Salinity*, U.S. Government Printing Office, Washington, D.C.

Levitus, S., and T. P. Boyer, 1994b: *World Ocean Atlas, Volume 4: Temperature*, U.S. Government Printing Office, Washington, D.C.

Lowell, T. V.., C. J. Heusser, B. G. Andersen, P. I. Moreno, A. Hauser, L. E. Heusser, C. SchlÜchter, D. R. Marchant, and G. H. Denton, 1995: Interhemispheric Correlation of Late Pleistocene Glacial Events, *Science*, **269**, 1541-1549.

Macdonald, A. M., and C. Wunsch, 1996: An estimate of global ocean circulation and heat fluxes, *Nature*, **382**, 436-439.

Manabe, S., and R. J. Stouffer, 1988: Two stable equilibria of a coupled ocean-atmosphere model, *J. Climate*, **1**, 841-866.

Manabe, S., and R. J. Stouffer, 1994: Multiple-century response of a coupled ocean-atmosphere model to an increase of atmospheric carbon dioxide, *J. Climate*, **7**, 5-23.

Mantyla, A. W., and J. L. Reid, 1983: Abyssal characteristics of the Worls Ocean waters, *Deep-Sea Research*, **30**, 805-833.

Marotzke, J., and J. Willebrand, 1991: Multiple equilibria of the global thermohaline circulation, *J. Phys. Oceanogr.*, **21**, 1372-1385.

Marshall J., F. Dobson, K. Moore, P. Rhines, M. Visbeck, E. d'Asaro, K. Bumke, S. Chang, R. Davis, K. Fischer, R. Garwood, P. Guest, R. Harcourt, C. Herbaut, T. Holt, J. Lazier, S. Legg, J. McWilliams, R. Pickart, M. Prater, I. Renfrew, F. Schott, U. Send, and W. Smethie, 1998, The Labrador Sea Deep Convection Experiment, *Bull. Amer. Meteor. Soc.*, **79**, 2033-2058.

Marshall, J., D. Olbers, H. Ross, and D. Wolf-Gladrow, 1993: Potential vorticity constraints on the dynamics and hydrography of the Southern Ocean, *J. Phys. Oceanogr.*, **23**, 465-487.

McCartney, M. S., 1977: Subantarctic Mode Water, In: A Voyage of Discovery: Geore Deacon 70th Anniversary Volume, ed. M. V. Angel, *Deep-Sea Research, Supplement*, 103-119, Pergamon Press.

McDermott, D. A., 1996: Interaction of the Northern and Southern Branches of the Thermohaline Circulation, Ph.D. thesis, Univ. Washington, Seattle, WA, 207pp.

McDermott, D. A., 1996: The regulation of northern overturning by southern hemisphere winds, *J. Phys. Oceanogr.*, **26**, 1234-1255.

Mertz, G. and D. G. Wright, 1992: Interpretations of the JEBAR term, *J.Phys. Oceanogr.*, **22**, 301-305.

Meyers, G., 1996: Variation of Indonesian throughflow and the El Nino - Southern Oscillation, *J. Geophys. Res.*, **101**, 12,255-12,263.

Michel, E., L. D. Labeyrie, J.-C. Duplessy, N. Gorfti, M. Labracherie, and J.-L. Turon, 1995: Could deep subantarctic convection feed the world deep basins during the last glacial maximum, *Paleoceanography*, **10**, 927-942.

Mikolajewicz, U., and E. Maier-Reimer, 1990: Internal secular variability in an ocean general circulation model, *Climate Dynamics*, **4**, 145-156.

Moore, D. W., and S. G. H. Philander, 1976: Modelling of the tropical oceanic circulation, In: *The Sea*, Vol. 6, Goldberg, et al., eds., Interscience, New York.

Munk, W. H., and E. Palmén, 1951: Note on the dynamics of the Antarctic Circumpolar Current, *Tellus*, **3**, 53-55.

Ostlund, H. G., and M. Stuiver, 1980: GEOSECS Pacific Radiocarbon, *Radiocarbon*, **22**, 25-53.

Pacanowski, R. C., K. Dixon, and A. Rosati, 1991: The GFDL Modular Ocean Model Users Guide, version 1.0, GFDL Ocean Group Tech. Rep. No. 2, 376 pp.

Petit, J. R., J. Jouzel, D. Raynaud, N. I. Barkov, J.-M. Barnola, I. Basile, M. Bender, J. Chappellaz, M. Davis, G. Delaygue, M. Delmotte, V. M. Kotlyakov, M. Legrand, V. Y. Lipenkov, C. Lorius, L. Pépin, C. Ritz, E. Saltzman, and M. Stievenard, 1999: Climate and atmospheric history of the past 420,000 years from the Vostok ice core, Antarctica, *Nature*, **399**, 429-436.

Power, S. B., and R. Kleeman, 1993: Multiple equilibria in a global ocean general circulation model, *J. Phys. Oceanogr.*, **23**, 1670-1681.

Rahmstorf, S., 1995: Multiple convection patterns and thermohaline flow in an idealized OGCM, *J. Climate*, **8**, 3028-3039.

Rahmstorf, S., 1995: Bifurcations of the Atlantic thermohaline circulation in response to changes in the hydrological cycle, *Nature*, **378**, 145-149.

Reid, J. L., 1989: On the geostrophic circulation of the South Atlantic Ocean: Flow patterns, tracers, and transports, *Progress in Oceanography*, **23**, 149-244.

Rind, D., and D. Peteet, 1985: Terrestrial Conditions at the last glacial maximum and CLIMAP sea-surface temperature estimates: Are they consistent?, *Quaternary Research*, **24**, 1-22.

Rintoul, S. R., 1991: South Atlantic interbasin exchange, *J. Geophys. Res.*, **96**, 2675-2692.

Robitaille, D. Y., and A. J. Weaver, 1995: Validation of sub-grid scale mixing schemes using CFC's in a global ocean model, *Geophysical Research Letters*, **22**, 2917-2920.

Roemmich, D., and C. Wunsch, 1984: Apparent changes in the climatic state of the deep North Atlantic Ocean, *Nature*, **307**, 447-450.

Sarmiento, J. L., T. M. C. Hughes, R. J. Stouffer, and S. Manabe, 1998: Response of the ocean carbon cycle to anthropogenic climate warming, *Nature*, **393**, 245-249.

Schmitz, W. J., 1995: On the interbasin-scale thermohaline circulation, *Reviews of Geophysics*, **33**, 151-173.

Schopf, P. S., 1983: On equatorial waves and El Nino. II: Effects of air-sea thermal coupling, *J. Phys. Oceanogr.*, **13**, 1878-1893.

Semtner, A. J. Jr., and R. M. Chervin, 1988: A simulation of the global ocean circulation with resolved eddies, *J. Geophys. Res.*, **93**, 15,502-15,522.

Severinghaus, J. P., T. Sowers, E. J. Brook, R. B. Alley, and M. L. Bender, 1998: Timing of abrupt climate change at the end of the Younger Dryas interval from thermally fractionated gases in polar ice, *Nature*, **391**, 141-146.

Shriver, J. F., and H. E. Hurlburt, 1997: The contribution of the global thermohaline circulation to the Pacific to Indian Ocean throughflow via Indonesia, *J. Geophys. Res.*, **102**, 5,491-5,511.

Sowers, T., and M. Bender, 1995: Climate records covering the last deglaciation, *Science*, **269**, 210-214.

Speer, K. G., and W. Zenk, 1993: The flow of Antarctic Bottom Water into the Brazil basin, *J. Phys. Oceanogr.*, **23**, 2667-2682.

Stocker, T. F., D. G. Wright, and W. S. Broecker, 1992: The influence of high-latitude surface forcing on the global thermohaline circulation, *Paleoceanography*, **7**, 529-541.

Stommel, H. and A. B. Arons, 1960a: On the abyssal circulation of the world ocean — I. Stationary planetary flow pattern on a sphere, *Deep-Sea Research*, **6**, 140-154.

Stommel, H. and A. B. Arons, 1960b: On the abyssal circulation of the world ocean — II. An idealized model of the circulation pattern and amplitude in oceanic basins, *Deep-Sea Research*, **6**, 217-233.

Stuiver, M., and H. G. Ostlund, 1980: GEOSECS Atlantic Radiocarbon, *Radiocarbon*, **22**, 1-24.

Stuiver, M., and H. G. Ostlund, 1983: GEOSECS Indian Ocean and Mediterranean Radiocarbon, *Radiocarbon*, **25**, 1-29.

Stute, M., M. Forster, H. Frischkorn, A. Serejo, J. F. Clark, P. Schlosser, W. S. Broecker, and G. Bonani, 1995: Cooling of tropical Brazil (5°C) during the last glacial maximum, *Science*, **269**, 379-383.

Teller, J. T., 1990: Meltwater and precipitation runoff to the North Atlantic, Arctic, and Gulf of Mexico from the Laurentide Ice Sheet and adjacent regions during the Younger Dryas, *Paleoceanography*, **5**, 897-905.

Thompson, L. G., E. Mosley-Thompson, M. E. Davis, P.-N. Lin, K. A. Henderson, J. Cole-Dai, J. F. Bolzan, and K.-b. Liu, 1995: Late glacial stage and Holocene tropical ice core records from Huascaran, Peru, *Science*, **269**, 46-50.

Toggweiler, J. R., and B. Samuels, 1993: New radiocarbon constraints on the upwelling of abyssal water to the ocean's surface, In: *The Global Carbon Cycle*, M. Heimann, ed., NATO ASI Series, Springer-Verlag, Berlin, pp. 333-366.

Toggweiler, J. R., and B. Samuels, 1995: Effect of sea ice on the salinity of Antarctic bottom waters, *J. Phys. Oceanogr.*, **25**, 1980-1997.

Toggweiler, J. R., and B. Samuels, 1995: Effect of Drake Passage on the Global Thermohaline Circulation, *Deep-Sea Research*, **42**, 477-500.

Trenberth, K. E., and A. Solomon, 1994: The global heat balance: heat transport in the atmosphere and ocean, *Climate Dynamics*, **10**, 107-134.

Veronis, G., 1975: The role of models in tracer studies, *Numerical Models of Ocean Circulations*, U.S. Natl. Acad. of Sci., pp. 133-145.

Warren, B. A., 1994: Driving the meridional overturning in the Indian Ocean, *Deep-Sea Research*, **41**, 1349-1360.

Weaver, A. J., 1995: Decadal-to-millennial internal oceanic variability in coarse-resolution ocean general-circulation models, In: *Natural climate variability on decade-to-century time scales.*, National Research Council, et al., National Academy Press, Washington, D.C., 365-383.

Weaver, A. J., and M. Eby, 1997: On the numerical implementation of advection schemes for use in conjunction with various mixing parameterizations in the GFDL ocean model, *J. Phys. Oceanogr.*, **27**, 369-377.

Weaver, A. J., J. Marotzke, P. F. Cummings, and E. S. Sarachik, 1993: Stability and variability of the thermohaline circulation, *J. Phys. Oceanogr.*, **23**, 39-60.

Weaver, A. J., and E. S. Sarachik, 1991: Evidence for decadal variability in an ocean general circulation model: An advective mechanism, *Atmosphere-Ocean*, **29**, 197-231.

Weaver, A. J., E. S. Sarachik, and J. Marotzke 1991: Freshwater flux forcing of decadal and interdecadal oceanic variability, *Nature*, **353**, 836-838.

Whitworth, T., III, W. D. Nowlin, Jr., and S. J. Worley, 1982: The net transport of the Antarctic circumpolar current through Drake Passage, *J. Phys. Oceanogr.*, **12**, 960-971.

Wijffels, S. E., J. M. Toole, H. L. Bryden, R. A. Fine, W. J. Jenkins, and J. L. Bullister, 1996: The water masses and circulation at 10°N in the Pacific, *Deep-Sea Research*, **43**, 501-544.

Winton, M., 1996: The role of horizontal boundaries in parameter sensitivity and decadal-scale variability of coarse-resolution ocean general circulation models, *J. Phys. Oceanogr.*, **26**, 289-304.

Yasuda, I., 1997: The origin of North Pacific Intermediate Water, *J. Geophys. Res.*, **102**, 893-909.

Vita

PAUL JOSEPH GOODMAN

16 March 1967	Born, New York City, NY, USA
1984	Graduate, Clarkstown High School South, West Nyack, NY
1988	B.A., Mathematics, University of Rochester, Rochester, NY
1996	M.S., Atmospheric Sciences, University of Washington
2000	PhD., Atmospheric Sciences, University of Washington

PUBLICATIONS:

Goodman, P. J., 1999: Thermohaline adjustment and advection in an OGCM, submitted to *Journal Physical Oceanography.*

Goodman, P. J., 1998: The role of North Atlantic deep water in an OGCM's ventilation and thermohaline circulation, *Journal Physical Oceanography,* **28**, 1759-1785.

Huang, R. X., M. A. Cane, N. Naik, and P. J. Goodman, 1999: Global adjustment of the thermocline in response to deep water formation, submitted to *Geophysical Research Letters.*

Kamenkovich, I. V., and P. J. Goodman, 1999: The dependence of AABW formation on vertical diffusivity, submitted to *Geophysical Research Letters.*